2-1-2019

Characteristics of linear alternator performance under thermoacoustic-power-conversion conditions

Ahmed Ibrahim

THE AMERICAN UNIVERSITY IN CAIRO

SCHOOL OF SCIENCES AND ENGINEERING

CHARACTERISTICS OF LINEAR ALTERNATOR PERFORMANCE UNDER THERMOACOUSTIC-POWER-CONVERSION CONDITIONS

BY

AHMED YASSIN ABDELWAHED IBRAHIM

A thesis submitted in partial fulfillment of the requirements for the degree of

Master of Science in Mechanical Engineering

Under the supervision of:

Prof. Ehab Abdel-Rahman

Professor, Physics Department

The American University in Cairo

Prof. Mohamed Amr Serag Eldin

Professor, Mechanical Engineering Department

The American University in Cairo

Dr. Abdelmaged Hafez Ibrahim Essawey

Research Post-Doctoral Scholar

The American University in Cairo

November 2018

Acknowledgement

The work that this thesis encompasses was made possible with the support of many individuals and organizations. First of all, I would like to thank my advisor Prof. Ehab Abdel-Rahman the head of the Thermoacoustics research team who provided me and the rest of the team with the needed scientific guidance and advanced facilities in the Thermoacoustic Research Lab throughout many years of research. Thanks also to my advisor Prof. Mohamed Amr Serag-Eldein who helped me a lot with his long and strong experience in the renewable energy field to produce this thesis work. For sure I would like to thank my advisor Dr. Abdelmaged H. Ibrahim Essawey whose experience, flexibility, technical guidance, and day-to-day follow up helped me produce the results of this work and made it easier to get over the many barriers in the field of the Thermoacoustics and linear alternators.

I also have a great deal of gratitude for Prof. Steven Garrett (Penn State University) and Dr. Kai Wang (Imperial College) whom knowledge and experience in thermoacoustic engines and their applications are great. Their prompt replies on my questions enabled me to significantly enhance the analytical model. Additionally, for sure I would like to thank Prof. Gregory W. Swift (Los Alamos Labs) for his great help in the modeling of the load resistance and the power-factor-correcting capacitor in DELTAEC software.

I am very thankful to John Corey, Phillip Spoor and Gordon Miller of Q-Drive (Rix Industries, Chart Industries in the past) for the technical support they provided on many aspects of linear alternators.

For sure, I would like to thank Dr. Islam Ramadan who assisted on the numerical simulations using DELTAEC software, Eng. Moamen Bellah Abdelmawgoud who built the initial form of the experimental setup, and Eng. Khaled El Beltagey who assisted in the development of the experimental setup along the years.

I am also thankful to every member in the thermoacoustic research team for the fruitful discussions, technical support, and the great time I had during this research period.

The American University in Cairo provided access to numerous scientific resources, a research grant, and two conference grants that enabled me to greatly develop this work and assisted

in the building, continuous and smooth running of the experimental setup and presenting nine publications in international conferences and meetings.

This work was possible with the financial assistance of the European Union. The contents of this document are the sole responsibility of the master student and can under no circumstances be regarded as reflecting the position of the European Union.

I am very thankful for the Egyptian Academy of Scientific Research and Technology which partly funded the development of the initial form of the experimental setup used.

This work is a new step of my research work in the space systems field that I have started under supervision of Dr.Mohammed Khalil Ibrahim, Prof. Atef Omar Sherif, Prof.Bahy-El Dein Argon and Dr.Ayman Kassem in Space Systems Technology Laboratory (SSTL), aerospace engineering department-Cairo University. I would like to thank all of these professors and the previous leader of this laboratory Eng.Samy Amin (Avelabs).

Many thanks go to my parents (Dr.Yassin Ibrahim and Mrs.Hanim El Saadany) who give me all what they have of love and support.

Contents

List of Figures

List of Tables

Nomenclature

A	piston area (m^2)
A_{opt}	optimum area for minimum total loss (m^2)
a	acceleration (m/s^2)
Bl	transduction coefficient (N/A)
C	capacitance of the tuning capacitor (F)
c	proportionality constant (Ω)
DELTAEC	Design Environment for Low-Amplitude Thermoacoustic Energy Conversion
d	piston diameter (m)
F	Lorentz force (N)
f	frequency (Hz)
I	generated current (A)
Im []	imaginary part of a complex number
j	imaginary unit
K	alternator intrinsic stiffness (N/m)
K_g	gas stiffness (N/m)
L	coil inductance (H)
L_e	effective coil inductance (H)
L_o	initial coil inductance (H)
l	seal length (m)
M	piston moving mass (Kg)
PF	power factor
P	dynamic pressure (Pa)
P_b	dynamic pressure at the back of the linear alternator piston (Pa)
P_f	dynamic pressure at front of the linear alternator piston (Pa)
P_m	mean gas pressure (Pa)
R_L	load resistance (Ω)
$R_{L,\ Opt}$	optimum load resistance for acoustic-to-electric-conversion efficiency (Ω)
R_e	total electric resistance (Ω)
Re []	real part of a complex number
R_m	damping coefficient (N.s/m)
r_e	stator resistance (Ω)
r_s	current-sensing resistance (Ω)
S	mechanical stroke (mm)

S_R	rated mechanical stroke (mm)
T	Temperature
t	time (s)
U	volume velocity (m^3/s)
u	piston's velocity (m/s)
V	voltage generated as a result of the movement of the magnet in the coil
V_L	voltage dissipated at the load (V)
V_b	enclosure volume (m^3)
V_{Gen}	voltage generated at the alternator's terminals (V)
X_e	electric reactance (Ω)
X_m	mechanical reactance (N.s/m)
Z_a	acoustic impedance ($Pa.s/m^3$)
Z_m	mechanical impedance (N.s/m)
Z_e	electrical impedance (Ω)
W_a	acoustic power (W)
$W_{applied}$	applied acoustic power in front of piston of the linear alternator(W)
W_e	electric power dissipated at the load (W)
W_{mech}	mechanical-motion loss (W)
W_{Ohmic}	Ohmic loss (W)
W_{seal}	Fluid seal loss (W)
α	helium molar fraction
β and PR	input dynamic pressure ratio
λ	wave length
γ	specific heat ratio
ΔP	pressure difference across the alternator's piston (Pa)
δ	piston's seal gap (m)
η	acoustic-to-electric conversion efficiency (%)
μ	relative permeability
μ	dynamic gas viscosity ($N.s/m^2$)
σ	Prandtl number
ϕ	phase angle between two signals

ω	angular frequency (rad/s)
ζ	Gas dispalcement amplitude
| |	magnitude of a complex number

Subscripts

e	electric
max	maximum
RMS	root-mean-square value

Superscript

*	conjugate of a complex number

Abstract

Recently, immense research work was done on the thermoacoustics power converters for their great potential in generating electricity by different types of heat sources, including solar energy, waste heat as well as conventional fuels. This work studies the performance of the linear alternator which is the part responsible for converting the acoustic power generated by the thermoacoustic engine into electric power. This work encompasses three parts: the first part is an analytical model that consists of algebraic equations that estimate the main acoustic, mechanical and electrical performance indices of the linear alternator and the relationships between them under linear loading case. These equations are experimentally validated under different conditions. These equations are used to analyze the effects of the operation conditions such as operation under mechanical resonance and electrical resonance, the values of linear alternator parameters and the load parameters on the performance of the linear alternator. This part of work introduces the relationship between the effective inductance of the linear alternator and the mechanical stroke. Additionally, this part introduces an optimization for the piston area to achieve the minimum sum of the mechanical motion loss and the Ohmic loss and an optimization for the load resistance to achieve the maximum electric power in the load and to achieve the maximum acoustic-to-electric conversion efficiency.

The second part of this work is an experimental parametric study using an experimental setup that was built for testing the linear alternator over a wide range of the thermoacoustic-power-conversion conditions that cannot be experimentally achieved in the case of testing the linear alternator with thermoacoustic engine. The parametric study covers the performance of the linear alternator under linear loading case and non-linear loading case. The effects of operating frequency, input dynamic pressure ratio, mean gas pressure, gas mixture, electric load value and the value of the power-factor-correcting capacitor on the performance indices are studied under the two types of loads. The results of the parametric study in the linear load case are compared to results of the analytical model and DELTAEC simulations and good agreement was found.

The third part of this work is a sensitivity analysis that utilizes design-of-experiment methodology to estimate how the factors and their combined interactions affect the performance indices of the linear alternator under linear loading.

The results of the study build a comprehensive study about the linear alternator performance under thermoacoustic-power-conversion conditions. The result are useful to properly select a linear alternator for an existing engine, or vice versa and to match the resulting system to an electric load. The results can be used to select the operating conditions that result in large generted power and or large efficiency. The results can be used to control the operating conditions in the correct proportions to achieve a certain required performance index, while observing the effects on other indices.

1. Introduction

Linear alternators are integral parts of thermoacoustic power converters. This chapter consists of three main sections. First section (1.1) discusses the types of the thermoacoustic engines, their operating cycles, their components, their advantages and their limitations. Second section (1.2) discusses the linear alternators' theory of operation, their types, their advantages ,their limitations, their connections in thermoacoustic power converters and the anti-drift network across the piston of the linear alternator. Third section (1.3) introduces the scope of the work of the thesis.

1.1 Thermoacoustic Engines

The main function of the thermoacoustic engine is to utilize the input heat rate (supplied by solar input, waste heat or electricity) to produce a net mechanical work in the form of an acoustic pressure wave, once the imposed temperature gradient across the stack/regenerator exceeds a certain critical value. There are two types of the thermoacoustic engines: standing-wave and travelling-wave engines

1.1.1 Standing wave thermoacoustic engine

In standing wave engines, the pressure and the displacement of the acoustic wave are in phase and there is a 90 degree as a phase difference between the pressure and the acoustic wave velocity. The produced acoustic power is a result of a dot product of the amplitude of the pressure wave and amplitude of the volumetric velocity [1].

The main parts of the standing wave engine are a stack housed between two heat exchangers in a resonator tube [2] .

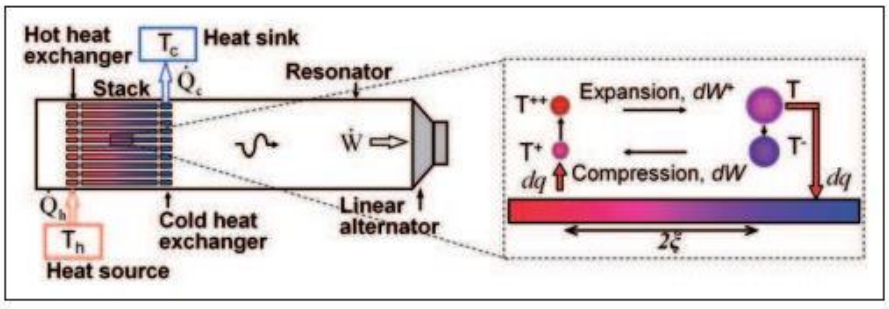

Figure 1-1.Simplified schematic drawing of a standing wave thermoacoustic engine [3].

As a result of the installed heat exchanger and cold exchanger on the two sides of the stack, a gas parcel experiences sweeping changes in temperature due to acoustic pressure stimulated adiabatic compression and expansion and the internal temperature of the stack. The parcel thermally expands in the hot side of the stack and absorbs heat as it is cooler than the surrounding hot stack. The thermal expansion takes place during the increase in the pressure of the parcel when the gas enters the stack. Then, the parcel rejects heat and thermally contracts in the cold side of the stack as it is warmer, the thermal contradiction happens while the pressure is decreasing at the exit of the stack, as shown in Fig. 1-2. There is a significant time delay between the expansion (or contraction) and movement of the gas parcel [2]. This delay is a result of imperfect thermal contact between the gas parcel and the solid material (Stack). Because of this imperfect heat transfer, the thermodynamic cycle of the standing-wave engines is intrinsically irreversible. Thus, standing wave engines have relatively low efficiencies [2].

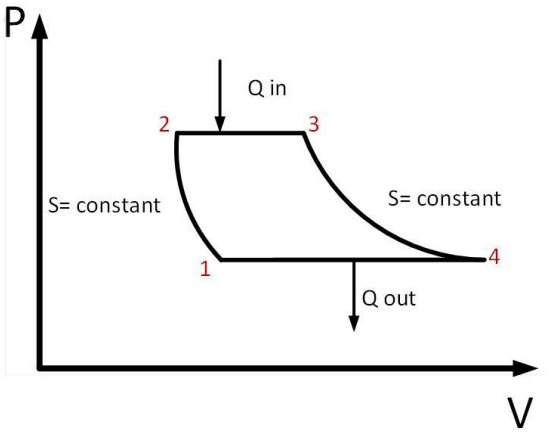

Figure 1-2. Ideal Brayton cycle diagram.

1.1.1.1 Standing wave thermoacoustic engine components

Each component has certain function and certain specifications.

1.1.1.1.1 Heat source

The nature of standing wave engine requires suitable quantity of heat to produce pressure wave with large amplitude to back up the effect of the angle (near 90) between the pressure and the velocity of the acoustic wave. The standing wave engine or thermoacoustics engines in

general can utilize any type of heat sources, such as the solar energy, the waste heat, combustion burners, electric heaters and even the produced heat of nuclear reactors [4].

1.1.1.1.2 Heat exchanger

The main function of the heat exchangers is to keep the temperature gradient across the stack. One of the main characteristics of the heat exchanger is having high overall heat transfer coefficient in addition to low acoustic power dissipation. The active heat exchange occurs between the working gas and a group of narrow spaced plates which are aligned in the direction of the wave propagation. The plate size and the spaces between the plates define the blockage ratio. Smooth flow of the gas can be achieved when the blockage ratios of the heat exchanger and the stack be the similar [4].

1.1.1.1.3 Stack

The stack is the place of generation the acoustic waves in standing wave thermoacoustic engine, so it is the main core of this engine. The sound wave is induced as a result of the temperature difference between the two sides of the stack, once the temperature gradient across the stack exceeds a certain limit [4].

The stack consists of very small channels with parallel arrangement. The hydraulic radius of the channels is comparable to the thermal penetration depth. The main function of the stack is to provide solid heat capacity and large cross section area to retain the thermal contact between gas particles and solid channels. The main characteristics of the stack are to minimize the viscous dissipation of acoustic power and the loss of the temperature gradient by conduction along the stack. The spacing between the stack plates is around two to four thermal penetration depth of gas, to achieve imperfect thermal contact between gas particle and the stack plate [4].

1.1.1.1.4 Working Gas

The working gas should have high speed of sound, low Prandtl number, high thermal conductivity (to increase the thermal penetration depth), non-flammable and commercially available. Inert gases usually satisfy these requirements and thus offer thermoacoustic devices the benefits of being environmentally friendly without global warming or ozone depletion issues [4].

1.1.1.1.5 Resonator

The resonator defines the resonance frequency of the system and houses the stack and the its surrounding heat exchangers [4].

1.1.2 Travelling wave thermoacoustic engine

Travelling wave engine or the Stirling engine, is the second type of thermoacoustic engines. The wave pressure and the wave velocity are in phase in the regenerator with large acoustic impedance at the regenerator. Ceperley was the first one to observe the similarity between the Stirling cycle and the thermodynamic cycle experienced by a gas parcel in acoustic field of a travelling-wave engine [5]. The travelling wave engine consists of a regenerator sandwiched between two heat exchangers. In the regenerator, the heat transfer between the regenerator and the gas parcel is nearly perfect because the hydraulic diameter, r_h, of the pores in the regenerator is much smaller than the thermal penetration depth, δ_k , at the frequencies of interest: $r_h \ll \delta\kappa$. Thus, the thermal expansions and contractions are in phase with the pressure and velocity oscillations.

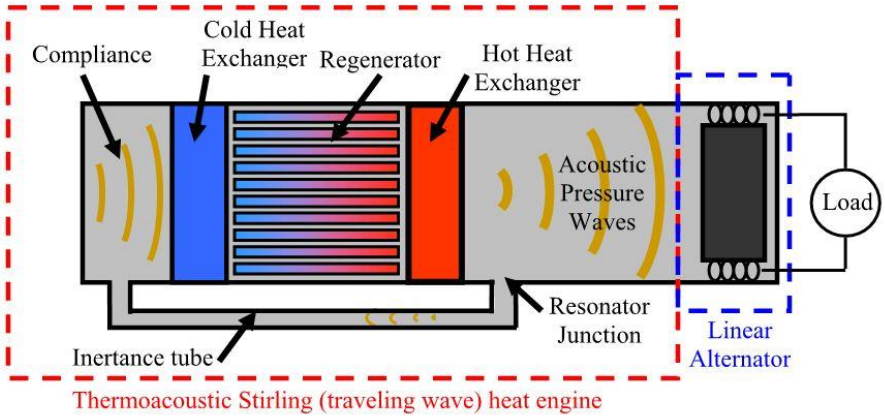

Figure 1-3.Thermoacoustic stirling engine [2].

Unlike the standing wave type of engine which requires a simple "closed-closed" or "closed-opened" resonator ends with length equal to $\lambda/2$ or $\lambda/4$ respectively, in a traveling wave Stirling-thermoacoustic engine acoustic power flows within a torus (doughnut) shaped resonator, as shown in Fig. 1-3. This enables the regenerator, with its steep temperature gradient, to thermoacoustically amplify the acoustic power that is fed into the cold end. This amplification gain is related to the absolute temperature ratio, between the hot and cold ends [2].

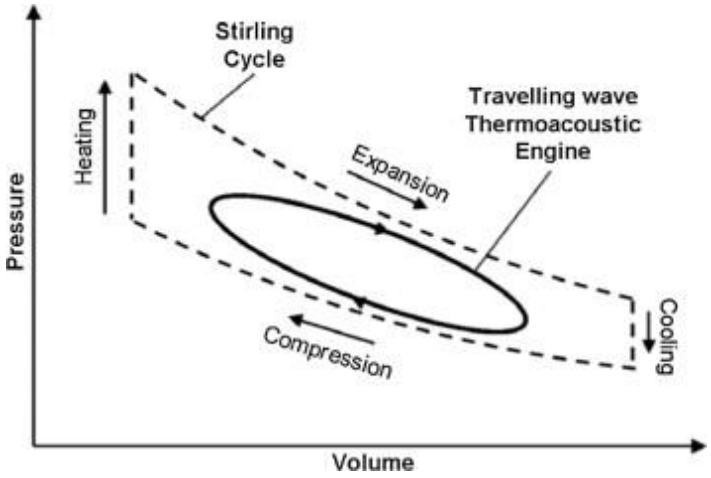

Figure 1-4.Stirling cycle (pressure versus volume) diagram [6].

Figure 1-4 shows that the gas parcel experience four phases within the regenerator, starting from the cold end.

First, at the cold end of the regenerator, the nearly-stationary gas parcel undergoes nearly isothermal compression (as a result of the excellent thermal contact and high heat capacity) as the acoustic wave compresses it [2]. Second, the gas parcel thermally expands as the acoustic wave forces it up the temperature gradient [2]. Third, nearly stationary at the hot end of the regenerator, the acoustic wave allows the gas to isothermally expand while it absorbs heat during the pressure reduction [2]. Fourth, parcel moves towards cold side and returns heat to the regenerator while thermally contracting at low pressure [2].

1.1.1.2 Travelling wave thermoacoustic engine components

The main components are main cold heat exchanger, regenerator, hot heat exchanger, thermal buffer tube, secondary heat exchanger, flow straightener, resonator, compliance and jet pump.

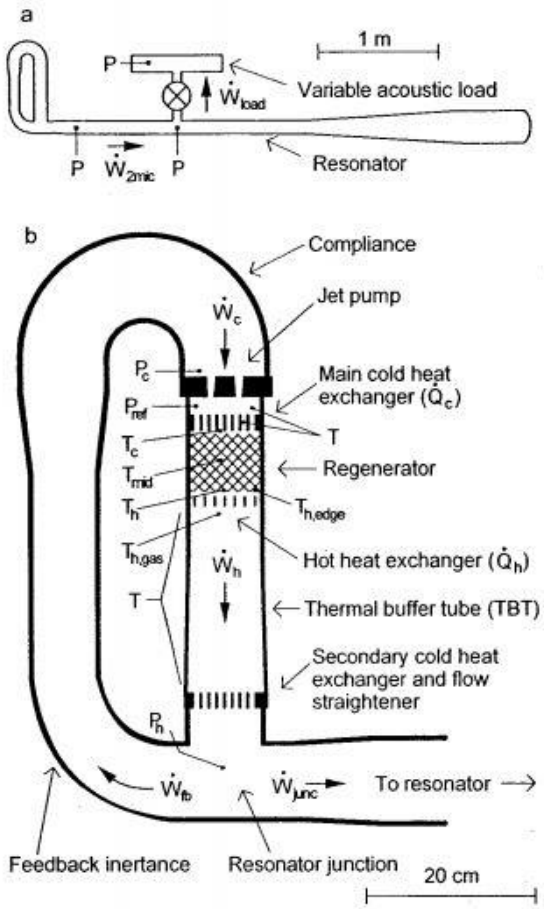

Figure 1-5.Torus travelling wave engine [7].

1.1.1.2.1 Main cold and hot heat exchangers

The main cold heat exchanger is placed near the top of the torus. The hot heat exchanger is placed below the regenerator. The length of the tubes should be roughly equal to the gas displacement (Peak-to-Peak).

1.1.1.2.2 Regenerator

The regenerator exists below the cold heat exchanger. The regenerator consists of randomly stacked screens contained in a metal can. The regenerator in this network plays the role of the

power amplifier to feed acoustic power to the cold side. There is a need for spacers between the regenerator and the heat exchangers so that at the upper end of the regenerator, the spacing permits the flow to spread over the entire regenerator cross section after exiting the narrow passages of the main cold heat exchanger [7].

1.1.1.2.3 Thermal buffer tube (TBT)

The main function of the thermal buffer tube is to provide a thermal buffer between the hot heat exchanger and the linear alternator, which should not be exposed to high temperatures. The inner diameter of TBT is much larger than the gas's thermal penetration depth, and its length is much greater than the peak-to-peak gas displacement at high amplitudes. The surface roughness of the TBT cylinder should be much less than the viscous and thermal penetration depths. There is a flow straightener at the lower end of TBT, which consists of mesh screens with very narrow diameters and its function is to ensure the uniformity of the flow entering the bottom of the TBT to avoid the jet flow, which would cause streaming within the TBT that convicts heat from the hot heat exchanger to the cold side [7].

1.1.1.2.4 Secondary cold heat exchanger

This heat exchanger is placed at the end of the lower end of the TBT. The main function of this heat exchanger is to decrease the temperature of the gas coming from the TBT, to ambient temperature levels to protect the linear alternators [7].

1.1.1.2.5 Feedback inertance tube

The main function of the feedback inertance tube is to feed-back the acoustic power into the ambient side of the regenerator [2].

1.1.1.2.6 Compliance

The compliance is a group of elbows. The length of the compliance determines the gas oscillating frequency. Additionally, the acoustic network between the inertance tube and compliance achieves the required traveling wave phasing in the regenerator [2].

1.1.1.2.7 Jet pump

The jet pump exists between the compliance and the cold heat exchanger. The jet pump works on reducing Gedeon streaming, which can be expressed as the net time-averaged DC mass flux away from the hot heat exchanger and counterclockwise around the loop of the engine. The jet pump is an annular diffuser that reduces the flow's velocity in one direction of the oscillation, which creates a time-averaged static pressure drop. The result of this pressure differential is a

steady DC flow in the opposite direction to the Gedeon streaming which can effectively cancel it out [2].

In the complete system, few notes should be considered: [2]

1. The traveling- wave requires a zero phase angle between the dynamic pressure and the velocity inside the regenerator.
2. During the cycle, the regenerator amplifies the acoustic power. This power is used to either drive the linear alternator or provide "new" acoustic power to the cold end of the regenerator that is in turn amplified. The acoustic network (specifically between the inertance and the compliance) enables the required traveling wave phasing in the regenerator.
3. In the network made of the regenerator (a resistance), inertance and compliance consists of channels that have different compliance, inertance and resistance, the compliance describes the compressibility of a gas within a certain channel's volume while the inertance describes the inertial properties of a gas in a channel. The acoustic resistance is a result of two parts: the oscillating-velocity dependent viscosity as the viscous penetration depth along the channel surface causes resistance; and the oscillating pressure within a channel causes an oscillating temperature, which develops a thermal relaxation resistance. This acoustic network controls the travelling wave phasing. Additionally, the magnitudes of compliance, inertance and resistance determine the amplitude of the acoustic impedance (ratio between pressure and volumetric velocity), which in turns determines the value of the viscous losses.
4. To reduce the viscous losses, the acoustic impedance at the exit of the regenerator should be very high (15 to 30 times rho_mean * C_mean).

1.1.3 Advantages and limitations of thermoacoustic engines

Thermoacoustics engines are considered to be attractive for many reasons.

- They operate at relatively low temperature difference. For instance, De Blok reported that the acoustic oscillations were induced at temperature difference of 65 C in his engine [8]. Thus, the thermoacoustic engines have a great potential in using low-grade waste heat in the industry field.

- They utilize renewable energy resources like the solar energy as a source of heat. Besides that, NASA utilizes nuclear reactors as a source of heat for thermoacoustic power converters to empower deep space missions.
- They have no moving parts except of the linear alternator, which make them attractive for their reliability and for maintenance needs.
- They use inert gases which make them attractive for being environmentally friendly more than the current sustainable energy technologies such as the solar panels which use the Silicon material.

On the other hand, thermoacoustic engines face some challenges:

- The complicated integration with the linear alternators and the electric loads, while keeping both the thermal-to-acoustic and the acoustic-to-electric efficiencies high.
- The limited power density with respect to conventional technologies.
- The generation of many non-linear phenomena that reduce the conversion efficiency at large amplitudes, such as streaming, harmonic generation, and turbulence.

1.2 Linear Alternators

The conventional technology used for acoustic-to-electric power conversion is the use of linear alternators. In this technology, the acoustic power generated by the thermoacoustic engine is applied to the alternator's piston causing the piston and the permanent magnet attached to it to oscillate, thus inducing an oscillating magnetic flux. This induces voltage in the stationary copper coils surrounding the reciprocating magnet and causes an electric current to flow into the load. These linear alternators utilize a carefully designed clearance seal between the piston and the cylinder, which allows operation without sliding seals nor lubrication and eliminate wearing parts, thus they enjoy large reliability and durability. In practice, some units have been in continuous operation for more than eight years without failure [9].

1.2.1 Types of linear alternators

The main three types of linear alternator are: [10]

1. Moving permanent magnet.
2. Moving iron with permanent magnet(s) fixed to the stator.
3. Moving coil with permanent magnet(s) fixed to the stator.

The moving permanent-magnet type is common in the Stirling engines. The moving permanent magnet has two designs or styles. The first style is a hollow cylinder of magnet (radial polarity) oscillating between an internal and external stator. The stator carries the cylindrically wound armature coil(s). The radial polarity magnet produces alternating flux directions in the radial laminations of the stator at the ends of the stroke. This style of linear alternator was used and modified by Sunpower, Inc., as well as the National Aerospace Laboratory of Japan (NAL) and Mechanical Technology Incorporated (MTI) [10].

Fig. (1-6) shows a schematic for this design of the moving permanent magnet linear alternator.

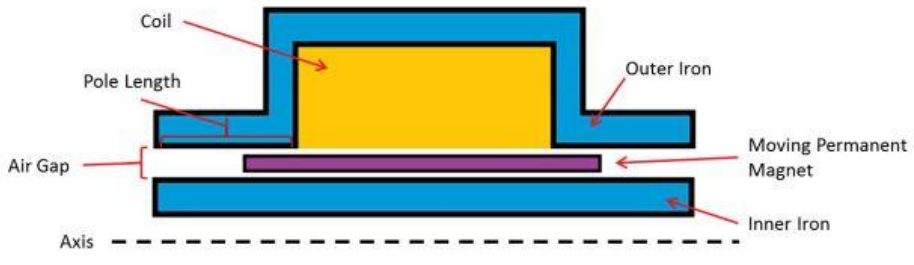

Figure 1-6.Sunpower linear alternator [11].

The second design of the moving permanent magnet, is the STAR alternator. This type of alternator is pioneered by Qdrive (Clever Fellows Innovation Consortium (CFIC), in the past). Fig. (1-7) shows a schematic for this design of moving permanent magnet linear alternator [10].

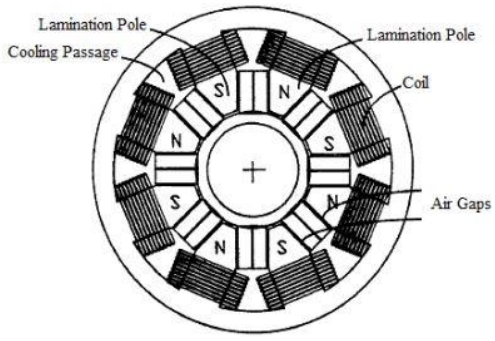

Figure 1-7.STAR linear alternator schematic [12].

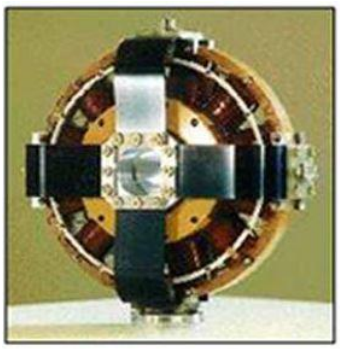

Figure 1-8.STAR linear alternator digital image [13].

In this type of linear alternators, the moving magnet is two layers with opposite polarity which alternately activate the axially stacked laminations, introducing flux reversal [10].

The second type of linear alternators is the moving iron type. There are many styles for this type. Stirling Technology Company (STC, also Infinia) developed the first one. This style has four poles, each one has two axially stacked magnets with opposite polarity and wounded coil around each pole. The moving iron will generate a flux path while its movement between the axially stacked magnets, producing flux reversal. Fig.1-9 shows that STC has also developed another style has a shape similar to the STAR alternator, with the magnets attached to the stator and the mover made of lamination material [10].

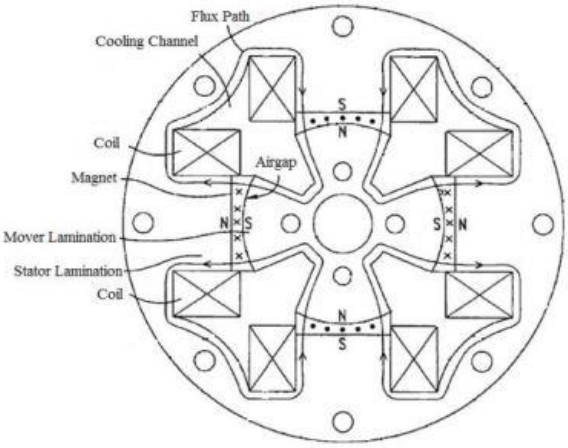

Figure 1-9.Moving iron linear alternator [14].

Another style of linear alternator has two magnets stacked axially for each pole, but the segment can be repeated axially with multiple lamination sections on the mover to increase power without increasing stroke [10].

The third type of linear alternator is the moving coil type. This type has a shape very similar to the speaker. The main advantage is cancellation of radial forces and torques on the moving mass, but this requires a larger permanent magnet in the stator [10].

1.2.2 Advantages and limitations of moving magnet linear alternators

The technology of the moving-magnet linear alternator is the dominant in the Stirling power converters. It has the following advantages

- There is no need for external power in the generation of the magnetic flux, which reduces the heat generation and eases up the cooling of the alternator.
- The flux density can be high and accurately controlled.

- This type of linear alternators has small weight and size, reasonable stroke limits (10mm-20 mm, peak to peak values) and reasonable power handling capacity.
- The windings are bonded directly to the yoke giving rise to high reliability and compact structure.
- They are designed without any wearing parts, no sliding seals and no traditional bearings.
- They operate without any lubrication because of the flexure bearing.
- The easy of setting and changing the operating frequency and the mechanical stroke of the linear alternator.
- They enjoy large acoustic-to-electric conversion efficiency if matched properly.
- The theoretical mean time between failures (per military standard method MIL-STD217F) is 129,760 hours so it enjoys long maintenance- free working periods, some linear alternators have been in a continuous operation for over eight years.

Linear alternators use flexure bearing to allow the piston to move softly in the axial direction while being extremely stiff with respect to radial, twisting, or rocking motion of the piston. They provide the counter-balancing force against the Lorentz force while allowing the axial motion with a radial clearance in the micrometer range. They are in the form of disk with spiral grooves going radially inwards. They form a "bearing" that is relatively soft in the axial. This stiff flexure is rigidly attached to the connecting rod and it keeps the alternator piston from touching its cylinder and the small clearance efficiently forms a non-wearing seal that requires no lubrication or moving seals.

Figure 1-10.Flexure bearing [15].

During operation, the flexure spring is deformed due to the linear motion of the connecting rod, which creates bending and torsional stresses. The working stress should be designed to be is less than the fatigue stress of the material. This fact puts a main limit on the peak-to-peak

piston stroke that can be used without experiencing excessive mechanical stress. In some applications, they are made of S-curve compliance to reduce their moving mass and to permit larger mechanical stroke [16]. In practice, these bearings have proven to be extremely reliable and robust.

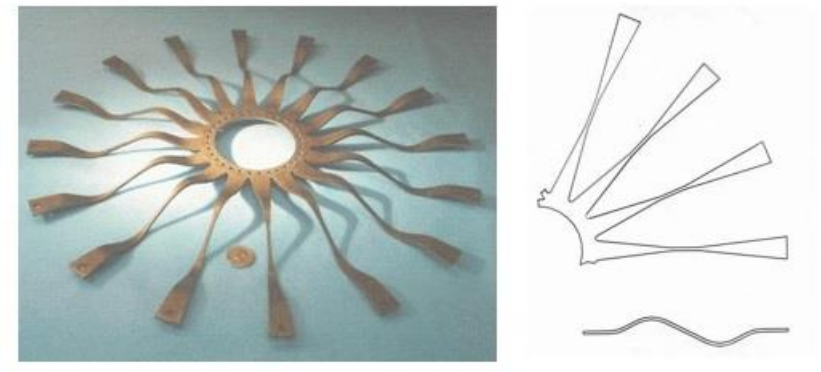

Figure 1-11.S curve flexure bearing [16].

On the otherwise, there are some complications and limitations in the moving magnet linear alternators. To comprehend the origin of these limitations, it is important to understand the physics of the equations which estimate the amount of the acoustic power and the generated electric power.

The acoustic power delivered to the linear alternator can be estimated using the time average of the dot product of the dynamic pressure and the piston velocity:

$$W_{applied} = P_f(t).U(t) \quad (1\text{-}1)$$

In the meantime, it should be realized that the time-averaged acoustic power, supplied by a moving piston of area A is given by:

$$W_{applied} = 0.5 * |P_f| * |U| * cos(\phi) \quad (1\text{-}2)$$

Noting that the volumetric piston velocity, U, is related to the piston stroke, S, via:

$$|U| = A * \omega * |S| \quad (1\text{-}3)$$

Thus

$$W_{applied} = 0.5 * |P_f| * A * \omega * |S| * cos(\phi) \quad (1\text{-}4)$$

Eq. (1-4) shows that the increase in the applied acoustic power requires an increase in the operating frequency, piston area, mechanical stroke or the dynamic pressure in the front of the piston of the linear alternator. **Accordingly, the following limits apply:**

Limitations on increasing the operating frequency:

- Increasing the operating frequency may require the mechanical resonance frequency to increase. The use of gas spring, leaf springs are possible methods to raise the mechanical resonance frequency, but up to a certain limit. Beyond this limit, further increase in mechanical resonance frequency is not practically possible.
- Increasing the operating frequency will complicate the heat transfer at the hot and ambient heat exchangers, since less time is available for the heat to diffuse.

Limitations on increasing the piston diameter:

- The increase in the piston diameter, which means an increase in the moving mass, causes an increase in the size of the linear alternator because the piston diameter should be always less than the linear alternator diameter to ease the mounting of the linear alternator, which decreases the power density.
- The increase of the moving mass results in extreme periodic forces which increase the difficulty in maintaining a stable clearance seals over large stroke amplitudes knowing that it increase the risk of seal friction or flexure fatigue because the suspension will have a harder time supporting the extra weight. An alternative solution to the increase in the moving mass is to have the piston hollowed out, but this means the piston will breathe in the response to the pressure fluctuations and together with the large area this will make the piston very prone to 'drifting' off axial center.
- The increase in the moving mass requires larger seal gap, which results in larger fluid seal loss. Additionally, the fluid seal loss will increase dramatically upon the increase of the seal gap, which reduces the acoustic-to-electric conversion efficiency.

Limitations on increasing the mechanical stroke:

- The mechanical stroke is limited by the stroke of the spring and requires larger seal gaps.
- Severe damage will take place if over-stroke occurs. For this reason, the current work employed a method to prevent over-stroking on a time scale short enough with respect to the inverse of the frequency of operation.

Limitations on increasing the dynamic pressure:

- The dynamic pressure in the front of the piston of the linear alternator is related to the working conditions like the mean gas pressure and the dynamic pressure ratio. The increase of the mean gas pressure is limited by the strength of the material of the resonator, while the increase in the dynamic pressure ratio is limited by avoiding non-linearities to avoid reductions in the conversion efficiency.

Other limitations:

- The generated voltage is equal to the product of the velocity of the moving magnet, the magnetic field strength of the magnet and the length of the winding of the coil. Thus, generating electric power at low frequencies (low magnet velocity) faces few challenges since it necessitates large mechanical stroke or strong magnetic field (higher expensive magnet material or larger moving mass) or both. Both options result in increasing complexity and cost. Consequently, linear alternators need to be operated at high frequencies (50-100 Hz) to get sufficient output electric power per unit mass.
- Unlike rotating generators, the nature of the reciprocating motion involves a point of zero velocity, at which the piston changes its direction, and thus no electric energy is generated at this point.
- There is a need of cooling for the temperature-sensitive components especially at high-generated power.
- Both the large cost of the complex manufacturing of the linear alternators and the few demand on it boost its price.

For the above reasons, some of the current research is focused on enhancing some of the characteristics of linear alternator, such as enhancing the acoustic-to-electric conversion efficiency of the linear alternator with less moving mass, minimizing the internal losses such as magnetic hysteresis, eddy currents, and flux leakage, easing of manufacturing of linear alternators by developing alternatives for high priced rare-earth magnets and complicated lamination geometries, providing suitable cooling for temperature-sensitive components, introducing new types of linear alternators (Non-Permanent Magnet) with high temperature capabilities such as linear induction and linear reluctance alternators [10].

1.2.3 Linear alternators' connections in thermoacoustic power converters

Typical thermoacoustic power converters have more than one linear alternators arranged in such a way to cancel or reduce vibration. A common arrangement is to use two linear alternators opposite to each and forming a balanced pair with minimal vibration. Using more than two alternators will cause more seal losses, but is justifiable if more output power is required.

The two linear alternators used should be synchronized together in such a way that they approach each other along a common line of motion when they both approach the secondary ambient heat exchanger, thus reducing the volume and increasing the dynamic pressure at the same time in the thermodynamic cycle. This can be achieved by proper electrical connection, either by connecting the linear alternators in series (e.g., [17], [18] and [19]) or in parallel (e.g., [2]).

Because the force is roughly proportional to the current, a series connection (one shared current) tends to balance the forces between the two linear alternators). On the other hand, the mechanical stroke is roughly proportional to the voltage, so a parallel connection (one shared voltage) tends to better match the mechanical strokes and the velocities (and thus less vibration).

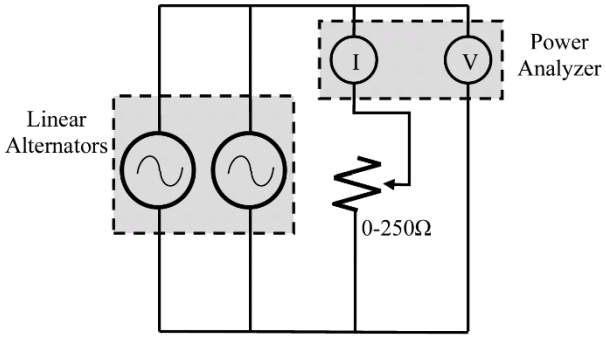

Figure 1-12. Parallel connection of the two linear alternators [2]

The series connection enjoys a safety advantage, since it forms a single circuit and thus a single switch (or any break in any linear alternator winding) produces a total stop, where in the parallel connection, one linear alternator may continue to run if the other linear alternator fails.

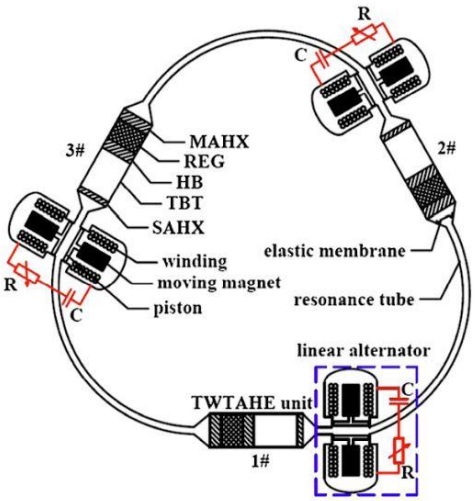

Figure 1-13.Series connection of the two linear alternators [17]

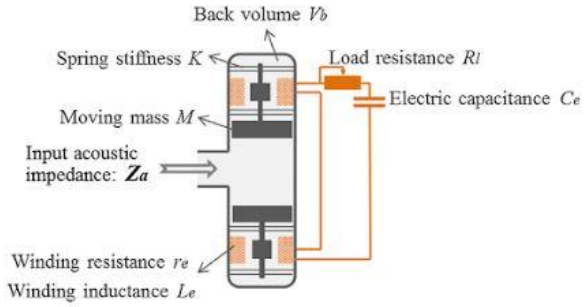

Figure 1-14.Series connection of the two linear alternators [18]

In the start of operation, when both linear alternators are connected as drivers to start the thermodynamic cycle, it should be noted that the series connection requires larger voltages while the parallel connection requires larger currents.

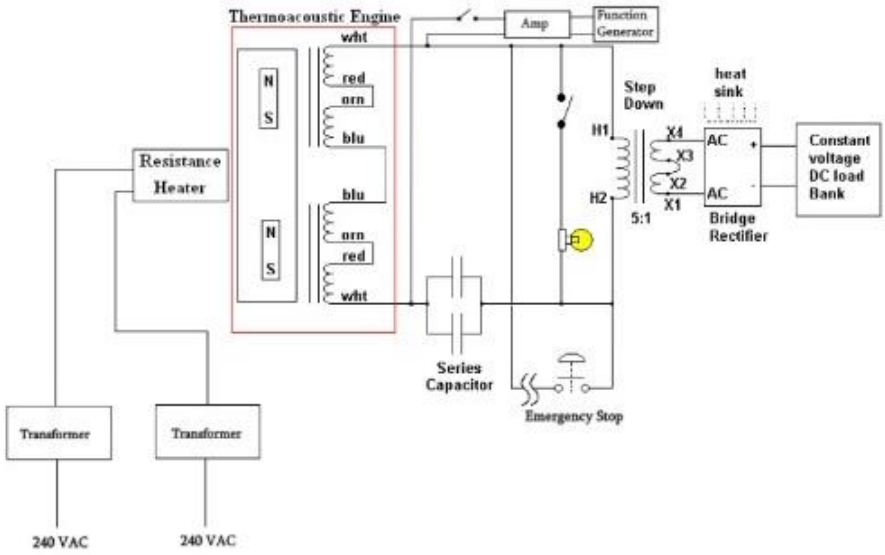

Figure 1-15.Series connection of the two linear alternators [19]

1.2.4 Anti-drift network across the linear alternator's piston

Because the flow of the working gas through the piston seal in the forward half of the cycle is not equal to what flows back in the return half of the cycle, thus over many repeated cycles,

the gas molecules and the gas dynamic pressure build up on one side of the linear alternator piston. In a configuration of two opposing pistons, this result in both pistons moving either toward each other or away from each other. This piston drift can be reduced or eliminated by an anti-drift network [20].

An anti-drift network can be either active or passive. The former uses a check and a control valve (e.g. needle valve) to move the working gas back to the other way; while the latter uses a tube (¼" or ½" in diameter) to connect the front and the back sides and rely on the pressure difference between them to create a DC return flow. The passive type can only reduce the piston drift but cannot eliminate it completely. The active network rectifies the AC oscillation to do the same thing, and can be tuned to cancel out the piston drift completely, at the expense of introducing wearing parts (valves) and at the expense of the fact that the tuning that cancels the drift is correct for only one amplitude [20].

Extreme care should be considered during the experiments to keep these valves opened during the filling/defiling of the setup, to avoid difference in the mean gas pressures during these processes. During startup experiments, these valves have to be closed to isolate the dynamic pressures [20].

1.3 Thesis Scope

The thesis work focuses on building a comprehensive study for the characteristics of the performance of the linear alternator under thermoacoustic-power-conversion conditions.

The first part of the study consists of algebraic model that describe the linear alternator performance indices' relationship with the linear alternator parameters, connected electric load parameters, and the thermoacoustic-power-conversion conditions. This enables linking the acoustic, mechanical and electrical parameters together, simulation of the linear alternator performance under different working conditions to achieve optimum performance and optimization of the linear alternator parameters such as the piston area and the load resistance. The model was validated via an experimental setup built specifically for this purpose [[21] and [22]].

The second part of the thesis work includes an experimental parametric study for the performance of the linear alternator. The ideal matching between the linear alternator and the thermoacoustic engine on one side and the electric load on the other side involves achieving the following eight conditions, simultaneously, namely (1) operating under mechanical and electrical resonances, (2) operating at the rated mechanical stroke, (3) real-time protection against over-stroking, (4) achieving the minimum sum of the mechanical motion and Ohmic losses, (5) operating at minimum fluid seal loss, (6) matching the real and imaginary parts of the impedance of thermoacoustic engine, (7) achieving the maximum thermal-to-acoustic conversion efficiency on the thermoacoustic engine side and (8) the maximum acoustic-to-electric conversion efficiency on the linear alternator side, and (9) generating the rated electric power. Needless to say, these conditions cannot be combined together; thus, the parametric study focuses on determining the best working conditions experimentally. The uniqueness of this parametric study stems from the availability of its results for linear loads and non-linear loads. This completes the image of the performance of the linear alternator under different types of load. The parametric study for the linear load is supported by DELTAEC simulation and by the algebraic model equations.

The third part of the thesis work is a sensitivity analysis of the effects of ± 10% variations in some of the operating factors on the performance of the linear alternators, where the most significant factors and their interactions are identified. This analysis classifies the effect of each working factor on the linear alternator performance indices.

The three parts of the thesis play different roles to produce a cogent and comprehensive analysis for the linear alternator performance under thermoacoustic-power-conversion conditions.

2. Literature Review

This chapter reviews the previous work reported in the literature on the performance of linear alternators as acoustic-to-electric power converters.

In this work, Chapter 4 derives and validates an analytical model for the linear alternator performance. This model is deduced from applying Netwon's second law and Kirchhoff's voltage law on the operation of the linear alternator and it estimates different performance indices of the linear alternator and the relationships between them and optimizes the load resistance and the piston area. These performance indices are: the acoustic impedance, mechanical stroke, generated current, absorbed acoustic power, dissipated electric power in the load, acoustic-to-electric conversion efficiency, power factor of the load, dissipated voltage in the load, mechanical motion loss and Ohmic loss.

In 2005, Liu and Garrett. [23] experimentally determined the mechanical and electrodynamic parameters of a small moving-magnet electrodynamic linear motor. These parameters were used to estimate the electro-mechanical efficiency of the motor. Additionally, they found that the transduction coefficient decreases with the increase of the mechanical stroke.

In 2008, Luo *et al* [24]. designed, analyzed and tested a thermoacoustic-Stirling electrical generator (TASEG). They made a numerical analysis on the linear alternator using the linear thermoacoustic theory. This simulation showed that the operating frequency and the electrical load greatly affect the linear alternator to achieve maximum efficiency and output electrical power as these two factors affect the mechanical and the electrical reactance of the linear alternator.

In 2008, Wu *et al.* [25] implemented theoretical investigations on a linear alternator to study the effects of the driving frequency, load resistance and piston diameter on alternator performance. They found that the efficiency of the linear alternator improves with achieving the electric resonance while it is dependent on the mechanical resonance. Additionally, they found that at mechanical and electrical resonance there is an optimum load resistance that achieves the maximum efficiency and another one that achieves the maximum generated electric power. Moreover, they found that under these conditions the generated electric power increases with the increase of the piston area.

In 2009, Rossi *et al.* [26] simulated four types of technologies (a moving iron generator and three moving-magnet machines) for linear electromagnetic alternators and categorized them in order to find the best solutions for the thermoacoustic based CHCP (combined heat , cooling and power). They simulated three configures using JMAG (Finite Element Software) that allows to build Finite Element analysis of two-dimensional electromagnetic systems. Using this software they calculated the shape of the generated voltage at no-load, the cogging force on the mover as a function of the displacement and the winding inductance. Moreover FEM (Finite Element Software) can be used to analyze the behavior of the e.m.f. with the current delivered to a load. They found that the FEM (Finite Element Method) software can be used to optimize various aspects of the electromagnetic system in terms of reducing the machine size and iron losses, reducing leakage flux and achieving the maximum flux density in order to decrease the size of coils and to diminish the cogging force.

Then in 2011, Yu *et al.* [27] developed a linear algebraic model for the performance of the audio loudspeakers for linear alternator applications. This model estimated the acoustic power acting on the diaphragm of the loudspeaker and the generated electric power based upon knowing the value of pressure difference across the diaphragm, thus they calculated the maximum acoustic-to-electric conversion efficiency and maximum dissipated electric power in the load under certain assumptions as functions of the speaker parameters. Their work investigated the feasibility of using commercially available loudspeakers as low-cost linear alternators for thermoacoustic applications and they found that some of the commercial loud speakers can reach acoustic–electric transduction efficiency of around 60%, when an optimum value of the load resistance is chosen.

Then, in 2012 Saha *et al.* [28] presented a theoretical analysis of the double Halbach array permanent magnet moving coil alternator at different coil configurations with the rectifier circuit is explained and analyzed with the finite elements simulation result. In this work they estimated the applied acoustic power, dissipated electric power in the load, the maximum generated electric power for this type of linear alternators under the assumption of the coil resistance is equal to the load resistance and the maximum acoustic-to-electric conversion efficiency. Their work achieved maximum acoustic-electrical efficiency of 57%.

In 2013, Sun *et al.* [29] utilized electro–mechano-acoustical analogy to analyze the equivalent acoustic circuit of a linear alternator. Thus, they obtained an equation for the acoustic impedance of the linear alternator as a function in the linear alternator parameters. Knowing the expression of the acoustic impedance the equations of the absorbed acoustic power, the dissipated electric power in the load, the acoustic-to-electric conversion efficiency, the mechanical stroke and the mechanical motion loss were estimated. They used the derived equations to show the importance of the acoustic coupling of the linear alternator to the traveling wave engine and the effects of the electrical and mechanical resonance on the performance of the thermoacoustic power converter.

Additionally, in 2014, Wu *et al.* [30] built a numerical model for double-acting thermoacoustic Stirling electric generator. This model is based on the classical thermoacoustic theory that was founded by Rott [31]. and advanced by Xiao ([32], [33] and [34]) and Swift [1]. Using the iteration method in the basic equations of this theory, the pressure amplitude, volume velocity amplitude and temperature distribution can be estimated. They used used Newton's second law and the Kirchhoff's voltage law to estimate the mechanical stroke amplitude, electric current amplitude, acoustic power and the generated electric power, acoustic-to-electric conversion efficiency. Additionally they presented a validation for the algebraic equations of the mechanical stroke, generated electric power and acoustic-to-electric conversion efficiency under different load resistances at an input dynamic pressure ratio of 4.5 %. Moreover, they presented the optimum load resistance that achieves the maximum acoustic-to-electric conversion efficiency under electric resonance condition.

Recently (2016), Wang *et al.* [35] used Newton's second law and the Kirchhoff's voltage law to get an expression for the acoustic impedance, electric-to-acoustic conversion efficiency. An analysis for the relationship between acoustic power and the acoustic-to-electric conversion efficiency was created and a validation was done for the relationship between the acoustic-to-electric conversion efficiency and the load resistance value.

A recent review article by Timmer, *et al.* [36] has evaluated a number of electro-acoustic transduction mechanisms for the extraction of electrical power from thermoacoustic engines including moving magnet linear alternators, but their analyses do not report all of the performance indices that are considered in this thesis.. Additionally, the presented algebraic model accounts for the change in the effective coil inductance of the linear alternator with the

mechanical stroke [37]. Moreover, the model that relates the performance indices is validated experimentally under different conditions, including different operating frequencies, mean gas pressures, gas mixtures, input dynamic pressure ratios (up to 1%), load resistances and power-factor correcting capacitors. Additionally, Chapter 4 introduces an optimization for the piston area to achieve the minimum sum of the mechanical motion loss and the Ohmic loss and an optimization for the load resistance to achieve the maximum electric power in the load. This optimization is not limited to mechanical or electrical resonances.

Chapter 5 presents an experimental parametric study that analyzes the effects of the different operating conditions such as different operating frequencies, mean gas pressures, gas mixtures, input dynamic pressure ratios , load values and power-factor correcting capacitors on the performance indices of the linear alternator such as the acoustic impedance, mechanical stroke, generated current, dissipated voltage in the load, absorbed acoustic power, dissipated electric power in the load, acoustic-to-electric conversion efficiency, mechanical motion loss, Ohmic loss and fluid seal loss under linear loading and non-linear loading. Furthermore, the simulated results are compared to experimental and to the DELTAEC results for the linear load.

The research work done in this area by other researchers can be summarized as:

In 1992, Kankam *et al.* [38] used the state-space technique to determine the effects of parametric variations of the dynamic stability of a free-piston Stirling engine/ linear alternator driving a dynamic load system on its performance.

In 2004, Petach *et al.* [39] introduced back-to-back Zener diodes as a part of the used non-linear load to allow the load's power - voltage slope to be sufficiently steeper than the alternator's power-voltage slope to manually control the mechanical stroke.

Then in 2008, Hoshino *et al.* [40] built a test rig to evaluate the performance of different types of linear alternators. They studied and validated the relationship between the generated electric power and the mechanical stroke and the relationship between the linear alternator's efficiency and the generated electric power for the different types of the linear alternator.

Additionally, in 2010 Metscher *et al.* [11] conducted two models for the performance of the linear alternator under Stirling-power-conversion conditions built using Sage software package that contain electromagnetic library that can be used to model the circuit of the linear alternator and the electric load. The first model relates the piston motion to electric current by means of a motor constant. The second uses an electromagnetic model components to model the

magnetic circuit of the alternator. They tuned both models to achieve results within 7% of the experimental data.

Then in 2011, Yu *et al.* [27] presented a study focused on performance of the loud speaker as a linear alternator in thermoacoustic electricity generators, under different operating frequencies, cone displacements and connected load resistance values. They found that the displacement amplitude does not affect the acoustic– electric transduction efficiency significantly.

In 2013, Sun *et al.* [29] conducted a theoretical analysis using the algebraic equations and found that the electric resonance increases the absorbed acoustic power, generated electric power and the acoustic-to-electric conversion efficiency and they experimentally validated this finding. In addition, they carried out an investigation for the effects of different load resistance values, pressure amplitude, mean gas pressures, mechanical strokes and operating at resonance on the three performance indices: acoustic power, electric dissipated power and acoustic-to-electric conversion efficiency. They found that the generated electric power increases with the increase of the pressure amplitude in front of piston of the linear alternator.

In 2015, Wang *et al.* [41] studied 500 W travelling wave thermoacoustic engine experimentally and numerically. They conducted DELTAEC simulations for the mechanical stroke, pressure amplitude in the front of the linear alternator piston, generated current and generated electric power under different load resistances. They found that the efficiency at low load resistance is relatively small due to the large pressure amplitudes inside the thermoacoustic system, which increases the dissipations. Additionally, they found that the behavior of the generated electric power with the change of the load resistance is a result of the changes of the corresponding acoustic impedance of the linear alternators.

The presented work in Chapter 5 includes the effects of six operating conditions on ten of the performance indices of the linear alternator under linear loading and non-linear loading. The parametric study under non-linear loading which is similar to the grid is a new contribution of this work. Additionally, this work utilizes the algebraic model equations to explain the behavior of the performance indices under the different working conditions.

The third part of this thesis work is presented in Chapter 6 and presents the sensitivity analysis that utilizes design-of-experiment methodology to estimate how the factors and their combined interactions affect the performance indices of the linear alternator under linear loading.

Previous work using this technique includes Kankam et *al.* [42] who conducted a sensitivity analysis by simulating the behavior of free-piston Stirling engine/linear alternator driving a dynamic load using MATLAB software. This analysis aimed at studying the controllability and dynamic stability of the system. This analysis studied the effects of variations in system parameters, engine controller, operating conditions and mechanical loading on the induction motor.

Second, Arafa *et al.* [43] who conducted a sensitivity analysis to study the effects of five factors of standing wave engine on the onset temperature, first law efficiency and the second law efficiency.

The research work carried-out in this thesis is the result and an extension of the accumulated experience acquired in the thermoacoustic research team at the American University in Cairo. Previous work in the team on linear alternators ([21], [22], [44], [37], [45], [46], [47], [48] and [49]), on thermoacoustic engines ([50], [51], [43], [52], [53], [54], [55], [56], [57], [58], [59], [60], [61] and [62]), on thermoacoustic refrigerators ([63] and [64]), and on fluid mechanics of oscillating flows ([65], [66], [67], [68], [69], [70] and [71]).

3. Experimental Setup and DELTAEC Simulations

In order to fully and deeply quantify the performance indices of the linear alternators, the authors built a platform designed specifically to test linear alternators under different operating conditions in a controlled environment with the acoustic power supplied in a controlled and a stable form). This is in opposition to testing the alternator in connection with a thermoacoustic engine, which inherently provides limitation in the ranges of frequency and intensity of the acoustic power as well as other limitations such as potential overheating, streaming, and turbulence as well as non-uniformity in the acoustic power distribution.

Figures. 3-1 and 3-2 show a schematic and digital image of the experimental setup, respectively. The set-up consists of a function generator (Model AFG3021B, supplied by Tektronix) that supplies a sine wave of a controlled frequency and amplitude to a power amplifier (model 2734, supplied by Bruel and Kjaer). The amplified wave then is supplied to an acoustic driver (Model 1S102D, supplied by Chart Industries). The reciprocating linear motion of the acoustic driver's piston supplies an acoustic wave to the linear alternator with the same frequency through an acoustic duct (5-cm long and 50.8-mm inside diameter).

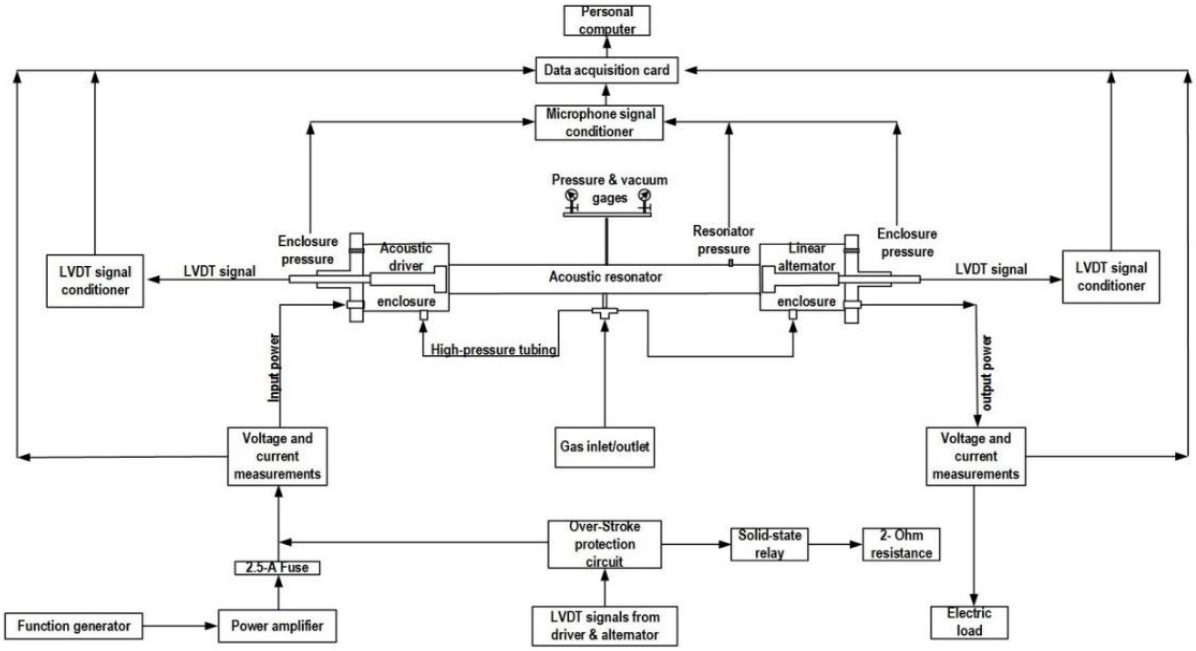

Figure 3-1. Schematic of the experimental setup [46]

The acoustic power applied to the alternator's piston causes the piston and the permanent magnet attached to it to oscillate, thus, induces an oscillating magnetic flux. This induces voltage in the stationary copper coils and causes an electric current to flow into the electric load and causes electric power to be delivered from the linear alternator to the electric load.

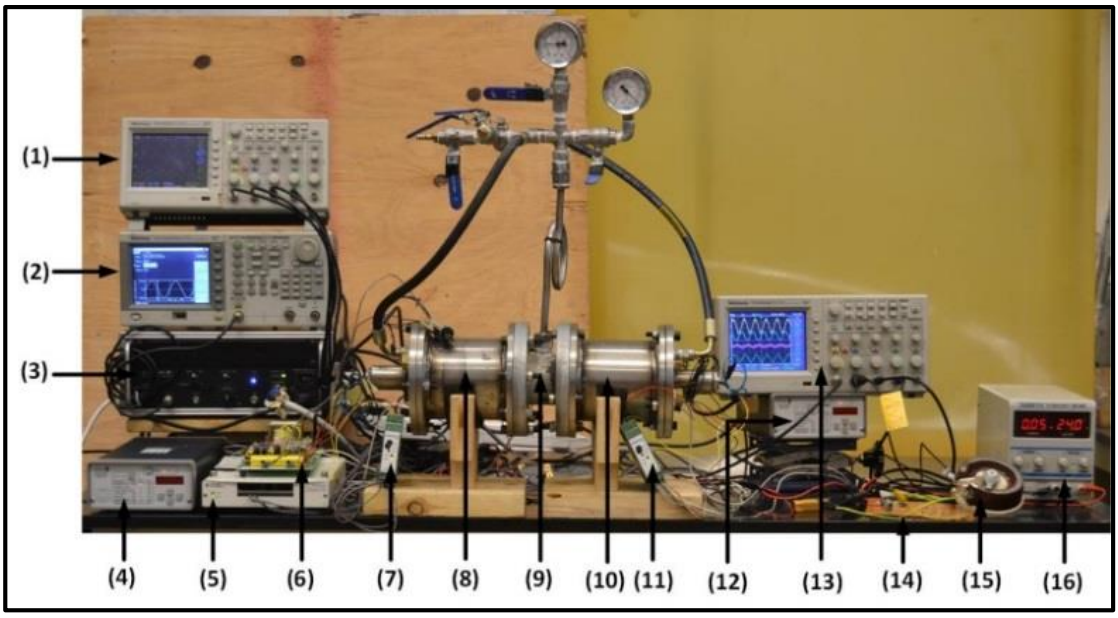

Figure 3-2. Digital image of the setup showing the digital storage oscilloscopes (1 and 13), function generator (2), power amplifier (3), signal conditioner of the pressure microphone (4 and 12), data acquisition card (5), over-stroke protection circuit (6), LVDT (7 and 11), Acoustic driver enclosure(8), Acoustic resonator (9), linear alternator enclosure(10), Power-factor-correcting capacitor and rectifier(14), load resistance (15) and LVDT power supply (16). [46]

The acoustic power applied to the alternator's piston causes the piston and the permanent magnet attached to it to oscillate, thus, induces an oscillating magnetic flux. This induces voltage in the stationary copper coils and causes an electric current to flow into the electric load and causes electric power to be delivered from the linear alternator to the electric load. The technical details of the acoustic driver and linear alternator used in this work are presented in Table 3-1.

In this experimental setup, the measured signals are the mean gas pressure, the dynamic pressures at different locations, the alternator's mechanical stroke, the generated current and voltage at the alternator terminals.

From the measured variables, the key performance indices can be inferred, namely the input acoustic power to the linear alternator, the acoustic impedance at the alternator's piston, the generated electric power, the mechanical-motion loss, the Ohmic loss, the fluid-seal loss and the acoustic-to-electric conversion efficiency.

Table 3-1. Technical specifications of the linear alternator and acoustic driver used in this work.

	Acoustic Driver	Linear Alternator
Model number	1S102-D218	1S102-D219
Stator's resistance, r_e (Ω)	6.70	6.72
Measured coil's inductance at rest, L_o (mH)	64.6	68
Transduction coefficient (BL product) (N/A)	47.7	48.01
Moving mass, M (Kg)	0.4922	0.478
Intrinsic stiffness, K (kN/m)	30.49	30.94
Damping coefficient, R_m (N.S/m)	4.69	4.55
Free-decay frequency, Hz	40.51	40.48
Piston's diameter, mm	50.8	50.8
Nominal mechanical stroke amplitude, mm	5.09	5.0
Moving magnet relative permeability (neodymium magnet-FeNdB or equivalent)	1.05	1.05
Magnet height, mm	31.8	31.8
Coil width (includes stator pole), mm	45.4	45.4
Coil depth (radial length), mm	17.3	17.3
Coil height (includes stator pole), mm	43.4	43.4

The mean gas pressure, or the vacuum pressure encountered prior to introducing the new gas mixture are measured via a Bourdon-tube gage and a vacuum pressure gauge installed at the middle of the acoustic duct. Both gauges are isolated from the acoustic duct via valves in order to protect them from exposure to acoustic oscillations and to prevent acoustic power from flowing out of the system in the direction of the gauges and confusing the data.

The dynamic pressure signals are measured upstream of the alternator's piston (P_f) and in the enclosure volume (P_b) using pressure microphones (model 8530B-500M5, piezo-resistive, range 0-500 PSI absolute, individually calibrated by the supplier, Meggitt). The pressure microphones receive bridge excitation from a programmable-gain signal conditioner unit (Model 136 amplifier, supplied by Meggitt).

The mechanical strokes of the acoustic driver and of the linear alternator pistons are measured using Linear Variable Differential Transformers (LVDT's) (Model XS-C 499,

sensitivity of 1.27 mm/V, supplied by Measurement Specialties), which receive excitation from a signal conditioner (Model LDM1000) powered by a power supply (Model RXN305D, supplied by Zhaoxin).

The generated voltage is reduced in amplitude using a phase-preserving transformer to match the input voltage range of the data acquisition card. The generated current is measured by monitoring the voltage drop on a precise 0.9 Ω high-power resistance.

All the data is digitized simultaneously using a data acquisition card (Model NI 6225, 40 differential-input analog channels, 16-bit resolution, maximum sampling rate of 250,000 Samples/S, quantization resolution of 0.3 mV and supplied by National Instruments).

The analog-to-digital sampling parameters were accurately selected to ensure sampling of an integer large number of cycles with fine time and spectral resolutions without aliasing and without significant amplitude leakage. The sampling rate is 22,400 Samples/s. When operating at 56 Hz, this corresponding to sampling 400 samples/cycle for 500 complete acoustic cycles with a total number of samples of 200,000 samples and a total sampling time of 8.92 seconds, yielding a time resolution of 45 ms and a spectral resolution of 1.36 Hz.

Signal integrity is achieved by isolating the signals via short shielded cables and by using differential sampling.

The generated electric power has to be dissipated into heat using a suitable electric load. Generally, either linear (resistive) or non-linear electric loads can be used for this purpose. In linear loads, the power is absorbed by the load is proportional to the square of the applied voltage. Non-linear loads do not have this proportionally and can be generated by different methods, including using back-to-back zener diodes [45], or by using DC electronic loads that provide operation under constant voltage or constant current modes [46].

An integral part of linear or non-linear electric loads is the power-factor-correcting capacitor, which is connected in series to with the linear alternator generated terminals to balance the inductance of its electric coils and achieve electrical resonance. The work presented in [37] shows that the effective impedance depends on the mechanical stroke. The work presented in [44] shows the performance at off-electric resonance when this power factor correction is ignored or the capacitance used is not optimized.

In this work, linear loads are used and they consists of high-power, low-inductance variable-resistances (Model RLS350E, maximum resistance of 350 Ω, power rating of 150 W

and supplied by Ohmite). This resistance is preceded by a power-factor correcting capacitor of the motor run-type and with sufficient voltage rating. In this work, polypropylene-film capacitors of 450-V rating with different capacitances are used. It is important to note that Ohmite resistance and current-sensing resistance (r_s) form the load resistance (R_L).

The working gas mixture consists of helium and argon gases with different molar fractions. This allows different combinations of speeds of sound and mixture densities and thus, covers a wide range of acoustic impedances as well as power densities. The helium and argon gases are supplied from high-pressure gas cylinders of purity 99.99%. Dalton's law is used to control the volumetric gas mixture composition in the resulting gas mixture. The lighter gas is filled first (helium), followed by the heavier gas (argon) and the acoustic wave is used to mix the two gases.

The presented experimental setup requires special protection against overheating, over-current and most importantly, over-stroke. The first two protections are achieved via a thermocouple measuring the gas temperature in proximity of the coils and a fast-acting fuse. Protection against over-stroke is more complicated since it requires control actions on a time scale is smaller than the inverse of the operating frequency. Consequently, in actual thermoacoustic power converters, just turning off the heat source, or de-focusing the solar concentrator, would not provide time-efficient protection. To resolve this issue, this work presents and implements a protection methodology that is electric in nature, as opposed to mechanical. The control logic used is described in Fig. 3-3. The stroke of each of the acoustic driver and the linear alternator is measured using a Linear Variable Differential Transducer (LVDT). Each LVDT signal is fed into a precision rectifier that produces its absolute value, to provide protection in either positive or negative directions. The generated signal then is fed into an analog comparator (LM324 Op-amp) in which it is compared against a pre-set voltage that corresponds to the maximum safe stroke limit allowed. When the measured stroke signal exceeds the set value, the comparator initiates two control signals: the first signal activates a normally-closed solid-state relay to open and thus, to disconnect the power from the acoustic driver, while the second signal activates a normally-open solid-state relay to close and thus, to connect a small electric resistance in parallel to the linear alternator.

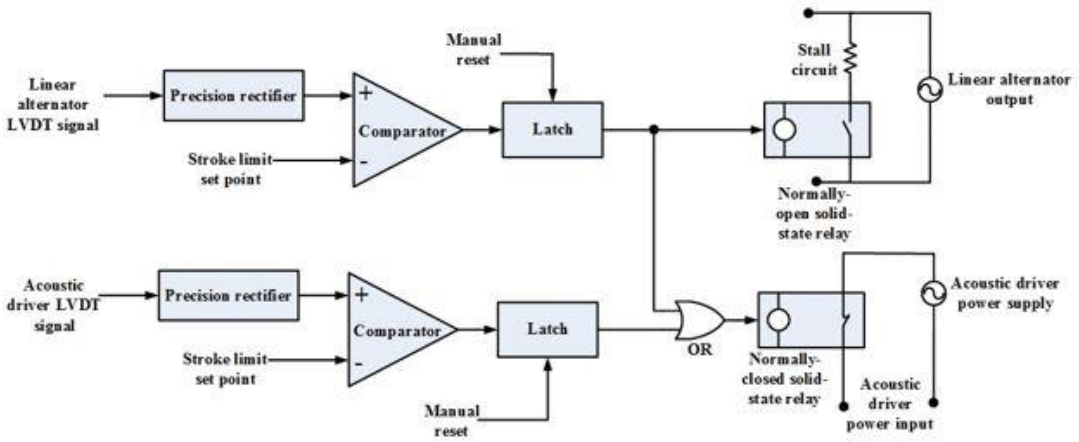

Figure 3-3. Control logic used to protect linear alternator against over-stroking [22]

The introduction of this low resistance in parallel to the alternator and any electric loads connected to it reduces the overall resistance seen by the alternator. This new electric load instantly withdraws a large current and thus, causes the alternator's generated voltage to drop. This resistance must have a low resistance and large power rating (2.2 Ω and 100 W in this work).

Because the stroke generally is proportional to the generated voltage in linear loads [48], the reduction in generated voltage corresponds to a reduction in the mechanical stroke on a time scale much smaller than the inverse of the frequency of operation and thus, provides a protection fast enough against potential combinations in operating conditions that may lead to over-stroke.

Once any of these two control actions is initiated, it remains in effect until a manual reset is made by a human action, to avoid further operation until the cause of over-stroking is identified and resolved.

In preparation for operation, the working gas mixture is introduced through three different ports *simultaneously* at a low filling rate. The three ports are located at the acoustic driver enclosure, the acoustic duct, and the linear alternator enclosure. This eliminates large internal pressure differentials inside the system during the pressurization process. A similar process occurs during the de-pressurization process.

Removal of existing air or other gas mixtures inside the system is achieved by purging three times using a vacuum pump. All parts of the systems are selected to withstand the vacuum pressure encountered during this process.

Then, the system is operated for approximately five minutes until steady-state operation is achieved before measurements are taken.

A Labview code (Appendix B) is used to provide visualization of all signals and real-time estimation of all the performance indices. This Labview code estimates the amplitude values of the mechanical stroke (S), the piston's velocity (u) can be estimated by time-differentiation of the mechanical stroke, generated current (I), generated voltage at the alternator's terminals (V_{Gen}), dynamic pressure in the front of the piston of the linear alternator, dynamic pressure at front of the linear alternator piston (P_f), dynamic pressure at the back of the linear alternator piston (P_b), the dynamic pressure difference across the piston of the linear alternator (ΔP) that is the difference between the signals of the P_f and the P_b. Additionally the Labview code estimates the angle between the generated voltage and the generated current, angle between the pressure signals and the piston velocity, absorbed acoustic power, dissipated electric power in the load (W_e), applied acoustic power($W_{applied}$), absorbed acoustic power(W_a), acoustic-to-electric conversion efficiency (η), mechanical motion loss(W_{mech}), Ohmic loss(W_{Ohmic}) and the RMS maximum value of the signal of the ΔP that is used to estimate the fluid seal loss (W_{seal}). The estimation of the performance indices is presented in in Sec.4.1.1. It is worth noting that the angle between the dynamic pressure difference across the piston of the linear alternator and the piston velocity can be estimated from Eq.(4-16).

The described experimental setup allows the operator to adjust the operating conditions (gas mixture composition, mean gas pressure, applied acoustic power, input dynamic pressure ratio, operating frequency and electric load settings).

The large range of the controlled variables allows for testing at the linear alternator's mechanical and/or electrical resonance, or under balanced or unbalanced mechanical/electrical losses, as well as under different angles between the dynamic pressure P_f and the particle velocity in order to test the effects of different imaginary parts of the gas acoustic impedance.

In this work, the experimental conditions are selected to simulate the conditions typically encountered in thermoacoustic power converters.

A working gas mixture of 60% helium and 40% argon is used because this gas mixture enjoys the least Prandtl number, and consequently the least viscous dissipation losses, amongst all argon/helium gas mixtures [72]. The mean gas pressure is selected as 30 bar, which is close to the lower range of mean gas pressures used in thermoacoustic power converters([73], [30]

and [19]). The operating frequency is selected to match the mechanical resonance frequency of the linear alternator at the mean gas pressure used, measured *in situ to* account for the gas spring effects in the linear alternator enclosure, and corresponds to 56 Hz (at 30 bar) in this work. In this work, the linear load consists of a resistance (nominal value of 122 Ω, rated power of 350 W, supplied by Ohmite) preceded by a power-factor correcting capacitor that corrects for the alternator inductance (polypropylene film capacitor, run type, maximum operating voltage of 450 V, a capacitance of 71-μF). The purpose and effects of the power-factor-correcting capacitors on the overall performance of the linear alternator has been discussed in detail [44].

In this work, the non-linear load consists of a power-factor correcting capacitor (65 μF) preceded by a bridge rectifier which is connected to a constant-voltage DC electronic load (model 8540, rated at 150 W, BK precision). This particular type of load is similar *in nature* to the electric grid, which is a very variable resistor that takes a near-zero resistance if the generated voltage is lower than that required by the grid, and a near-infinite resistance if the generated voltage is higher than that required by the grid. Performance of the linear alternators under other types of non-linear loads have been studied in [45].All the datasheets of the experimental setup devices are available in Appendix A.

3.1 DELTAEC Simulations

DELTAEC (Design Environment for Low-Amplitude Thermoacoustic Energy Conversion) is a computer program that solves one-dimensional wave equation in gases to determine the spatial dependence of the acoustic pressure and velocity in thermoacoustic devices.

DELTAEC contains different types of segments (purely acoustic, lumped impedances, electro-acoustic transducers, thermoacoustic stacks and thermoacoustic heat exchangers).It is important noting that DELTAEC does not directly model electric loads such as the load resistance and the load capacitance. It is worthy to note that other software such as Sage [11] which is a 1-D Stirling device modeling software package developed by Gedeon Associates, contains electromagnetic library that can be used in simulating the linear alternator circuit and the load circuit. This section introduces a method for simulating the load resistance and the power-factor-correcting capacitor in DELTAEC software which is a free and available software.

The experimental setup was modelled in the DELTAEC by 28 segments as shown in Appendix C. The values of the applied acoustic power on the piston of the linear alternator, the load resistance and the power-factor-correcting capacitor are RPN targets in the DELTAEC code. When the code achieves these targets it simulates the performance of the linear alternator in the experimental setup as the linear alternator (IESPEAKER in the code) is exposed the value of the experimental acoustic power and it is forced to modify the ratio between the generated voltage and generated current and the phase angle between them to achieve the mentioned targets. These targets, operating frequency, mean gas pressure, gas mixture are changed in the code upon the conditions of the experimental data.

The load resistance is modelled as the magnitude of the real part of the load impedance that is seen by the linear alternator (IESPEAKER in the code)- RPN 18 in the DELTAEC code.

$$R_L = \frac{|V_{Gen}|}{|I|} * \cos(\varphi) \tag{3-4}$$

And the power-factor-correcting capacitor is modelled from the equation of the power factor (Eq.(4-26)) as-RPN 21 in the DELTAEC code:

$$C = \frac{-1}{\omega R_L \tan(\varphi)} \tag{3-5}$$

4. Results: Analytical Model

The purpose of this chapter is to derive an analytical model that relates the mechanical and electrical variables across the acoustic and electrical sides of the linear alternator. Such a model will lead to estimate the key performance indices of the linear alternator and thus, to optimize them for different purposes (e.g., maximizing the generated power or the acoustic-to-electric conversion efficiency). The estimation of the performance indices of the linear alternator using this model depends on knowing the stroke or the dynamic pressure difference across the piston and the operation factors (frequency, mixture composition, mean gas pressure, the input dynamic pressure ratio, load resistance and power-factor correcting capacitance) and the linear alternator parameters. This chapter is divided into three sections. The first section presents a derivation for the analytical model equations. The second one introduces a validation for the equations of this model using experimental data. The third one presents an optimization for the load parameters and the linear alternator parameters.

4.1 Analytical Model Derivation

The model assumes laminar regime in the velocity and dynamic pressures and thus neglects the dissipation of kinetic energy into heat via turbulent fluctuations. The model also neglects harmonic generation and thus assumes that all the acoustic power is carried-out in the fundamental mode only. The model simulates the two main losses (mechanical-motion loss and Ohmic loss) while it ignores the minor losses (e.g., pressure drops and secondary flows associated with variations of the flow cross sectional area or fluid seal loss) for the sake of simplicity. The model ignores variations in the linear alternator parameters either with time or with the operating conditions, except for the variation of the effective inductance with the mechanical stroke, which was found to strongly affect the electric resonance and is discussed in Sec 4.1.2 below. The model considers electric loads made of resistive and capacitive components and does not consider non-linear loads (e.g., the electric grid).

The measurements carried-out of the different variables (mechanical stroke, dynamic pressures, current and voltage) at the low pressure ratios used support these assumptions up to

the maximum pressure ratio allowed by the experimental setup, which is 1% at a mean gas pressure of 30 bar.

The equations are presented in terms of the alternator's impedance, which should match the engine's impedance simulated on DELTAEC, and in terms of the rated stroke, which is one of the alternator's parameters.

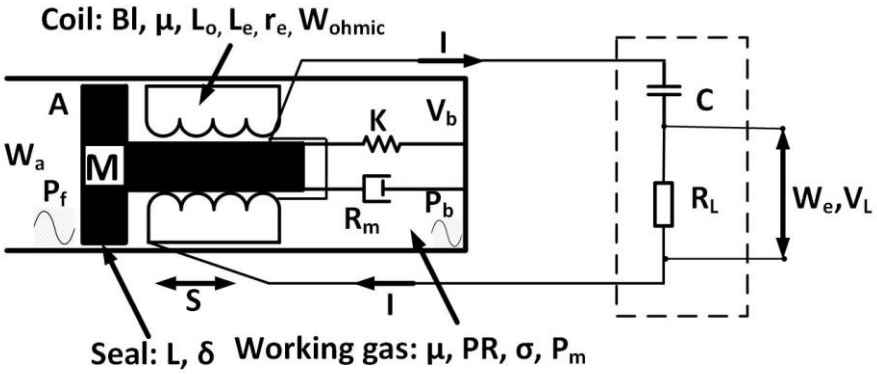

Figure 4-1. A schematic for the linear alternator main parts

First, the acoustic, mechanical and electrical impedances are defined as:

$$Z_a = \frac{\Delta P}{U}, \tag{4-1}$$

$$Z_m = R_m + jX_m, \tag{4-2}$$

$$Z_e = R_e + jX_e, \tag{4-3}$$

where the mechanical reactance is expressed as:

$$X_m = \omega M - \frac{K}{\omega}, \tag{4-4}$$

and the real part of the electrical impedance is expressed as:

$$R_e = r_e + R_L \tag{4-5}$$

and the electrical reactance is expressed as:

$$X_e = \omega L_e - \frac{1}{\omega C} \tag{4-6}$$

The estimation of the effective inductance is illustrated in detail in Sec (4.1.2)

Now, the mechanical stroke signal motion of the alternator piston can be expressed as:

$$S = |S|e^{j\omega t}, \tag{4-7}$$

where the angular frequency ω is defined as:

$$\omega = 2\pi f. \tag{4-8}$$

The piston's velocity and acceleration can be estimated from the sinusoidal mechanical stroke signal as:

$$u = \frac{ds}{dt} = j\omega S, \tag{4-9}$$

and

$$a = \frac{d^2s}{dt^2} = j\omega u \tag{4-10}$$

Now, applying Netwon's second law on the alternator piston (Fig. 4-1) yields:

$$A\Delta P = (Bl)\, I + R_m \frac{dS}{dt} + K\, S + M\, \frac{d^2S}{dt^2}, \tag{4-11}$$

A current (*I*) flowing through a conductor, placed in a magnetic field, produces a force *BL*I* (Lorentz force) on the conductor.

The velocity (*u*) of a conductor in a magnetic field induces a voltage (*V*) across the conductor, this voltage can be expressed as:

$$V = (Bl)\left(\frac{U}{A}\right) = I * \left(R_L + r_e + j\omega L_e - \frac{j}{\omega C}\right) \tag{4-12}$$

Substituting equations (4-7), (4-9) and (4-10) into equation (4-11) yields:

$$A\Delta P = ((Bl) * I) + \left(R_m \frac{U}{A}\right) - j\left(\frac{KU}{\omega A}\right) + j\left(\omega M \frac{U}{A}\right) \tag{4-13}$$

If the damping is insignificant, at mechanical resonance, the force applied to the piston is not consumed to accelerate the moving mass nor to deflect the linear alternator stiffness. Under this condition, the applied force is used only to generate electric current, as shown in Eq. (4-13). Thus, the mechanical resonance frequency is almost the point of the maximum generated current.

It is important to notice that the alternator intrinsic stiffness (*K*) represents the total mechanical stiffness of the linear alternator without taking the gas stiffness in the consideration because these equations utilize the dynamic pressure difference across the piston of the linear alternator (*ΔP*). The pressure difference across the piston of the linear alternator is a function of two parameters. The first one is the dynamic pressure in front of the piston of the linear alternator (P_f), the value of which depends on the applied/absorbed acoustic power, so setting this pressure is a controllable process. The second parameter is the dynamic

pressure in the back volume of the linear alternator, which is a reaction of the linear alternator's response to the applied acoustic force. This response depends on the parameters of the linear alternator, the operating frequency, the mechanical stroke and the generated current, as shown in Eq. (4-11). Setting the value of the pressure difference is an impossible process because the dynamic pressure in the back volume changes with the change in the dynamic pressure in the front of the piston of the linear alternator.

In the high-power thermoacoustic-power-converters, the mean gas pressure and the input dynamic pressure ratio determine the value of the pressure difference across the linear alternator's piston, as the dynamic pressure in the front of the linear alternator's piston is much higher than the dynamic pressure in the back volume. Conversely, in the case of small power thermoacoustic converters (which is the case in our experimental setup), the value of the dynamic pressure in the front of the linear alternator's piston is minor compared to the value of the pressure difference in the most of the operating conditions and it does not reflect the value of the absorbed acoustic power for instance ΔP changes from 10 to 32 kPa over the change in the operating frequency on the other hand the P_f=constant=14.4 kPa as shown in Fig.5-1,additionally, ΔP changes from 5.6 to 62.4 kPa over the change in the input dynamic pressure ratio from 0.1% to 1% on the other hand the P_f changes from 2.9 to 29.7 kPa as shown in Fig-5-2. Thus, in this section's work, the mechanical stroke is used to understand the behavior of the linear alternator's performance indices under different working conditions.

Eqs. (4-12) and (4-13) couple the mechanical and electrical variables. Solving them simultaneously yields expressions for the current and the volumetric velocity in complex form, as:

$$I = \frac{A(Bl)\left(((Bl)^2 - X_m X_e + R_e Rm) - j\left(X_m R_e + R_m X_e\right)\right)}{\left((Bl)^2 - X_m X_e + R_m R_e\right)^2 + \left(X_m R_e + X_e R_m\right)^2}\Delta P \tag{4-14}$$

Now, the acoustic impedance can be deduced as:

$$U = \frac{A^2\left(((Bl)^2 R_e + R_e^2 R_m + R_m X_e^2) + j((Bl)^2 X_e - X_m R_e^2 - X_m X_e^2)\right)}{\left((Bl)^2 - X_m X_e + R_m R_e\right)^2 + \left(X_m R_e + X_e R_m\right)^2}\Delta P \tag{4-15}$$

Thus,

$$Z_a = \left(\frac{1}{A^2}\right)\left[\left(R_m + \frac{R_e(Bl)^2}{R_e^2 + X_e^2}\right) + j\left(X_m - \frac{X_e(Bl)^2}{R_e^2 + X_e^2}\right)\right]. \quad (4\text{-}16)$$

Which yields an expression for the complex acoustic impedance in terms of the alternator parameters and the electric load imposed on the alternator. This alternator's impedance should match the acoustic impedance at the thermoacoustic power converter at the piston's location, which is one of the challenges met during matching a linear alternator to a thermoacoustic engine. Operating at mechanical resonance and electric resonance cancels the imaginary part of the acoustic impedance thus it causes a decrease in the acoustic impedance magnitude. These two conditions can be achieved by working at the mechanical resonance frequency and by using a power factor correcting capacitor, respectively. However, the results indicate that the overall performance is certainly not guaranteed to coincide with mechanical/electrical resonances. The overall performance will be optimal around a certain operating frequency, but this frequency may not be the mechanical resonance frequency necessarily.

4.1.1 Estimation of linear alternator performance indices

Now, as the linear alternator is located at the interface between the thermoacoustic engine and the electric load, it is useful to utilize the developed analytical model to derive useful relationships between the different variables across the input and generated sides of the linear alternator.

The amplitude of volumetric flow rate can be derived directly from Eq. (4-15):

$$|U| = \frac{A^2\sqrt{(R_{e+}^2 X_e^2)}}{\sqrt{((Bl)^2 - X_m X_e + R_m R_e)^2 + (X_m R_e + X_e R_m)^2}}|\Delta P| \quad (4\text{-}17)$$

The acoustic impedance amplitude can be derived from Eq. (4-16):

$$|Z_a| = \frac{\sqrt{((Bl)^2 - X_m X_e + R_m R_e)^2 + (X_m R_e + X_e R_m)^2}}{A^2\sqrt{(R_{e+}^2 X_e^2)}} \quad (4\text{-}18)$$

The load resistance not only strongly affects the impedance value (and thus, the thermal-to-acoustic conversion efficiency in the thermoacoustic engine) but also affects the acoustic-to-electric conversion efficiency and the generated electric power as shown in Eq. (4-22) and Eq. (4-23), respectively, and thus, an optimization should be carried-out for the proper balance between these three key performance indices.

The amplitude of the mechanical stroke can be derived from Eq. (4-9) and (4-17) as:

$$|S| = \frac{A\sqrt{(R_{e+}^2 X_e^2)}}{\omega\sqrt{(\,(Bl)^2 - X_m X_e + R_m R_e)^2 + (\,X_m R_e + X_e R_m\,)^2}}\,|\Delta P| \tag{4-19}$$

A simpler form of Eq. (4-19) can be obtained for the special case of working at mechanical resonance (X_m = 0) and ignoring the value of damping coefficient (Rm) with respect to transduction coefficient (Bl). In this case, the relationship between the mechanical stroke (|S|) and the pressure difference across the piston of the linear alternator (|ΔP|), can be described as:

$$|S| = \frac{A\sqrt{(R_{e+}^2 X_e^2)}}{\omega(Bl)}\,|\Delta P| \tag{4-20}$$

Revealing that the mechanical stroke decreases as the electrical reactance, Xe, decreases, giving more stroke allowance to generate electric power.

The amplitude of the generated current can be estimated from Eqs. (4-14) and (4-19):

$$|I| = \frac{A\,(Bl)}{\sqrt{(\,(Bl)^2 - X_m X_e + R_m R_e)^2 + (\,X_m R_e + X_e R_m\,)^2}}\,|\Delta P| = \frac{\omega(Bl)}{\sqrt{(R_{e+}^2 X_e^2)}}\,|S| \tag{4-21}$$

and the absorbed acoustic power by the linear alternator can be related to the amplitudes of the stroke and the acoustic impedances from Eqs. (4-1), (4-9), (4-16), (4-18) and (4-19) as:

$$\begin{aligned} W_a &= \frac{1}{2}\mathrm{RE}[\Delta P.\,U^*] = \frac{1}{2}|\Delta P|^2\,\frac{\mathrm{RE}[Z_a]}{|Z_a|^2} \\ &= \frac{1}{2}\frac{A^2((Bl)^2\,R_e + R_m\,R_e^2 + X_e^2 R_m)}{(\,(Bl)^2 - X_m X_e + R_m R_e)^2 + (\,X_m R_e + X_e R_m\,)^2}\,|\Delta P|^2 \\ &= \frac{1}{2}\frac{\omega^2((Bl)^2\,R_e + R_m\,R_e^2 + X_e^2 R_m)}{(R_e^2 + X_e^2)}\,|S|^2 \end{aligned} \tag{4-22}$$

The electric power dissipated at the load can be estimated from Eq. (4-21) as:

$$\begin{aligned} W_e &= |I| * |V_L| * PF = \frac{1}{2}R_L|I|^2 \\ &= \frac{1}{2}\frac{A^2(Bl)^2}{(\,(Bl)^2 - X_m X_e + R_m R_e)^2 + (\,X_m R_e + X_e R_m\,)^2}\,R_L|\Delta P|^2 \\ &= \frac{1}{2}\frac{\omega^2(Bl)^2 R_L}{(R_e^2 + X_e^2)}\,|S|^2, \end{aligned} \tag{4-23}$$

which identifies the main factors that affect the generated electric power and their orders and thus, allows for maximization of this key performance indicator.

The acoustic-to-electric conversion efficiency (η) can be estimated from Eqs. (4-22) and

(4-23) as:

$$\eta = \frac{W_e}{W_a} = \frac{R_L}{(R_e) + \frac{R_m}{(Bl)^2}((R_e)^2 + X_e^2)} \tag{4-24}$$

This equation gives many insights on the acoustic-to-electric power conversion. First, it shows that the maximum efficiency occurs when the electrical reactance, X_e, is adjusted to zero. Second, it shows a complicated dependence on the load resistance, R_L, suggesting an optimal load resistance that maximizes the acoustic-to-electric conversion efficiency. However, this load resistance must still be selected to generate an acoustic impedance that is reasonable to the thermoacoustic engine, as shown in Eq. (4-18). Third, the equation shows that the efficiency improves as R_m decreases, r_e decreases and Bl increases.

The relationship between acoustic power and the generated current can be estimated from Eqs. (4-21) and (4-22):

$$|I| = \frac{2(Bl)\sqrt{(R_{e+}^2 X_e^2)}}{\omega((Bl)^2 R_e + R_m R_e^2 + X_e^2 R_m)|S|} W_a \tag{4-25}$$

The power factor of the electric power can be estimated as:

$$PF = \cos(\tan^{-1}\left(\frac{-1}{\omega C R_L}\right)) = \frac{1}{\sqrt{1 + \frac{1}{(\omega C R_L)^2}}} \tag{4-26}$$

The dissipated voltage in the load, can be estimated from Eqs. (4-21), (4-23) and (4-26):

$$\begin{aligned} |V_L| &= |V_{Gen}| * \frac{R_L}{R_e} = \frac{W_e}{|I| * PF} \\ &= \frac{A * (Bl) * R_L * \sqrt{1 + \frac{1}{(\omega C R_L)^2}}}{\sqrt{((Bl)^2 - X_m X_e + R_m R_e)^2 + (X_m R_e + X_e R_m)^2}} |\Delta P| \\ &= \frac{\omega (Bl) R_L \sqrt{1 + \frac{1}{(\omega C R_L)^2}}}{\sqrt{(R_{e+}^2 X_e^2)}} |S| \end{aligned} \tag{4-27}$$

The relationship between acoustic power and dissipated voltage in the load can be estimated from Eq. (4-21) and (4-26):

$$|V_L| = \frac{2(Bl)R_l\sqrt{(R_{e+}^2 X_e^2)}\sqrt{1 + \frac{1}{(\omega C R_l)^2}}}{\omega|S|((Bl)^2 R_e + R_m R_e^2 + X_e^2 R_m)} W_a \tag{4-28}$$

The fluid-seal loss through the clearance gap was shown by [74] as:

$$W_{seal} = \frac{\pi d \delta |\Delta P|^2_{RMS(Max)}}{12 \mu l}, \tag{4-29}$$

where $|\Delta P|_{RMS}$, max is the maximum root mean square difference between the pressure difference across the linear alternator's piston. Typical values of the ratio between the fluid seal loss to the sum of the mechanical-motion and Ohmic losses are in the range of 3-4% during the operating conditions of this work.

The two main losses affecting the performance of the linear alternator can be incorporated into the model through the mechanical energy loss represented by R_m and the electrical losses represented by r_e that are associated by Joule heating in the copper wire. In addition to the viscous dissipation, the value of R_m also includes eddy current losses and magnetic hysteresis losses related to the changes in the magnetic flux through the motor's materials due to the motion of the piston. The mechanical motion loss can be estimated from Eq. (4-9), as:

$$\begin{aligned} W_{mech} &= \frac{1}{2} R_m \left|\frac{U}{A}\right|^2 = \frac{1}{2} \frac{A^2 (R_e^2 + X_e^2)}{((Bl)^2 - X_m X_e + R_m R_e)^2 + (X_m R_e + X_e R_m)^2} R_m |\Delta P|^2 \\ &= \frac{1}{2} \omega^2 R_m |S|^2, \end{aligned} \tag{4-30}$$

and the Ohmic loss can be estimated from Eq. (4-21) as:

$$\begin{aligned} W_{Ohmic} &= \frac{1}{2} r_e |I|^2 = \frac{1}{2} \frac{\omega^2 (Bl)^2}{(R_e^2 + X_e^2)} r_e |S|^2 \\ &= \frac{1}{2} \frac{A^2 (Bl)^2}{((Bl)^2 - X_m X_e + R_m R_e)^2 + (X_m R_e + X_e R_m)^2} r_e |\Delta P|^2 \equiv c * A^2 * |U|^2 * |Z_a|^2 \end{aligned} \tag{4-31}$$

where the proportionality constant in Eq. (4-31) is defined as:

$$c \equiv \frac{1}{2} \frac{r_e (Bl)^2}{((Bl)^2 - X_m X_e + R_m R_e)^2 + (X_m R_e + X_e R_m)^2} \tag{4-32}$$

It is evident that the mechanical-motion loss is inversely proportional to the piston's area, while the Ohmic loss is proportional to the piston's area. Physically, for a fixed input acoustic power, the mechanical-motion loss can be reduced by increasing the piston's area and thereby decreasing the required velocity. This, however, reduces the mechanical stroke and the generated voltage and thus, a larger current and larger Ohmic loss are encountered.

The equations of this section reflect many important findings. Operation at electric resonance reduces the mechanical stroke (and thus reduces the mechanical-motion loss) which

provides allowance to do over-stroke control on the mechanical stroke. Additionally, this operation reduces the pressure difference across the piston of the linear alternator, the dissipated voltage in the load and the fluid seal loss. Operation at electric resonance causes an increase in the generated current, Ohmic loss, generated electric power and the acoustic-to-electric conversion efficiency (Figs. 5-6 and 5-12).

The benefits of operating at mechanical and electric resonances are estimated and the losses associated with operating at off-mechanical and/or off-electrical resonance conditions can be estimated from the model. These two conditions can be achieved by working at the mechanical resonance frequency and by using a power factor correcting capacitor that cancels the effective inductance at the mechanical stroke of operation. This process involves trial and error because the mechanical stroke affects the effective inductance of the linear alternator as shown in Sec.(4.1.2).

4.1.2 Estimation of effective coil inductance

In this work [37], the effective linear alternator coil's inductance is measured during operation by driving the linear alternator as an acoustic driver using a function generator, which is a voltage source without an inductive or capacitive components. A power-factor-correcting capacitor (of the run type and of sufficient voltage rating) is connected in series with the alternator to balance its inductance. The current and voltage signals across the combination made of the alternator's coil and the power-factor-correcting capacitor are measured simultaneously on a digital storage oscilloscope (Model TDS2024 B, supplied by Tektronix), as shown in Fig. 4-2. The capacitance of the power-factor-correcting capacitor is varied until the measured current and voltage signals are in phase indicating that the power-factor-correcting capacitor has balanced the effective coil's inductance. When this condition is achieved, the effective inductance at this operating condition can be inferred from the power-factor-correcting capacitor value using:

$$L_e = \frac{1}{\omega^2 C} \tag{4-33}$$

This method allows estimation of the effective inductance at different operating conditions, unlike as direct measurement of the inductance with an LCR meter which necessitates that the alternator is not energized and thus, provides a single data point of an effective inductance of 68 mH at zero mechanical stroke.

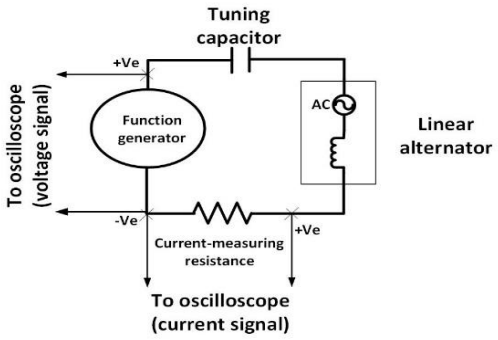

Figure 4-2. Experimental setup used to measure the effective linear alternator coil's inductance for a wide range of mechanical stroke values. [37]

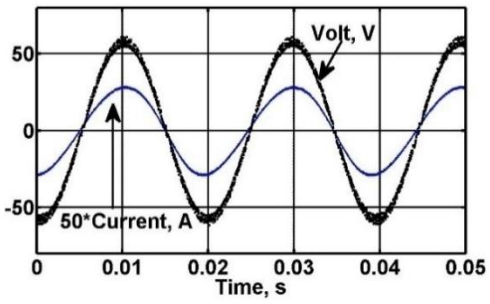

Figure 4-3. Sample of the measured in-phase current and voltage signals at the linear alternator's electric resonance. Data acquired at an input voltage of 40.5 V_{RMS}, an operating frequency of 51 Hz, a mechanical stroke amplitude of 2.95 mm and a power-factor-correcting capacitor. [37]

A sample of this measurement showing in-phase current and voltage signals is shown in Fig. 4-3 at an operating frequency of 51 Hz (which is the mechanical resonance of the linear

alternator at a mean gas pressure of 20 bar) and at a mechanical stroke amplitude of 2.95 mm. Under these conditions, the power-factor-correcting capacitance needed to balance the effective inductance was 72 μF, yielding an effective inductance of 135 mH, which is larger than the inductance value measured at zero mechanical stroke and suggesting that the effective coil's inductance increases with the mechanical stroke amplitude. This increase was measured up to 83 % of the rated stroke amplitude and the results are shown in Fig. 4-4, showing a linear increase in the measured effective coil's inductance with the mechanical stroke beyond an initial stroke value of 3 % of the rated stroke.

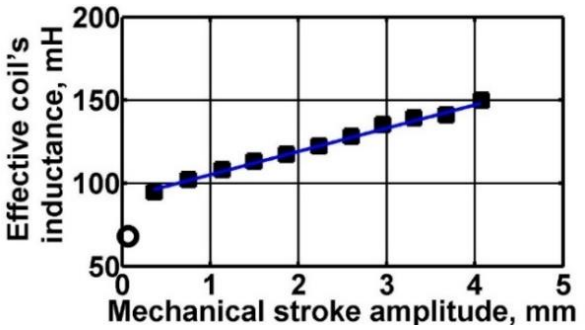

Figure 4-4. The dependence of the effective coil's inductance on the mechanical stroke amplitude. The symbols denote measured values. The solid line shows the relationship presented in Eq. (4-34) assuming Lo of 68 mH and μ of 2.6. [37]

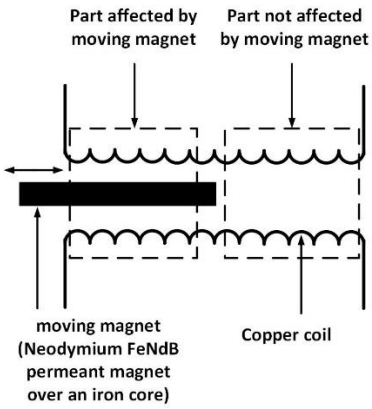

Figure 4-5. An illustration showing the moving magnet oscillating inside the stationary copper coils. During this oscillatory motion, one part of the coil feels the existence of the magnet and its iron core while the other part does not. [37]

The reason for this measured performance can be explained in view of Fig. 4-5 at large values of mechanical stroke amplitudes, the penetration of the iron rod holding the reciprocating magnet is significant. The increased exposure of the iron rod causes an increase in the effective core permeability, which in turns increases the effective coil's inductance [75], since the effective coil's inductance is proportional to the effective core permeability.

As a result, the effective inductance can be modelled as a sum of two terms: the first term corresponds to the part of the electric coil affected by the existence of the iron rod carrying the permanent magnet, which experiences larger core permeability and increased effective inductance. The second term corresponds to the part of the electric coil that is not affected by the rod, and thus, has the nominal core permeability and the nominal coil inductance, hence

$$L_e = \mu L_o \left(\frac{|S|}{|S_R|}\right) + \frac{L_o(|S_R| - |S|)}{|S_R|}, \tag{4-34}$$

where the linear alternator's inductance at rest was measured as 68 mH and μ is the relative permeability of the system made of the electric copper coil, the moving permanent magnet, its iron holder and the gas between the copper coil and the magnet under reciprocating conditions.

The measured effective inductances at different mechanical stroke amplitudes are compared to the values estimated using Eq. (4-34) in Fig. 4-4: the straight line in the figure presents the simulated inductance using a relative permeability of 2.6. For comparison, the relative permeability of neodymium magnet, typically used a moving permanent magnet in linear alternators, is 1.05 [76]. The difference between the two values may arise from the existence of other materials, such as the iron rod holding the magnet, the gas between the magnet and the copper coil as well as due to the reciprocating motion. Additionally, because the presented model does not account for any non-linear effects, such as the non-uniformity of the magnetic field fringes when the alternator's piston is first introduced into the magnetic field, the measurements made at near-zero mechanical strokes (circular symbol in Fig. 4-4) deviate from the model.

4.2 Analytical Model Validation

In this section, there is an experimental validation for the model equations over a wide range of load resistance values and under different input dynamic pressure ratios. The validation under different load resistance values is important because the effect of the load resistance on the linear alternator performance indices is a complex one as shown in Sec (4.1). Table 4-1 shows the basic case conditions for the validation process.

Table 4-1 Basic case working factors and performance indices for the analytical model validation

Operation factor	**Nominal value**	**Operation factor**	**Nominal value**
A	0.60 %	P_m	30 bar
R_L	122 Ω	β	0.48%
C	71 μF	f	56 Hz
Performance index	**Nominal value**	**Performance index**	**Nominal value**
|S|	2.2 mm	$\|Z_a\|$	21.5 Mpa. s/m^3
W_{mech}	1.37 W	W_{Ohmic}	0.3 W
|VL|	38 V	|I|	0.28 A
W_e	5 W	W_a	7 W
η	71.3 %	W_{seal}	0.17 W
X_e	0.68 Ω	X_m	80 N.s/m
P_f	14.4 kPa	|ΔP|	33.8 kPa

The theoretical analysis for the linear alternator performance indices in Sec (4.1) shows that the increase of the pressure difference across the linear alternator piston increases the value of the parameters of the linear alternator except for the acoustic-to-electric conversion efficiency. This increase of the pressure difference greatly affects the acoustic power, generated electric power, Ohmic loss and mechanical motion loss, which are functions of the square value of the stroke. Thus, they are functions of the pressure difference square. The increase of the pressure difference is a direct result of the increase in the working mean gas pressure and the pressure ratio, and an indirect result of the other parameters as illustrated in detail in Sec (5.1.3). Figure. 5-2 reveals the effects of the increase of the input dynamic pressure ratio and the load resistance on the linear alternator performance indices. These effects are illustrated in detail in Sec (5.1.2).

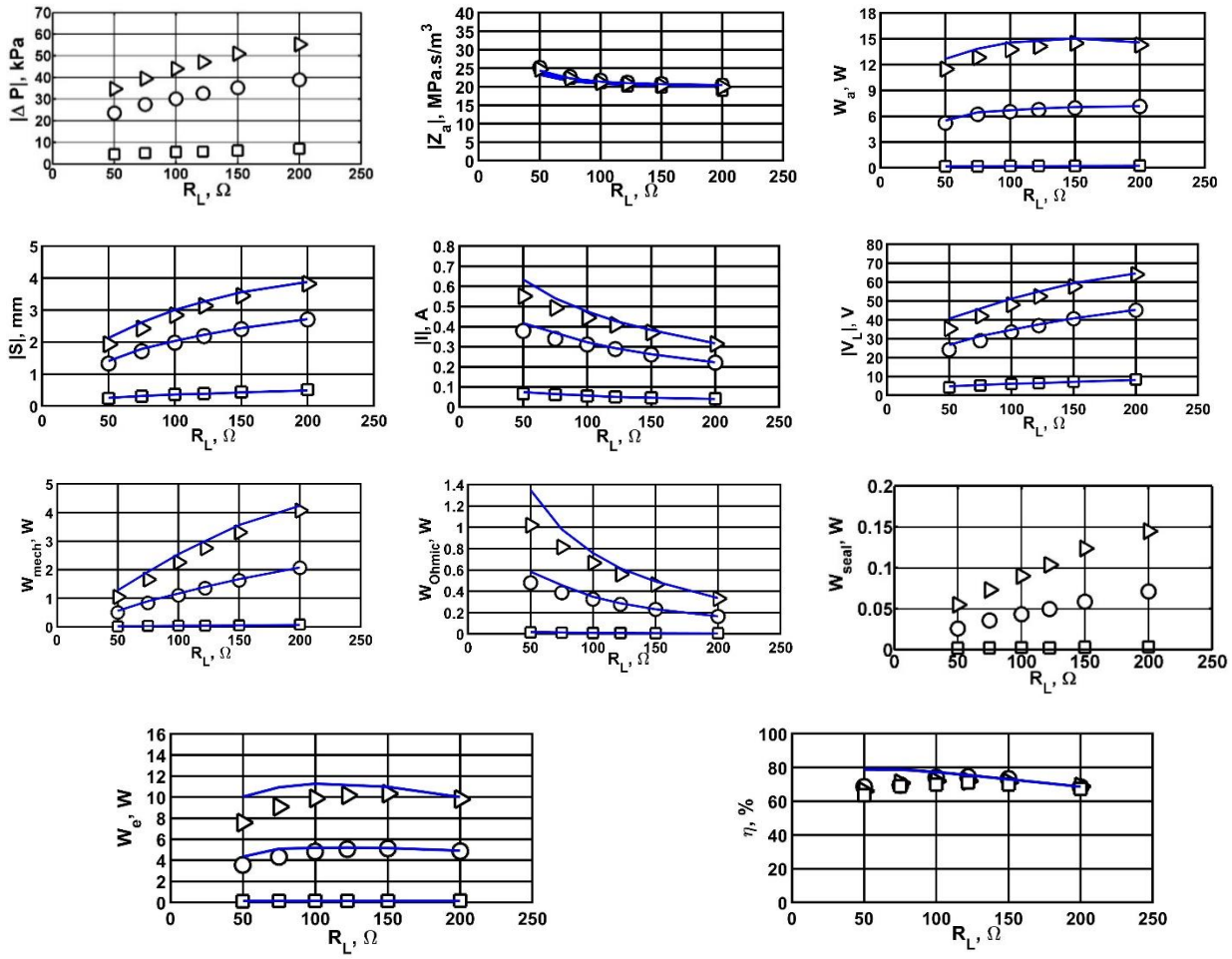

Figure 4-6. Linear alternator performance indices under different load resistances (50-200 Ω) and three input dynamic pressure ratios; and under the stated conditions in Table 4-1. Symbols represent experimental data at different pressure ratios: 0.1% (rectangular), 0.5% (circular), 0.7% (triangular).The solid lines represent the results of the analytical model at the different input dynamic pressure ratios.

It is worthy to note that the experimental data and the analytical model equations are in good agreement and the driver-dependent performance indices, particularly the electroacoustic efficiency, η, are in agreement with the earlier analysis of Wakeland [77] which predicts η_{max} = 79.5% based on the values of (Bl), R_m, and r_e provided by the manufacturer in Appendix A. The values of the experimental data are lower than the expected results of the analytical model under high input dynamic pressure ratio for two main reasons. The first one is that the analytical model equations are based on two controlling equations that do not account for the effect of all types of losses in the linear alternator. For example, these equations do not include the effect of the fluid seal loss and the hysteresis losses; however, these equations include the effects of the mechanical motion loss and the Ohmic loss. Secondly, the main parameters of the linear alternator experience a change in their values. For instance, Sec (4.1.2) shows the

relationship between effective inductance of the linear alternator's coil and the mechanical stroke. Additionally, it was reported that the increase in the dynamic pressure difference across the linear alternator piston area causes an increase in the value of the damping coefficient (R_m) of the linear alternator [30]. Moreover, it was presented that the transduction coefficient (Bl) decreases with the increase of the mechanical stroke [23].

The discrepancy between the results of the model equations and the experimental data is about 20% in the dissipated electric power in the load and 10.4% in the mechanical stroke at input dynamic pressure ratio of 0.7% and load resistance of 50 Ω.

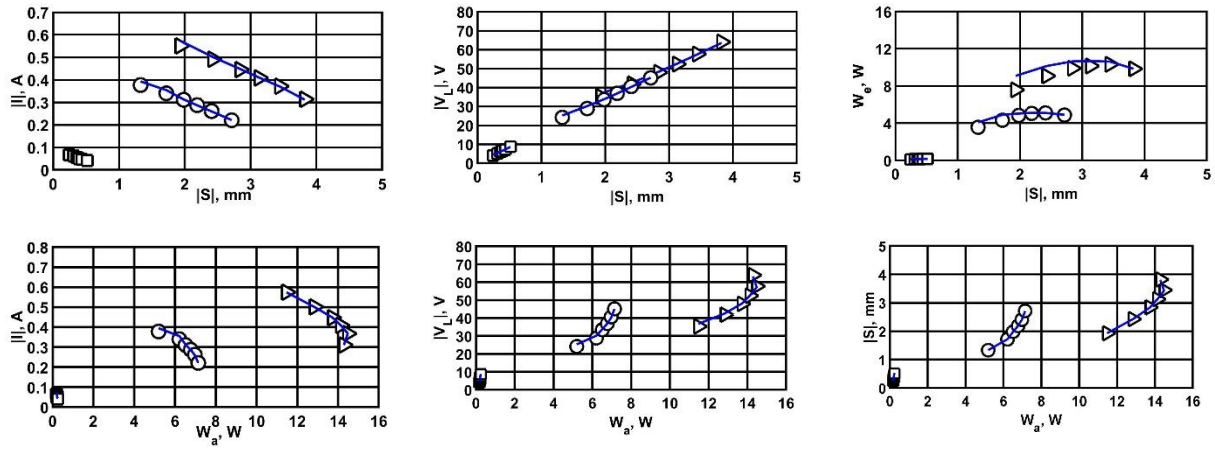

Figure 4-7. The relationships between the acoustic, mechanical and electric performance indices under different load resistances (50-200 Ω) and three input dynamic pressure ratios; and under the stated conditions in Table 4-1. Symbols represent experimental data at different pressure ratios: 0.1% (rectangular), 0.5% (circular), 0.7% (triangular).The solid lines represent the results of the analytical model at the different input dynamic pressure ratios.

Figure. 4-7 shows the relationships between the mechanical, electrical and acoustical performance indices of the linear alternator. These relationships are validated with experimental data under the same conditions stated in Table 4-1 and under different load resistance values (50-200 Ω) for three input dynamic pressure ratios. Showing these relationships over a range of load resistance values simulates the operation under thermoacoustic power conversion conditions. This is because in testing the thermoacoustic power converter, load resistance (or the load parameters) is the most flexible tool to enhance the generated electric power and the efficiency of the linear alternator and to change the acoustic and electric impedances for the purpose of the acoustic and load matchings.

The relationships between the mechanical, electrical and acoustical performance indices of the linear alternator are very important for two main reasons. The first one is that all the

performance indices of the linear alternator can be estimated knowing one of the performance indices, the electric load parameters and the parameters of the linear alternator. Secondly, all the performance indices of the linear alternator are interdependent; for example, the value of the mechanical stroke greatly affects all the other parameters. Conversely, the mechanical stroke is affected by the absorbed acoustic power and the dissipated voltage in the load. Another example is the absorbed acoustic power, which in general reflects the value of the generated current by the linear alternator. On the other hand, if the load resistance increases, then the generated current decreases and the absorbed acoustic power increases as shown in Fig. 4-7.

Fig.4-7 shows that there is a linear relationship between the mechanical stroke and the dissipated voltage in the load under different values of the load resistance. Eq. (4-27) includes the load resistance in the numerator and the denominator, producing no effect for the load resistance on the relationship between the mechanical stroke and the dissipated voltage. In general the dissipated voltage in the load increases and the value of the current decreases with the increase in the load resistance value (Ohm's law).

4.3 Optimization of Piston Area and Load Resistance

An optimum piston area minimizes the sum of these two losses. The total losses can be estimated from Eq. (4-30) and (4-31). By differentiating the equation of the total losses, the optimum area can be estimated as shown in Eq. (4-35).This optimization is valid under constant acoustic impedance, volumetric velocity, load resistance, electric reactance and mechanical reactance.

$$A_{opt} = \frac{R_m^{0.25}((Bl)^2 - X_m X_e + R_m R_e)^2 + (X_m R_e + X_e R_m)^2)^{0.25}}{r_e^{0.25}\sqrt{(Bl)}\sqrt{|Z_a|}} \quad (4\text{-}35)$$

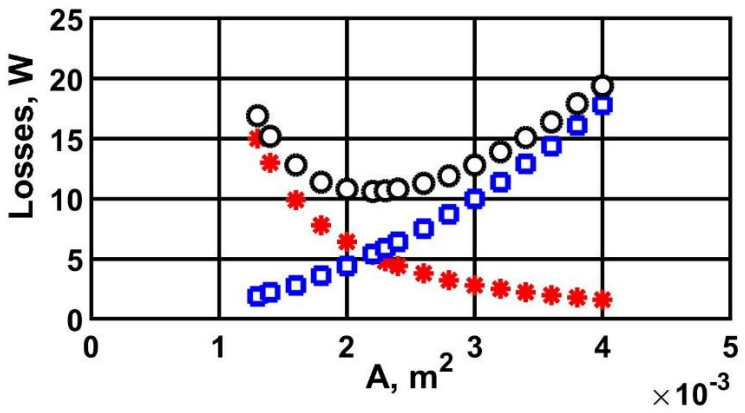

Figure 4-8. Mechanical motion loss, Ohmic and their sum of mechanical motion loss under different piston areas. At $|U|=3.5*10^{-3}$, m^3/s, $|Z_a|=20MPa.s/m^3$,$R_L=60\ \Omega$, $X_e=-16\ \Omega$ and $X_m=80.25$ N.s/m. Star symbols represent the mechanical motion loss, rectangular symbols represent the Ohmic loss and circular symbols represent the total losses.

Figure 4-8 shows that the minimum total losses= 10.63 W, at piston area (*A*) of 0.0022 m^2, which is 110% of the original piston area under the specified conditions. The increase in the value of the piston area that achieves the minimum total loss will enhance the value of the most of the performance indices of the linear alternator as shown in Sec 4.1.1 .

The value of this optimum piston area is a function of the linear alternator parameters, load parameters, acoustic impedance and the operating frequency. The value of the optimum piston area should be estimated at the frequency of the mechanical resonance to harvest the benefits of operating at mechanical resonance and at the resistance value in between the value of the maximum electric power and the maximum efficiency. Nevertheless, the load resistance must achieve a linear alternator impedance that matches that of the thermoacoustic engine.

From the results of the parametric study (Fig.(5-5)) it is shown that the acoustic impedance is low and constant at high load resistance values. Thus increasing the chosen

electric load resistance increases the optimum piston area value that causes an increase of the mechanical stroke, electric power and the absorbed acoustic power and other performance indices.

Similarly, the optimum load resistance for maximum acoustic-to-electric conversion efficiency (Fig.(4-9)) is obtained by differentiating Eq. (4-24) with respect to the load resistance and can be expressed as:

$$R_{L\,(Max\,\eta)} = \frac{\sqrt{R_m((Bl)^2 r_e + R_m X_e^2 + R_m r_e^2)}}{R_m} \tag{4-36}$$

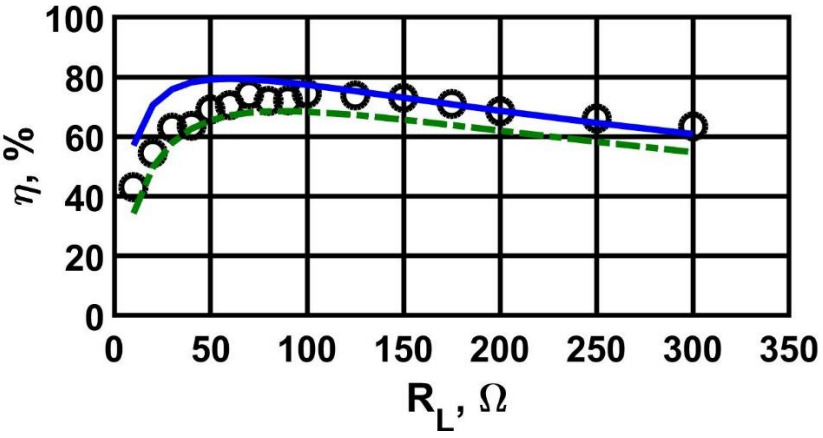

Figure 4-9. Acoustic-to-electric-conversion efficiency under different load resistances at the stated conditions in Table [4-1]. The circular symbol represents the experimental data, the solid blue line represents the analytical model results and the dashed green line represents the DELTAEC results.

When using this load resistance, the resulting conversion efficiency can be expressed as:

$$\eta_{max} = \frac{2R_m^2 X_e^2 + 2R_m r_e((Bl)^2 + R_m r_e) + (Bl)^2\sqrt{R_m}\sqrt{(Bl)^2 r_e + R_m(r_e^2 + X_e^2)} + 2R_m\sqrt{R_m}\,\sqrt{(Bl)^2 r_e + R_m(r_e^2 + X_e^2)r_e}}{(Bl)^2\sqrt{R_m(Bl)^2 r_e + R_m^2(r_e^2 + X_e^2)}} \tag{4-37}$$

It is worthy to note that η_{max}=79.46 % at electrical resonance case which is in agreement with the earlier analysis of Wakeland [77] which predicts ηmax = 79.5% based on the values of (Bl), R_m, and r_e provided by the manufacturer in Appendix A. Fig. 4-9 verifies the findings of Eqs. (4-36) and (4-37).

Additionally, there is a load resistance that yields a maximum dissipated electric power in the load at constant operating mechanical stroke. It is obtained by differentiating Eq. (4-23) with respect to the load resistance and can be expressed as:

$$R_{L(Max\,We)} = \sqrt{(X_e^2 + r_e^2)} \tag{4-38}$$

It is worthy to note that $R_{L(We\,(Max))} = 6.72\ \Omega$ at electrical resonance. When using this load resistance, the resulting generated electric power can be expressed as:

$$W_{e(max)} = \frac{1}{2}\frac{\omega^2 (Bl)^2 \sqrt{(X_e^2 + r_e^2)}}{(((\sqrt{(X_e^2 + r_e^2)}) + r_e)^2 + X_e^2)} |S|^2, \qquad (4\text{-}39)$$

It should be noted that the load resistance, which achieves the maximum generated electric power, could be used under the condition of constant mechanical stroke, constant operating frequency and constant value of power-factor-correcting capacitor. Achieving maximum electric power should be conducted at off-electric resonance condition by using the value of the power-factor-correcting capacitor that causes a high-magnitude electric resonance, this will increase the value of the optimum load resistance which achieve the maximum electric power. Increasing the value of the optimum load resistance decreases the generated current and the Ohmic loss.

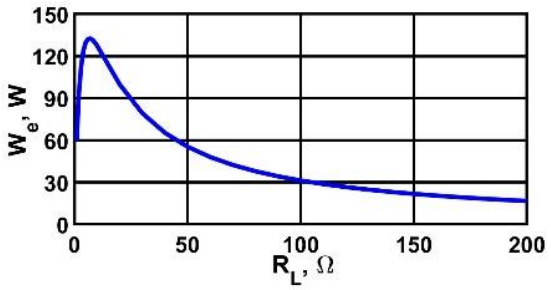

Figure 4-10. Effect of load resistance (1-200 Ω) on the dissipated electric power in the load at conditions of rated stroke ($|S_R|$=5 mm) and electrical resonance using a 46 μF power-factor-correcting capacitor and an operating frequency of 56 Hz.

Eq (4-37) and Eq (4-39) reveal that the points of the maximum generated electric power and the maximum acoustic-to-electric conversion efficiency cannot intersect with each other's because the maximum efficiency occurs at the point of the electric resonance that decreases the value of the generated electric power.

The findings of Eq.(4-38) and Eq. (4-39) are verified using a numerical simulation for Eq.(4-23) under different load resistances as shown in Fig. 4-10. This simulation is achieved at the conditions of Table 4-1, a constant rated stroke ($|S_R|$=5 mm) and a constant operating frequency (f=56 Hz) and a constant power-factor-correcting capacitor (C=46 μF).

4.4 Summary of Analytical Model Results

In conclusion, the benefits of operating at mechanical and electric resonances are estimated and the losses associated with operating at off-mechanical and/or off-electrical resonance conditions can be estimated from the model. These two conditions can be achieved by working at the mechanical resonance frequency and by using a power factor correcting capacitor that cancels the effective inductance at the mechanical stroke of operation. This process involves trial and error because the mechanical stroke affects the effective inductance of the linear alternator.

The results indicate that the overall performance is certainly not guaranteed to coincide with mechanical/electrical resonances. Any specific performance index, like the acoustic-to-electric conversion efficiency, is not guaranteed to be optimal around the mechanical resonance frequency necessarily, but should be close to it. However, the overall performance should be optimal when both resonance conditions are fulfilled.

Operation at electric resonance reduces the mechanical stroke (and thus reduces the mechanical-motion loss) which provides allowance to do over-stroke control on the mechanical stroke. Additionally, this operation reduces the pressure difference across the piston of the linear alternator, the dissipated voltage in the load and the fluid seal loss. Operation at electric resonance causes an increase in the generated current, Ohmic loss, generated electric power and the acoustic-to-electric conversion efficiency (Figs. 5-6 and 5-12).

If the damping coefficient of the linear alternator is insignificant, at mechanical resonance, the force applied to the piston is not consumed to accelerate the moving mass nor to deflect the linear alternator stiffness. Under this condition, the applied force is used only to generate electric current, as shown in Eq. (4-13).

The model presented in this work is validated by experimental measurements at different input dynamic pressure ratios (0.1 %, 0.5 % and 0.7 %) and load resistance values (50-200 Ω) under the conditions of operating frequency of 56 Hz, a gas mixture of 60% Helium-40% Argon, a mean gas pressure of 30 bar and a power-factor-correcting capacitor that cancels the linear alternator inductance at these conditions (71 μF).

The comparison between the simulated and measured results show reasonable agreement, with the discrepancy caused by two main reasons: The analytical model only accounts for the mechanical-motion loss, the Ohmic loss and the fluid seal loss and not for all losses; and

because the model assumes constant alternator parameters under different operating conditions, except for the variation of the effective coil inductance with the mechanical stroke. The discrepancy was about 20% in the absorbed acoustic power and 10.4% in the mechanical stroke.

Upon validating the model, optimization process for the optimum load resistance was carried-out. It was found that one load resistance achieves the maximum acoustic-to-electric conversion efficiency and another one achieves the maximum generated electric power. The later should be used carefully since if operation would occur at electrical resonance, this optimal resistance would be extremely small and would withdraw excessive current and would result in excessive Ohmic loss and poor acoustic-to-electric conversion efficiency. In practice, a load value in between the two resistance values is more practical. This load resistance has the advantages of relatively-high generated electric power and relatively-high acoustic-to-electric conversion efficiency. Additionally, this chapter introduces an optimum piston area for achieving minimum sum of the main losses (mechanical loss and Ohmic loss). The value of this optimum piston area is a function of the linear alternator parameters, load parameters, acoustic impedance and the operating frequency. The value of the optimum piston area should be estimated at the frequency of the mechanical resonance to harvest the benefits of operating at mechanical resonance and at the resistance value in between the value of the maximum electric power and the maximum efficiency. Nevertheless, the load resistance must achieve a linear alternator impedance that matches that of the thermoacoustic engine.

From the results of the parametric study it is shown that the acoustic impedance is low and constant at high load resistance values. Thus increasing the chosen electric load resistance increases the optimum piston area value (Eq. (4-35)) which causes an increase of the mechanical stroke, electric power and the absorbed acoustic power and other performance indices.

As expected, the equations show that the decrease in the damping coefficient, the stator resistance, and/or the increase in the transduction coefficient cause an increase in the conversion efficiency and the generated electric power. This is consistent with the earlier analysis by Wakeland [77] which showed that the maximum efficiency can depend only upon a dimensionless combination of those driver parameters: $\beta = (Bl)^2/(R_m r_e)$ Moreover, the model shows that the generated voltage is linearly proportional to the mechanical stroke and that the

proportionality constant is function of the operating frequency, the transduction coefficient, the stator's resistance, the coil inductance, the capacitance of the power-factor correcting capacitor and the load resistance. Additionally, the generated current is linearly proportional with the mechanical stroke (Eq.(4-21)) and that the proportionality constant is function of the total operating frequency, the transduction coefficient, the stator's resistance, the coil inductance, the capacitance of the power-factor correcting capacitor and the load resistance.

The results of this work show that low load resistances result in withdrawing large current, generating lower voltages from the alternator and thus lower mechanical strokes. Accordingly, during the start of operation, low resistance values should be used first to avoid over-stroking. Then, after the engine starts to self-oscillate at a certain load resistance, the load resistance can be increased gradually while the stroke is monitored carefully until the desired stroke is reached safely.

5. Results: Experimental Parametric Study

The parametric study experimentally investigates the optimum performance for the linear alternator under thermoacoustic-power-conversion conditions. There are typically several conditions describing the optimum performance of the linear alternator under thermoacoustics-power-conversion conditions and they cannot be combined together; thus, the parametric study focuses on determining the effects of the different working conditions such as different operating frequency, different mean gas pressure, different gas mixtures, different input dynamic pressure ratios, different load resistance and different operating power-factor correcting capacitors on achieving the optimum performance. The understanding for these effects contributes in determining the best working conditions experimentally. The uniqueness of this parametric study stems from the availability of its results for linear loads and non-linear loads. This completes the image of the performance of the linear alternator under different types of load. The parametric study under linear load condition is supported by the results of the analytical model and the DELTAEC simulations for two reasons. First, they support the validity of the analytical model and DELTAEC simulations within a wide range of operation and under different working conditions. The second reason is that the equations of the analytical model provide an explanation for the change of the linear alternator's performance under different working conditions.

5.1 Experimental Parametric Study under Linear Load Condition

This section introduces the performance of the linear alternator under different working conditions with a linear load consisting of load resistance and a power-factor-correcting capacitor. Table 5-1 shows the basic case working conditions and the values of the performance indices under linear load condition.

Table 5-1 Basic case operating factors and performance indices of the parametric study under linear load condition.

Operation factor	**Nominal value**	**Operation factor**	**Nominal value**
α	0.60 %	P_m	30 bar
R_L	122 Ω	β	0.48%
C	71 μF	f	56 Hz
Performance index	**Nominal value**	**Performance index**	**Nominal value**
$\|S\|$	2.2 mm	$\|Z_a\|$	21.5 Mpa. s/m^3
W_{mech}	1.37 W	W_{Ohmic}	0.3 W
$\|V_L\|$	38 V	$\|I\|$	0.28 A
W_e	5 W	W_a	7 W
η	71.3 %	W_{seal}	0.17 W
X_e	0.68 Ω	X_m	80 N.s/m
P_f	14.4 kPa	$\|\Delta P\|$	33.8 kPa

The conditions of the basic case are selected such that the operating frequency is determined to achieve the mechanical resonance. Additionally, the power-factor-correcting capacitor is selected according to Eq. (4-6) and (4-33) to achieve the electrical resonance at the presented value of the mechanical stroke (X_e=0.68 Ω).The operating frequency (56Hz) is the free damping frequency of the linear alternator at mean gas pressure of 30 bar and mixture of 60% He and 40%Ar. The mechanical reactance (X_m) is equal to 80 N.s/m at this frequency. The load resistance value is selected to create a harmonized mode of operation by achieving equal mechanical stroke for the acoustic driver and the linear alternator. The gas mixture and the mean gas pressure selection is illustrated in detail in Chapter 3.

The pressure ratio is chosen to be suitable under different working conditions within the limitations of the configuration of the experimental setup. Despite working at a constant pressure ratio, the value of the pressure difference across the linear alternator piston varies. The increase

in the pressure difference causes an increase in the values of the linear alternator performance indices. As illustrated in the algebraic model equations, the main factors to determine the value of the performance indices are the operating frequency, load parameters, mean gas pressure, gas mixture, the input dynamic pressure ratio and the parameters of the linear alternator.

The pressure difference across the piston of the linear alternator is a function of two parameters. The first one is the dynamic pressure in front of the piston of the linear alternator (P_f), the value of which depends on the absorbed acoustic power, so setting this pressure is a controllable process. The second parameter is the dynamic pressure in the back volume of the linear alternator (P_b), which is a reaction of the linear alternator's response to the applied acoustic force. This response depends on the parameters of the linear alternator, the operating frequency, the mechanical stroke and the generated current, as shown in Eq. (4-11). Setting the value of the pressure difference is an impossible process because the dynamic pressure in the back volume changes with the change in the dynamic pressure in the front of the piston of the linear alternator.

In the high-power thermoacoustic-power-converters, the mean gas pressure and the input dynamic pressure ratio determine the value of the pressure difference across the linear alternator's piston, as the dynamic pressure in the front of the linear alternator's piston is much higher than the dynamic pressure in the back volume. Conversely, in the case of small power thermoacoustic converters (which is the case in our experimental setup), the value of the dynamic pressure in the front of the linear alternator's piston in the most of the cases is minor compared to the value of the pressure difference and it does not reflect the value of the absorbed acoustic power (ΔP changes from 10 to 32 kPa over the change in the operating frequency on the other hand the P_f=constant=14.4 kPa) as shown in Fig-5-1**.** Thus, in this section's work, the mechanical stroke is used to understand the behavior of the linear alternator's performance indices under different working conditions.

From Eq. (4-12), the dissipated voltage in the electric load is an indicator of the mechanical stroke at constant operating frequency. Under the different operation conditions, the generated voltage and the mechanical stroke have the same behavior.

5.1.1 Effects of the operating frequency

Figure. 5-1 demonstrates the effect of the change in the operating frequency on the linear alternator performance indices at the working conditions stated in Table 5-1.

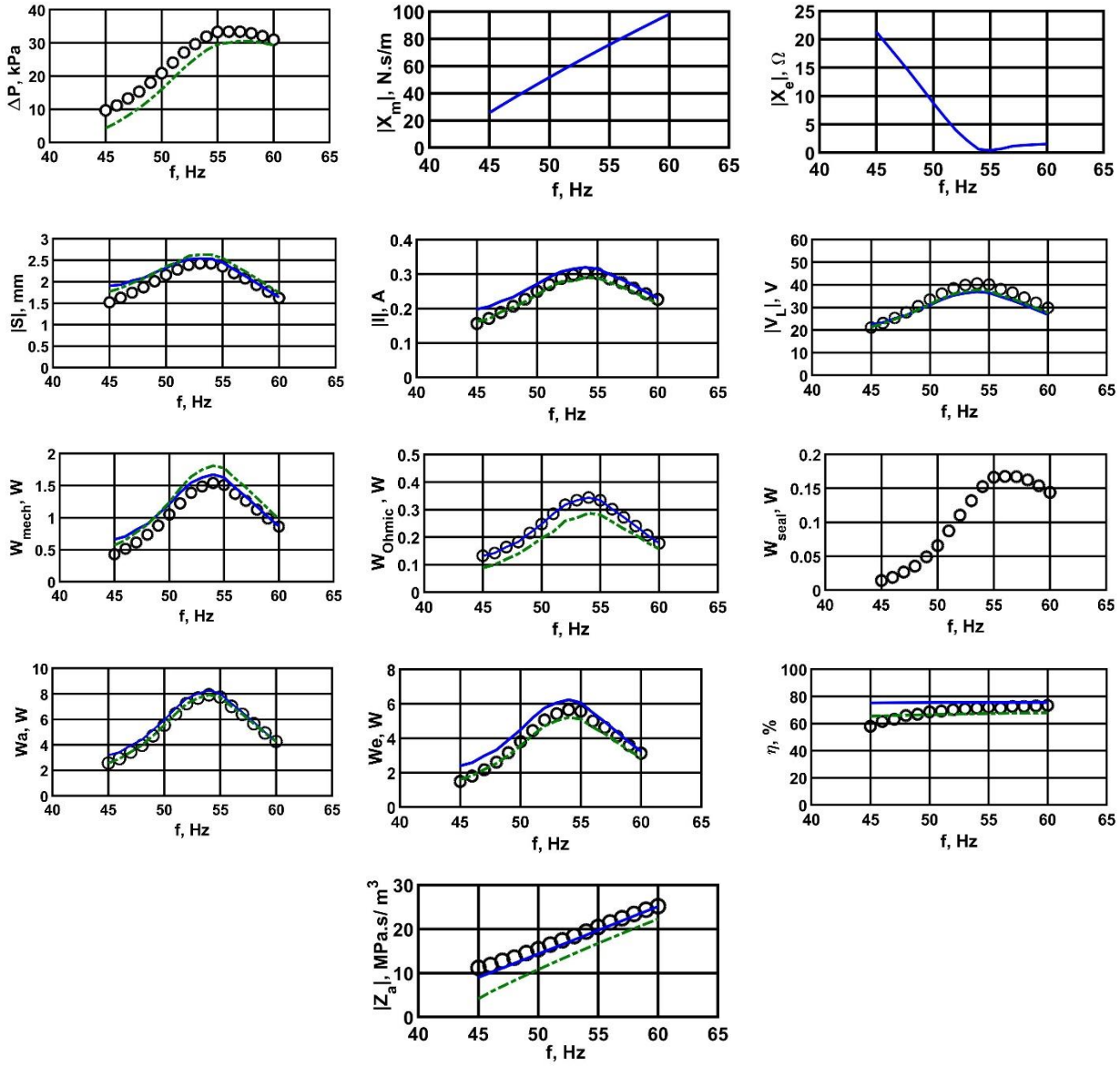

Figure 5-1. Linear alternator performance indices under frequency range 45-60 Hz, this data is for a gas mixture consists of 60% helium/40% argon, a mean gas pressure of 30 bar and dynamic pressure ratio 0.48%. The load is a 122-Ω resistance in series with a 71 μF power-factor-correcting capacitor. The circular symbol represents the experimental data, the solid blue line represents the analytical model results and the dashed green line represents the DELTAEC results.

The mechanical reactance increases due to the increase in the operating frequency conversely the magnitude of electric reactance decreases until reach to the resonance point (56 Hz) then starts to increase (the value of the electric reactance is negative before the frequency of 56 Hz) . It should be noted that the electric reactance is a function of the radial frequency,

effective inductance of the coil that is a function of the mechanical stroke and the power-factor-correcting capacitor. The acoustic impedance increases with the increase in the operating frequency under these conditions because the mechanical reactance increases with the increase in the operating frequency and the electric reactance is negative and it decreases until 56 Hz. The increase of the mechanical reactance and the decrease of the electric reactance (from negative to zero) cause an increase in the numerator and a decreases of the denominator of the equation of the acoustic impedance (eq. (4-18)).

The experimental data shows that the pressure difference has a peak point at frequency of 57 Hz that is near to the electric resonance point and the free damping frequency of the linear alternator under conditions of mean gas pressure of 30 bar and gas-mixture of 60%He-40%Ar that are the basic case conditions of this work. From the definition of the acoustic impedance the mechanical stroke can be defined as: $|S|=|\Delta P|/(A*\omega*|Z_a|)$, the mechanical stroke decreases when the rate of the increase of the pressure difference is less than the rate of the increase of the radial frequency and the acoustic impedance.

It should be noted that the magnitude of the electric reactance reaches a minimum (almost electric resonance) at nearly 54 Hz. At this point, the mechanical stroke, the generated current, voltage, electric power, absorbed acoustic power, mechanical-motion loss and Ohmic loss all reach their peaks at the same frequency. Beyond this frequency, the increase in the electric reactance and the decrease in the mechanical stroke forced most of the performance indices to decrease, despite the increase in the radial frequency.

From Eq. (4-21) it can be deduced that the generated current is proportional to the mechanical stroke as well as the radial frequency. Furthermore, the generated current is inversely proportional to the electrical reactance and has a peak at frequency of 54 Hz. Because, this point is almost at electric resonance.

At a higher frequency point, the severe decrease in the mechanical stroke combined with an increase in the absolute value of the electrical reactance causes a decrease in the generated current. This decrease in the generated current occurs, despite the increase in the radial frequency. The dissipated voltage (Eq. (4-27)) is similar to the generated current, which is both directly proportional to the mechanical stroke and the radial frequency and inversely proportional to the electrical reactance at conditions of constant values of load resistance and power-factor-correcting capacitor. Therefore, the dissipated voltage enjoys a peak point at frequency 54 Hz.

On the other hand, the acoustic-to-electric conversion efficiency from Eq. (4-24) is a function of the load resistance and the electrical reactance. Concurrently, the efficiency is inversely proportional to the electrical reactance squared. The increase in the operating frequency causes an increase in the value of the electrical reactance, as well as a decrease in its magnitude at the value of the power factor correcting capacitor stated in Table 5-1. Thus, the efficiency increases with the increase in the operating frequency. The rate of this increase diminished because of the value of the (R_e) squared. Noting that, the (R_e) squared is significantly higher compared to the square of the decreasing electrical reactance (X_e).

According to Eq. (4-22), the acoustic power absorbed by the linear alternator increases with the increase of the radial frequency squared and the mechanical stroke. Thus, it enjoys the same peak as the mechanical stroke at frequency 54 Hz. The dissipated electric power (Eq. (4-23)) and the Ohmic loss (Eq. (4-31)) are in proportionality relationships of the generated current squared, thus they have the same peak point as the generated current (54 Hz). The mechanical motion loss is proportional to the product of the mechanical stroke squared and the radial frequency squared but still peaks at the peak of the mechanical stroke (54 Hz).

The results of the algebraic model equations and the DELTAEC simulations are consistent with the experimental results over a wide range of operating frequencies. From the presented results, it can be observed that the value of the mechanical stroke is proportional to most of the linear alternator parameters. All these parameters exhibit similar behavior to the linear alternator's mechanical stroke, except for the acoustic-to-electric conversion efficiency and the acoustic impedance.

This is because the maximum efficiency occurs at the electric resonance assuming constant load resistance. Thus, the maximum acoustic-to-electric conversion efficiency and the maximum generated electric power cannot occur simultaneously.

The electric reactance magnitude decreases down to zero at the electric resonance point and then increases. It should be noticed that there is no single frequency that achieves the optimum performance in all indices.

5.1.2 Effects of the input dynamic pressure ratio

The increase in the input pressure ratio results in an increase in the pressure difference across the piston of the linear alternator. Thus, the mechanical stroke increases, causing changes in all other performance indices. Furthermore, the increase of the mechanical stroke causes an increase of the linear alternator's effective inductance, so the electrical reactance increases. Thus, the mechanical stroke and the electrical reactance magnitude both affect the value of the linear alternator performance indices, but with varying degrees.

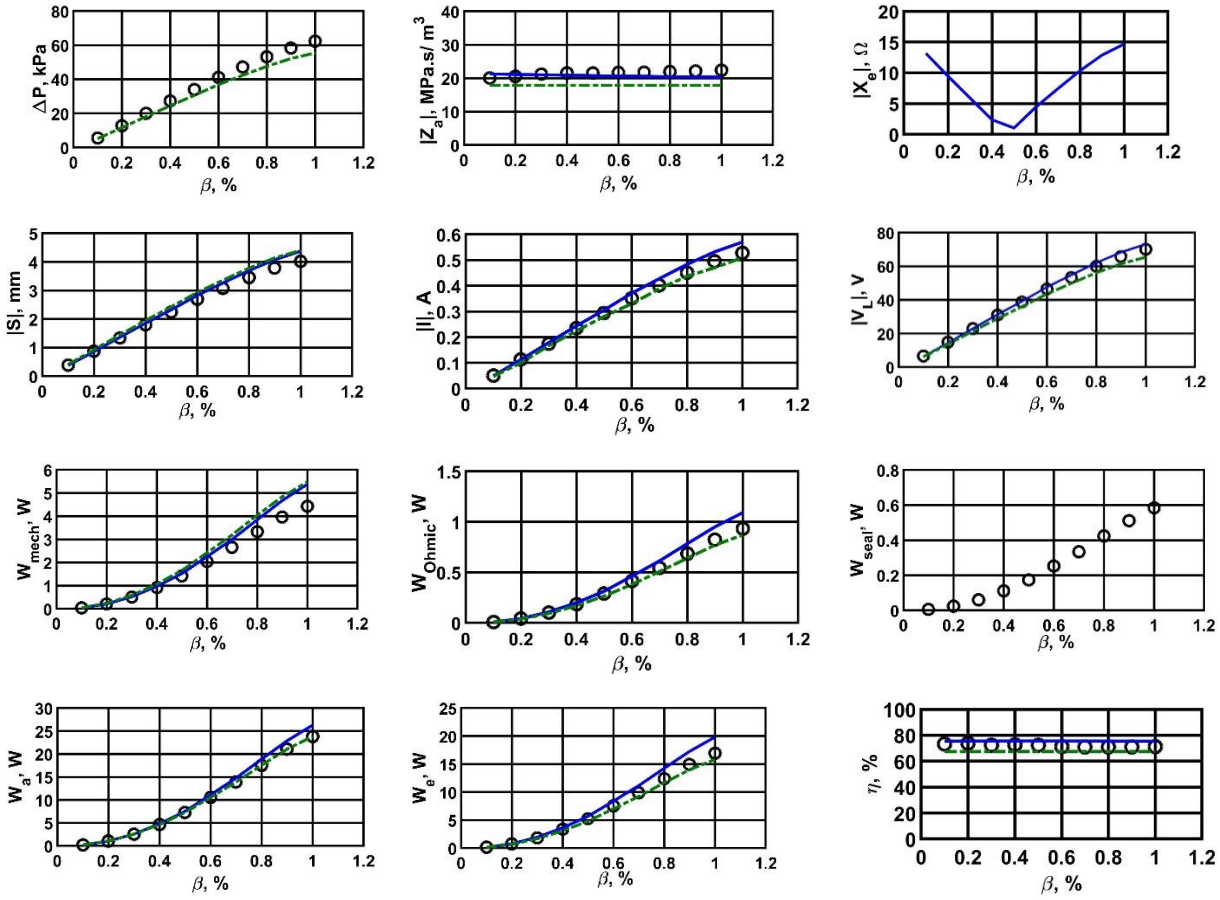

Figure 5-2. Linear alternator performance indices under dynamic pressure ratio range 0.1-1 %, This data is for a gas mixture consists of 60% helium/40% argon, a mean gas pressure of 30 bar and an operating frequency of 56 Hz. The load is a 122-Ω resistance in series with a 71 μF power-factor-correcting capacitor. The circular symbol represents the experimental data, the solid blue line represents the analytical model results and the dashed green line represents the DELTAEC results.

The generated current and the dissipated voltage are proportional with the mechanical stroke.

The dependence of the current and voltage on the mechanical stroke and the electric reactance are described in Eq. 4-21, and 4.27, respectively. These equations show that the relationship would be linear if the electric reactance was constant. The change in the electric

reactance induced by the change in the mechanical stroke is the reason behind the slight non - linearity observed.

The effects of the electric reactance in these equations are minor because they are masked behind a large total resistance R_e.

Similarly, the mechanical motion loss, the Ohmic loss, the absorbed acoustic power and dissipated electric power in the load have quadratic relationships with the mechanical stroke. So, there is a quadratic relationship between these parameters and the input dynamic pressure ratio. Moreover, the seal loss is a function of the maximum pressure difference across the piston of the linear alternator, so it always has the same behavior of the pressure difference.

The acoustic-to-electric conversion efficiency experiences a very insignificant decrease with the dynamic pressure ratio because of the minor increase in the magnitude of the electrical reactance away from electric resonance.

For the acoustic impedance, the electric reactance appears in the numerator and the denominator so its effect on the value on the acoustic impedance is insignificant. The electrical reactance behaves as before.

At high input dynamic pressure ratio, the experimental results are lower than the simulated results. This happens because of several reasons. The first one is that, the losses which include the mechanical motion loss, Ohmic loss, fluid seal loss and some minor losses related to the non-linearities in the linear alternator, increase dramatically with the increase of the pressure difference across the piston of the linear alternator.

The second reason is that; the main parameters of the linear alternator experience a change in their values. For instance, Sec (4.1.2) shows the relationship between effective inductance of the linear alternator's coil and the mechanical stroke. Additionally, it was reported that the increase in the dynamic pressure difference across the linear alternator piston area causes an increase in the value of the damping coefficient (R_m) of the linear alternator [30]. Moreover, it was presented that the transduction coefficient (Bl) decreases with the increase of the mechanical stroke [23].

5.1.3 Effects of mean gas pressure

The effects of the change of the mean gas pressure on the linear alternator performance indices are presented in the figure below. Essentially, the increase in the mean gas pressure improves the acoustic coupling between the acoustic driver and the linear alternator. Thus, the absorbed acoustic power increases and the mechanical stroke increases forcing a change in the electrical reactance as well and causing changes in all other performance indices.

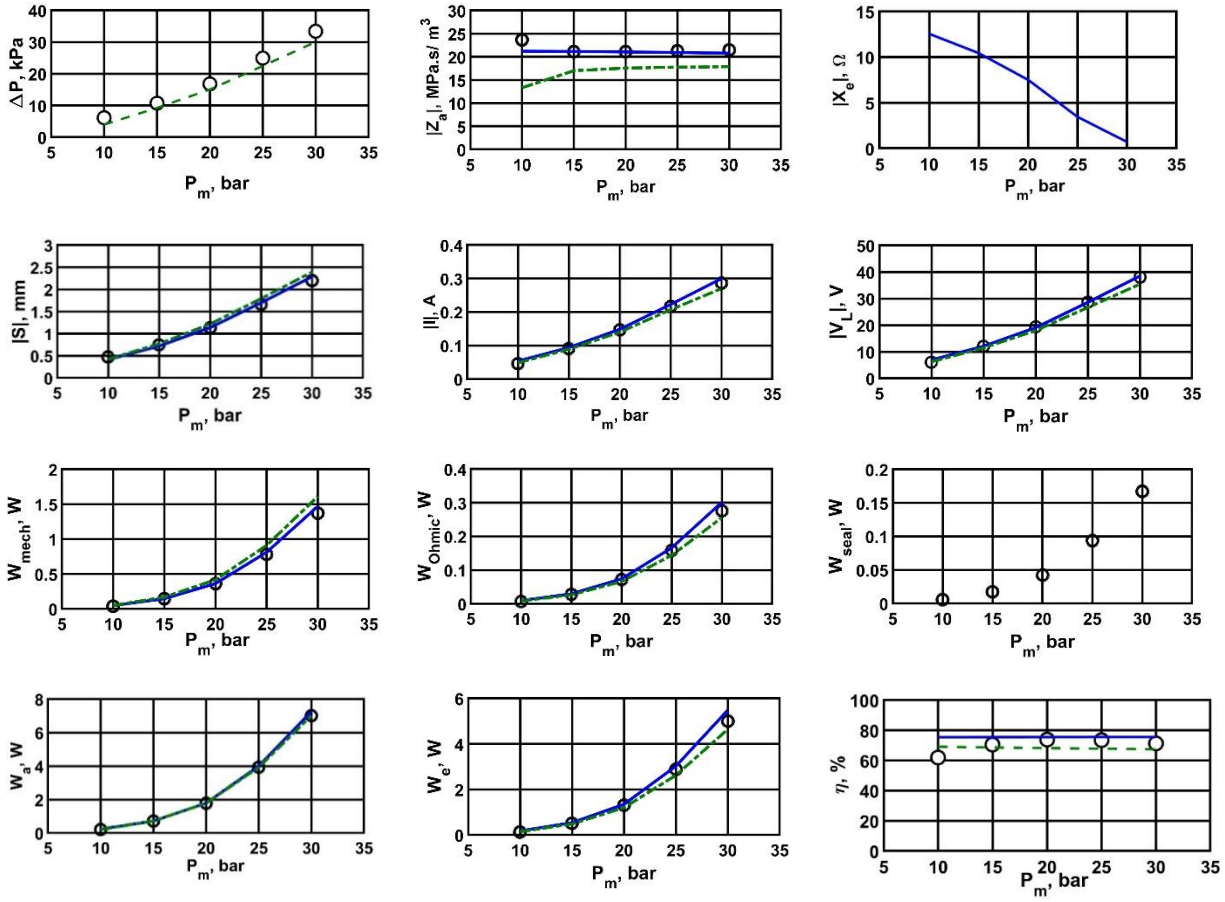

Figure 5-3. Linear alternator performance indices under mean gas pressure range 10-30 bar, This data is for a gas mixture consists of 60% helium/40% argon, dynamic pressure ratio 0.48% and an operating frequency of 56 Hz. The load is a 122- Ω resistance in series with a 71 μF power-factor-correcting capacitor. The circular symbol represents the experimental data, the solid blue line represents the analytical model results and the dashed green line represents the DELTAEC results.

The acoustic impedance and the acoustic-to-electric conversion experience a small change compared to the other performance indices. This small change is a result of the change of the electric reactance and the linear alternator's parameters where the damping coefficient increases with the increase of the dynamic pressure difference across the piston of the linear alternator [30] and the transduction coefficient decreases with the increase of the mechanical

stroke [23] that increases with the increase of the dynamic pressure difference across the piston of the linear alternator. The electrical reactance behaves as before.

5.1.4 Effects of gas mixture

Vesely [78] studied the effects of the increase of the helium molar fraction in different gas mixtures that commonly used in the thermoacoustic engines. It was found that the increase of the helium molar fraction in the gas mixture causes an increase in the speed of sound and the acoustic intensity in the thermoacoustic engine.

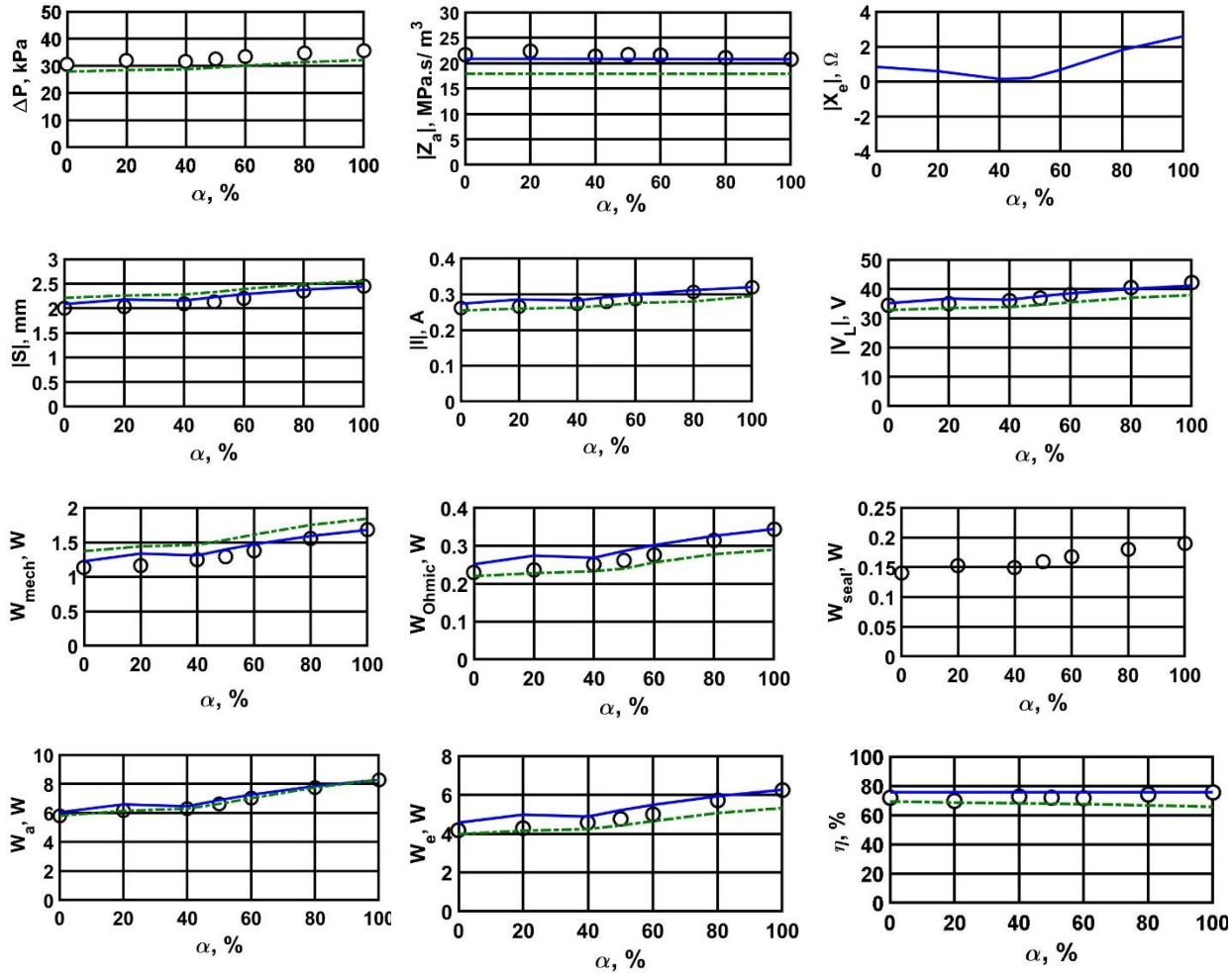

Figure 5-4. Linear alternator performance indices under helium molar fraction range 0-100 %, This data is for a mean gas pressure of 30 bar and dynamic pressure ratio 0.48% and an operating frequency of 56 Hz. The load is a 122- Ω resistance in series with a 71 μF power-factor-correcting capacitor. The circular symbol represents the experimental data, the solid blue line represents the analytical model results and the dashed green line represents the DELTAEC results.

The studied gas mixtures consist of helium and argon gases. Figure 5-4 shows the effect of the increase of the helium molar fraction (α) in the gas mixture. The increase of the helium molar fraction means an increase in the speed of the sound in the mixture. Consequently the particle velocity increases which causes an increase in the applied acoustic power (Eq.(1-4)) and the absorbed acoustic power. It is worthy to note that in this work the P_f (dynamic pressure in the

front of the piston) is a constant because the input dynamic pressure ratio is a constant, thus, the increase in the absorbed acoustic power arises only from the increase of the piston velocity as a result of the increase of the particle velocity.

The increase in the piston velocity means an increase in the mechanical stroke ($|S|=|u|/\omega$, ω=constant in this work). From Eq. (4-19), the dynamic pressure difference across the piston of the linear alternator increases with the increase of the mechanical stroke. Consequently, as shown in Sec (4.1.1), most of the performance indices increase with the increase of the mechanical stroke and the dynamic pressure difference across the piston of the linear alternator.

The electric reactance is a function of the effective inductance of the linear alternator that change with the change in the mechanical stroke. The change in the electrical reactance is negligible with respect to the large value of total resistance (R_e) used. The electrical reactance behaves as before.

From the experimental data of Fig.5-4, it is worthy to note that, the factor of the increase in the mechanical stroke ($|S|$) over the range of the change in the helium molar fraction from 0% to 100%, is similar to the factor of the increase (1.22) in the generated current ($|I|$) and the dissipated voltage in the load ($|V_L|$), over the same range of change in the helium molar fraction (α).

Table 5-2. The increase factors of the main performance indices over the change in the helium molar fraction

Performance index	Value of the index at α = 0%	Value of the index at α = 100%	Ratio between two values
($|S|$), mm	1.99	2.44	1.22
(W_{mech}), W	1.13	1.67	1.48 (=1.22^2)-(Eq. 4-30)
(W_a), W	5.80	8.28	1.42 (Eq.4-22)
($|I|$), A	0.26	0.32	1.22 (Eq.4-21)
(W_{Ohmic}), W	0.23	0.34	1.49(=~1.22^2)- (Eq.4-31)
($|V_L|$), V	34.49	42.18	1.22 (Eq. 4.-27)
(W_e), W	4.17	6.23	1.49 (=~1.22^2)-(Eq.4-23)

Additionally, the factor of the increase (1.48) in the dissipated electric power in the load (W_e), mechanical motion loss (W_{mech}), Ohmic loss (W_{Ohmic}) is equal to the square of the factor of the increase in the mechanical stroke ($|S|$), generated current ($|I|$) and the dissipated voltage

in the load ($|V_L|$), over the mentioned range of the change in the helium molar fraction (α). These observations are summarized in the Table 5-2 above.

5.1.5 Effects of load resistance

Determining the exact effect of the load resistance on the linear alternator's performance indices is a complex process. It can be found that the mechanical stroke is proportional to the load resistance as shown in Eq. (4-20).

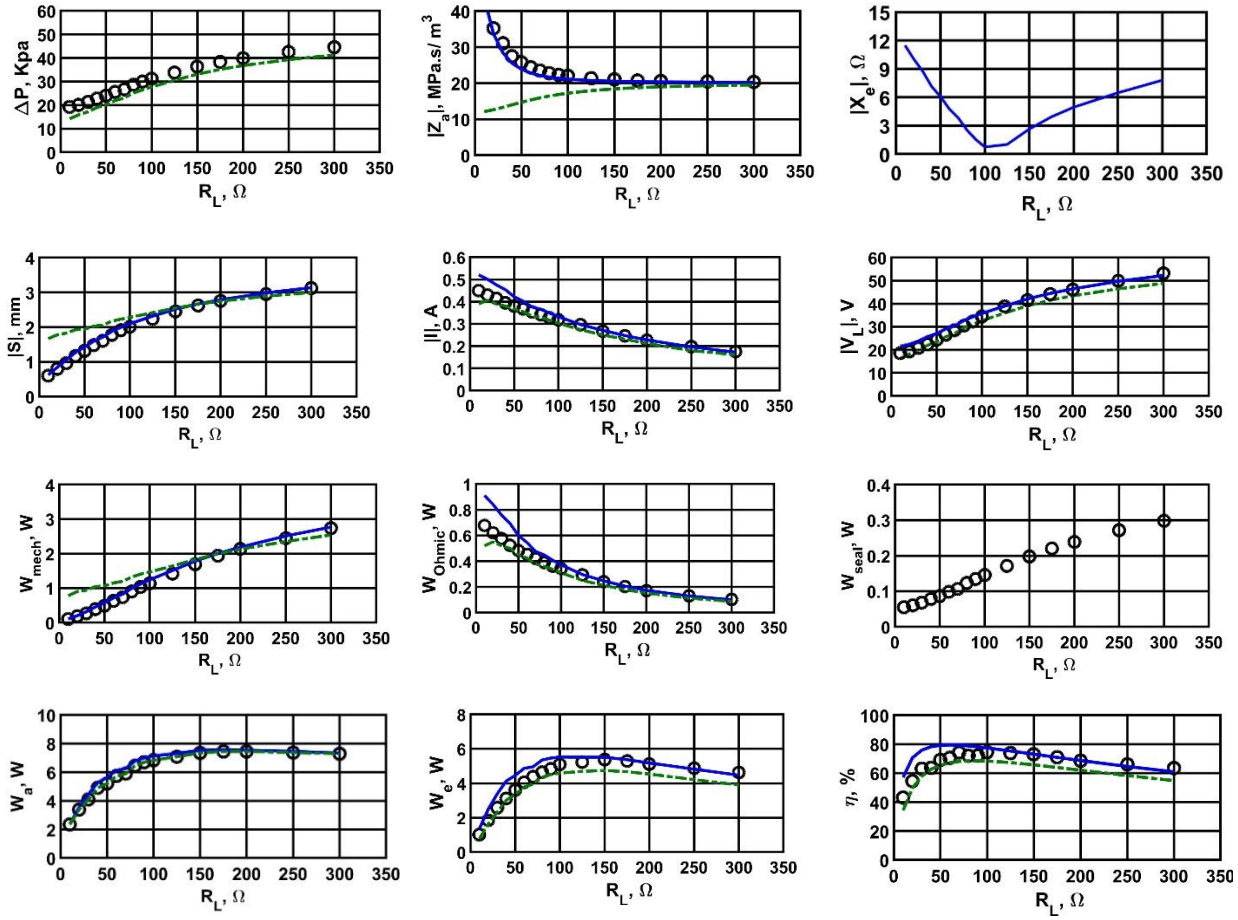

Figure 5-5. Linear alternator performance indices under simple load resistance range 100-300 Ω, This data is for a gas mixture consists of 60% helium/40% argon, 30 bar and dynamic pressure ratio 0.48% and an operating frequency of 56 Hz. The load is a simple resistance in series with a 71 μF power-factor-correcting capacitor. The circular symbol represents the experimental data, the solid blue line represents the analytical model results and the dashed green line represents the DELTAEC results.

Additionally, from Eq. (4-27), at constant operating frequency, constant power-factor-correcting capacitor and constant electric reactance it can be found that the mechanical stroke and the dissipated voltage in the load resistance are proportional, even with the change in the load resistance in this range. This is because the load resistance appears in the numerator and the

denominator of the relationship between the mechanical stroke and the dissipated voltage in the load, so the change in the load resistance has limited effect on this proportionality.

Conversely, from Eq. (4-21), the generated current is proportional to the mechanical stroke and inversely proportional with the load resistance. From the last two facts, the increase in the load resistance causes an increase in the dissipated voltage in the load resistance, and a decrease in the generated current.

The increase of the generated voltage with the load resistance, while the current decreases lead to an optimum load resistance for the maximum generated electric power, as estimated in Eq. (4-38).

Eq. 4-24 describes the dependence of the acoustic-to-electric conversion efficiency in the load resistance, which appears in the numerator and the denominator, causing a peak in the acoustic-to-electric efficiency with the load resistance, as estimated in Eq. 4-36.

It should be noted that the Eqs. 4-36 and 4-38 include the effects of the electric reactance, which varies with the mechanical stroke in this work, which should be taken into account when using these two equations at variable mechanical stroke.

From Eq. (4-18), the effect of the load resistance on the denominator of the acoustic impedance is greater than its effect of the numerator at small load resistance because the value of the load resistance is small relative to the *Bl* product. Thus the acoustic impedance decreases with the increase of the load resistance then reaches an almost constant value where the value of the load resistance is high.

The DELTAEC simulations results match the model and the experimental results very well at large load resistances. It is not clear why the DELTAEC under-estimate the acoustic impedance at low load resistance values.

5.1.6 Effects of power-factor-correcting capacitor

The effect of the power factor power-factor-correcting capacitor, whose value is the main factor in determining the value of the electric reactance, is significant and yields very important findings.

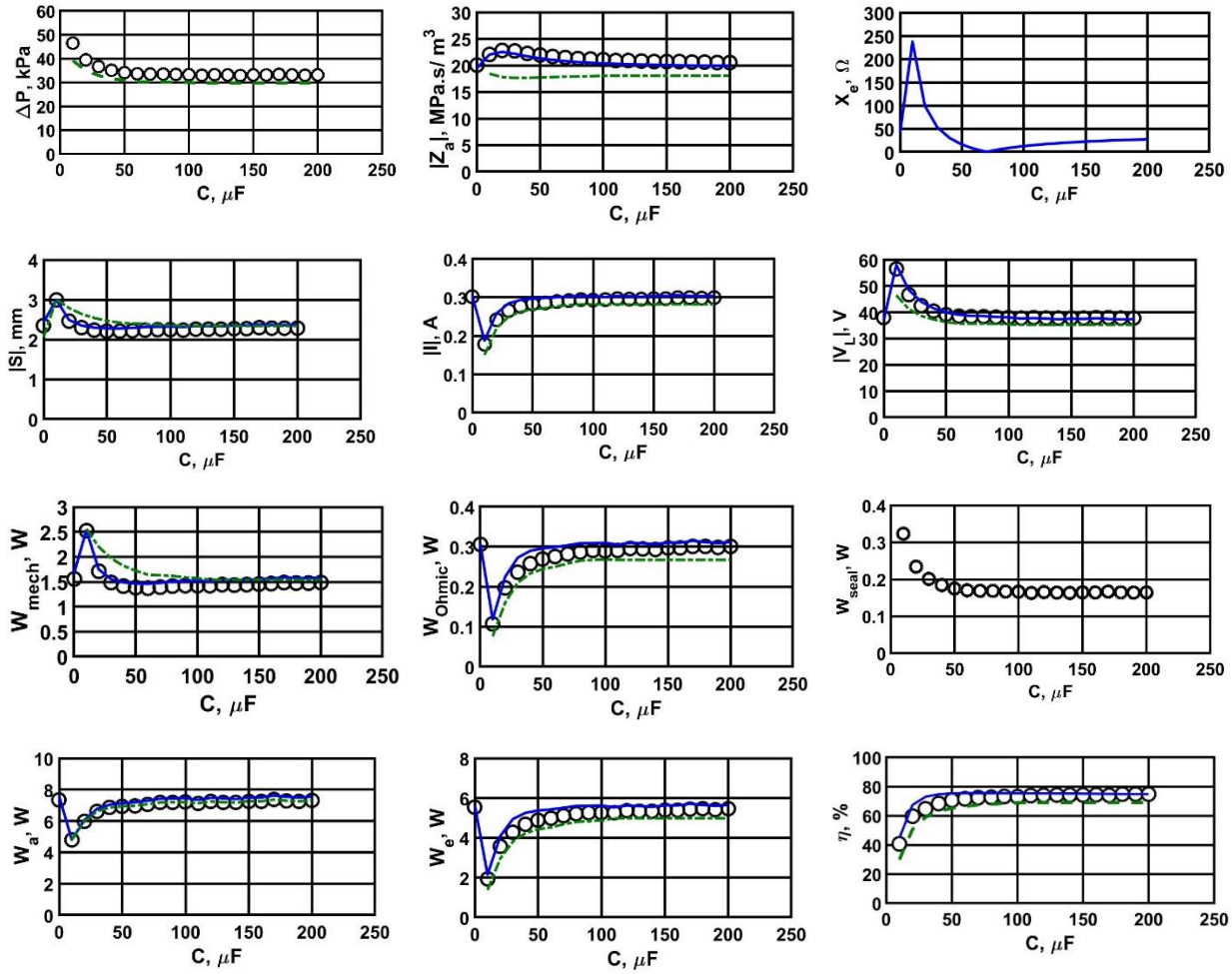

Figure 5-6. Linear alternator performance indices under power-factor-correcting capacitor range 0-204 μF, This data is for a gas mixture consists of 60% helium/40% argon, a mean gas pressure of 30 bar, dynamic pressure ratio 0.48% and an operating frequency of 56 Hz. The load is a 122- Ω resistance in series with the power-factor-correcting capacitor. The circular symbol represents the experimental data, the solid blue line represents the analytical model results and the dashed green line represents the DELTAEC results.

The first important finding shows that the different performance indices experience different increasing or decreasing behaviors. Increasing the power-factor-correcting capacitor in the linear load case and in the non-linear load case under the mentioned operating conditions in Table 5-1 and Table 5-3 causes a decrease in the magnitude of the electric reactance that causes a decrease in the mechanical stroke, dissipated voltage in the load, dynamic pressure difference across the piston of the linear alternator, fluid seal loss and the mechanical motion loss. On the

other hand, this decrease causes an increase in the generated current, the Ohmic loss, the absorbed acoustic power, the dissipated electric power in the load, the acoustic-to-electric conversion efficiency. Additionally, the acoustic impedance has a peak at certain value of the power-factor-correcting capacitor

The difference between the behaviors is largest when the deviation of the electric reactance from zero (resonance) is largest. It is worth noting that generated current, Ohmic loss, absorbed acoustic power, dissipated electric power in the load, acoustic-to-electric conversion efficiency are low values at the largest deviation of the electric reactance from zero despite of the large values of the mechanical stroke, dynamic pressure difference across the piston and the dissipated voltage in the load. This shows the significant effect of the electric reactance on the performance indices.

Eq.(4-20) shows that the mechanical stroke has a direct proportionality with the magnitude of the electric reactance thus the mechanical stroke decreases with the decrease of the magnitude of the electric reactance then starts to increase after the electric resonance point. On the other hand, Eq.(4-21), Eq. (4-22), Eq.(4-23) and Eq.(4-31) show that the generated current, absorbed acoustic power, the dissipated electric power in the load and the Ohmic loss have an inverse proportionality with the magnitude of the electric reactance that increases the denominator of these equations.

Equation (4-18) shows that the acoustic impedance is a function of the electric reactance that appear in the numerator and denominator of this equation. Thus, the effect of the change in the electric reactance on the acoustic impedance is not significant especially in the case of high values of the load resistance and the mechanical reactance that is the case of this work. The acoustic impedance has a peak at point of 20μF then it has a minor decrease over the increase of the power-facto-correcting capacitor.

Additionally, Eq. (4-1) reveals that the direct relationship between the mechanical stroke and the dynamic pressure difference across the piston of the linear alternator depends on the magnitude of the acoustic impedance as $|S|=|\Delta P|/(\omega*A*|Za|)$. From this relationship, it is clear that the mechanical stroke and the pressure difference display the same behavior when the operating frequency and the acoustic impedance are constants. This is supported by the results presented in Fig.5-6. Consquently, the dissipated voltage in the load (Eq. (4-27)), the mechanical

motion loss (Eq. (4-30)) and the fluid seal loss (Eq. (4-29)) have the same behavior of the mechanical stroke and the dynamic pressure difference across the piston.

From Eq.(4-27), it is worthy to note that the change in the value of the power-factor-correcting capacitor and the electric reactance does not affect the proportionality between the mechanical stroke and the dissipated voltage in the load as the change in the value of the power-factor-correcting capacitor affects the numerator and the denominator (electric reactance). Thus the dissipated voltage in the load display the same behavior of the mechanical stroke.

The second significant finding can be deduced from comparing the values of the different indices of the linear alternator's performance under different power-factor-correcting capacitors. The usage of a power-factor-correcting capacitor of 71 μF (point of electric resonance) demonstrates that this point enjoys high generated electric power and linear alternator's efficiency (Eq.(4-24)) accompanied by low operating mechanical stroke (Eq.(4-20)), mechanical motion loss and generated voltage with respect to points at off-electric resonance conditions.

It is important to notice that the mechanical motion loss is always significantly higher than the Ohmic loss under these working conditions. Thus, working at electric resonance greatly affects the sum of the mechanical-motion loss and the Ohmic loss. Moreover, the resonance case as shown in Fig. 5-6 requires acoustic power less than the points of the high values of the power-factor-correcting capacitor.

The parametric study under linear load condition is supported by the results of the analytical model and the DELTAEC simulations. The point of no power-factor correcting capacitor is not simulated by the DELTAEC because the impedance of the load in the DELTAEC cannot be purely real.

5.2 Experimental Parametric Study under Non-Linear Load

Testing the performance of the linear alternator under non-linear loading with different operating conditions is a unique type of testing, no researches are available about this kind before except our work on the Zener load as non-linear type of load [45]. As mentioned before the chosen non-linear load is a constant voltage DC load to simulate the condition of connecting the linear alternator with the Grid. The linear alternator is connecting with a power factor power-factor-correcting capacitor then to rectifier to convert the AC power to DC power to be suitable for the constant voltage DC load.

For the comparison between working under linear loading and non-linear loading, the basic case conditions of the non-linear load have the same pressure ratio of the basic case of the working under linear loading. Additionally the two basic cases enjoys very similar mechanical stroke values.

Table 5-3.Basic case operating factors and performance indices of the parametric study under non-linear load condition

Operation factor	**Nominal value**	**Operation factor**	**Nominal value**
A	0.60%	P_m	30 bar
V_{DC}	37- V	β	0.48%
C	65 μF	f	56 Hz
Performance index	**Nominal value**	**Performance index**	**Nominal value**
|S|	2.51 mm	$\|Z_a\|$	20.04 MPa. s/m^3
W_{mech}	1.77 W	W_{Ohmic}	0.77 W
| V |	44.7 V	|I|	0.53 A
W_e	6.48 W	W_a	10.5 W
η	61.7 %	W_{seal}	0.18 W
X_e	-0.56 Ω	X_m	80 N.s/m
$\| P_f \|$	14.4 kPa	|ΔP|	35 kPa

The value of the DC load voltage (basic case) is chosen to provide mechanical stroke value almost equals the mechanical stroke value of the basic case of the working under linear loading

This section introduces an illustration for the behavior of the linear alternator under the non-linear loading and a comparison between this performance and the performance of the linear alternator under the linear loading. Table 5-3, shows the basic case operating conditions that are identical to the operating conditions under linear load, except for the load variables.

5.2.1 Effects of operating frequency

The experimental data of the operating frequency is limited up to 58 Hz to avoid the vibrations in the experimental setup. The nature of the constant voltage DC load forces the linear alternator to reach the set voltage on the DC electronic load (37 V in this case).

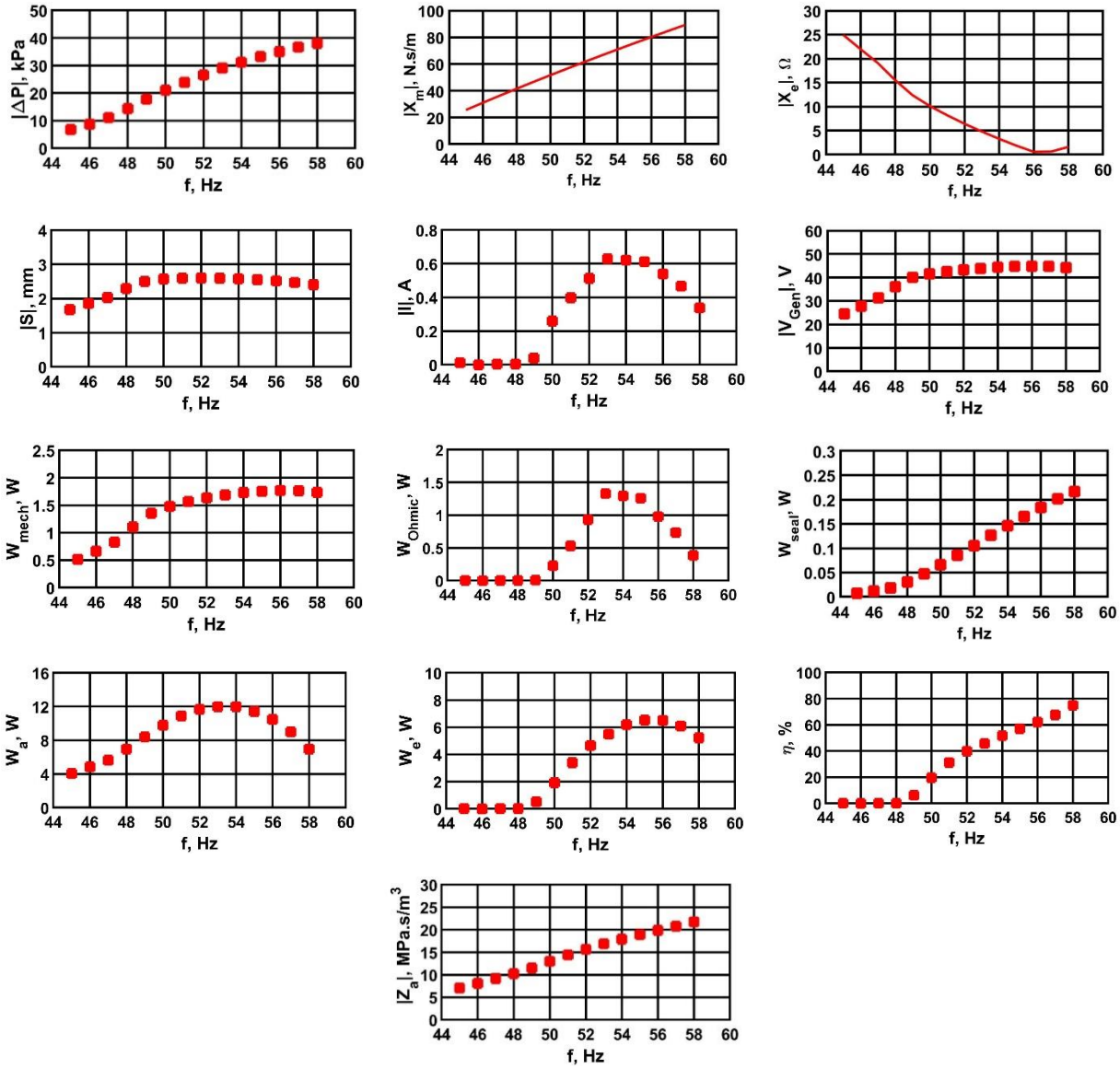

Figure 5-7. Linear alternator performance indices under frequency range 40-58 Hz, this data is for a gas mixture consists of 60% helium/40% argon, a mean gas pressure of 30 bar and dynamic pressure ratio 0.48%. The load consists of a rectifier in series with a 65 μF power-factor-correcting capacitor then connected with a 37V constant voltage DC-load.

The increase in the operating frequency produces a rise in the absorbed acoustic power, most of which is consumed to increase the generated voltage of the linear alternator. Thus, at low frequencies (45-49 Hz) and at the specified input dynamic pressure ratio, the generated current is almost zero.

The equations of the algebraic model are descriptive for the main relationships between the linear alternator performance indices despite the difference in the nature of the load.

In the linear load case under different operating frequencies, as shown in Fig. (5-1), the change in the mechanical stroke was significant; thus, the absorbed acoustic power, generated current, dissipated electric power and voltage in the load feature the same peak point of the mechanical stroke. This is not applicable in the non-linear load case because working under constant DC voltage will minimize the change in the mechanical stroke after achieving the targeted DC load voltage. The relationship between the mechanical stroke and the generated voltage can be demonstrated by Eq. (4-12) as $|V|=Bl^{*}\omega*|S|$, as illustrated in detail in Sec (5.1.5).

From Eqs. (4-21), (4-22), (4-23) and (4-27), the generated current, absorbed acoustic power, dissipated electric power, and dissipated voltage in the load increase with the increase in the operating frequency and the decrease in the magnitude of the electric reactance. This accounts for the negligible increase in the generated voltage after achieving the targeted DC load voltage.

This is also the case in the pressure difference across the piston of the linear alternator which increases according to the operating frequency and with the decreasing magnitude of the electric reactance, Eqs. (4-19) and (4-20). Similarly, the acoustic impedance and the fluid seal loss increase according to of the pressure difference across the piston of the linear alternator.

In contrast, the mechanical stroke features an inverse proportionality with the operating frequency and direct proportionality with the magnitude of the electric reactance thus the mechanical stroke starts to decrease at low magnitude of the electric reactance and this explains the decrease in the absorbed acoustic power that is a function of volume velocity. Additionally, the mechanical motion loss features a different peak as the effect of the increasing operating frequency overcomes that of the insignificant decline in the mechanical stroke, Eq. (4-30).

As previously illustrated, the peak of the mechanical stroke (52 Hz), does not represent the point of the electric resonance. Conversely, it can be observed that the peak of the generated voltage indicates the electric resonance, at 56 Hz.

The perfect operation point under non-linear loading from the operating frequency perspective is the point of 56 Hz, which offers the advantages of maximum generating power with acceptable efficiency and suitable total loss and mechanical stroke.

The comparison between the linear load and the non-linear load at the same pressure ratio and semi equal operating mechanical stroke (|S|=2.2 mm in the linear load case and |S|= 2.5 mm in the non-linear load case), yields several significant findings.

As shown in Fig.5-7, the first significant finding is that, at a frequency of 54 Hz, the non-linear load consumes 12 W of the acoustic power to produce 6 W of electric power. In contrast, at the same frequency (54 Hz) under linear loading, the linear alternator consumes 8W of the acoustic power to produce the same value of the electric power as shown in Fig.5-1. In general, from comparing the values of the acoustic-to-electric conversion efficiency in Fig.5-1 and Fig. 5-7 it can be noticed that operating under the linear loading is more efficient than operating under the non-linear loading for a wide range of operating frequencies.

The second remarkable finding is that the value of the generated current and the Ohmic loss in the non-linear loading case is much higher than in the case of the linear loading while the mechanical motion loss under the two types of loads is almost the same . Thus, testing the linear alternator under an insignificant amount of total losses calls for operating under linear loading.

The third finding is that the acoustic impedance of the linear alternator under the previous specified conditions is almost the same. It is worthy to note that the mentioned differences between the two types of loads are valid under the stated operating conditions in Table 5-1 and Table 5-3.

5.2.2 Effects of the input dynamic pressure ratio

Figure (5-8) demonstrates the effect of the input dynamic pressure ratio on the performance indices of the linear alternator under non-linear loading.

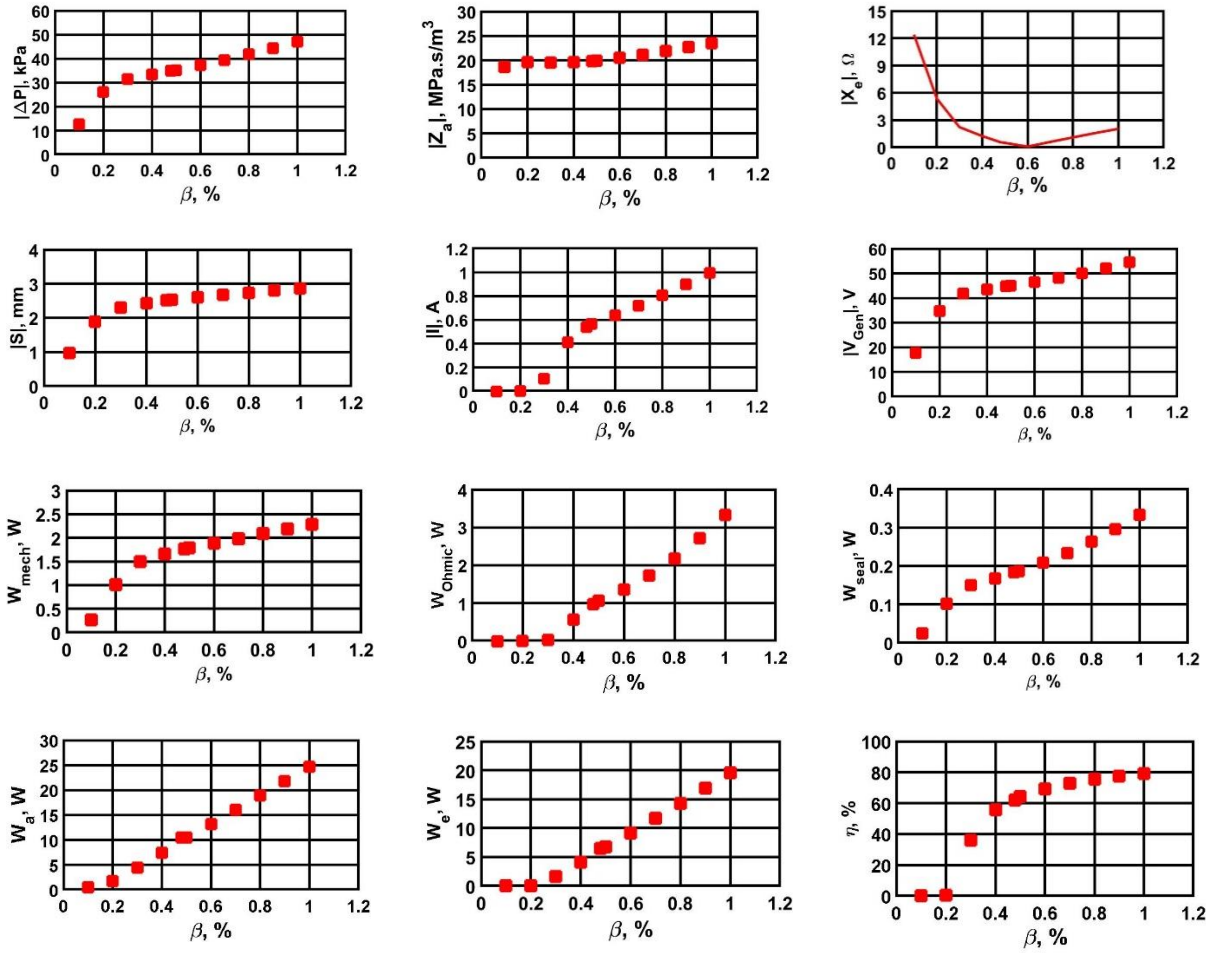

Figure 5-8. Linear alternator performance indices under dynamic pressure ratio range 0.1-1 %, This data is for a gas mixture consists of 60% helium/40% argon, a mean gas pressure of 30 bar and an operating frequency of 56 Hz. The load consists of a rectifier in series with a 65 μF power-factor-correcting capacitor then connected with a 37V constant voltage DC-load.

As previously illustrated in Sec (5.1.2), the increase in the pressure ratio results in an increase in the dynamic pressure difference across the linear alternator‘s piston. This increase causes an increase in the performance indices with different degrees. Additionally, the increase in the pressure difference causes an increase in the mechanical stroke that causes an increase in the electric reactance, as described in Sec. (4.1.2). The change in the value of the electric reactance affects some of the performance indices. The electrical reactance behaves as before.

The relationships between mechanical stroke, mechanical motion loss, generated voltage and the dynamic pressure difference across the linear alternator‘s piston on the one hand and the

input dynamic pressure ratio on the other are different than the same relationships in the linear load case. This difference can be easily recognized by comparing these relationships in Fig (5-2) and in Fig (5-8).

The nature of the DC load is the main cause of this difference as DC load focuses on achieving the targeted DC voltage (37 V) by limiting the increase in the generated voltage and allowing the increase in the generated current. Thus, the rate of increase in the generated voltage after achieving the target DC voltage is small over the increase in the input dynamic pressure ratio. This small rate of increase affects the increase of the mechanical stroke as shown in Eq.(4-12).

The dynamic pressure difference across the linear alternator's piston mechanical motion loss are affected by the change of the mechanical stroke as shown in Eq. (4-18) and Eq. (4-30).

The increase in the dynamic pressure difference over the increase in the input dynamic pressure ratio is more the than the increase in the mechanical stroke over the increase in the input dynamic pressure ratio. This is because the dynamic pressure difference is a function of the P_{res} and the mechanical stroke (Eq. 4-19) which increase with the increase of the input dynamic pressure ratio.

Regarding the acoustic impedance (Eq. 4-1), it increases because the increase in the dynamic pressure difference is more than the increase of the mechanical stroke.

Regarding seal loss, it is a function of the maximum pressure difference across the piston of the linear alternator, so it always has the same behavior of the pressure difference.

The acoustic-to-electric conversion efficiency increases with the increase in the input dynamic pressure ratio because of two reasons. The first significant one is that the rate of the increase in the generated electric power is more than the rate of increase in the absorbed acoustic power. The second reason is the decrease in the magnitude of the electric reactance (Eq.(4-24)).

The main differences between operation under linear loading and non-linear loading are mentioned in Sec. 5.2.1. These differences are mainly valid at β =0.48% as at high input dynamic pressure ratio (β=1) the working under non-linear loading is more efficient than working under linear loading as shown in Fig.5-2 and Fig.5-8 ((η) =71 % in the linear load case on the other hand (η) =79.2 % in the non-linear load case). Additionally, it can be found that over the studied range of input dynamic pressure ratios, the generated current, generated electric power and the

Ohmic loss are higher in the case of the non-linear load. These performance indices significantly increase with the increase of the input dynamic pressure ratio.

5.2.3 Effects of mean gas pressure

From the experience with linear loading and from the fact of at low mean gas pressure the absorbed acoustic power is low and this not effective in the case of set DC Voltage of 37 V with operating pressure ratio of 0.48%. Thus, the experimental data were acquired at range of (25-35 bar).

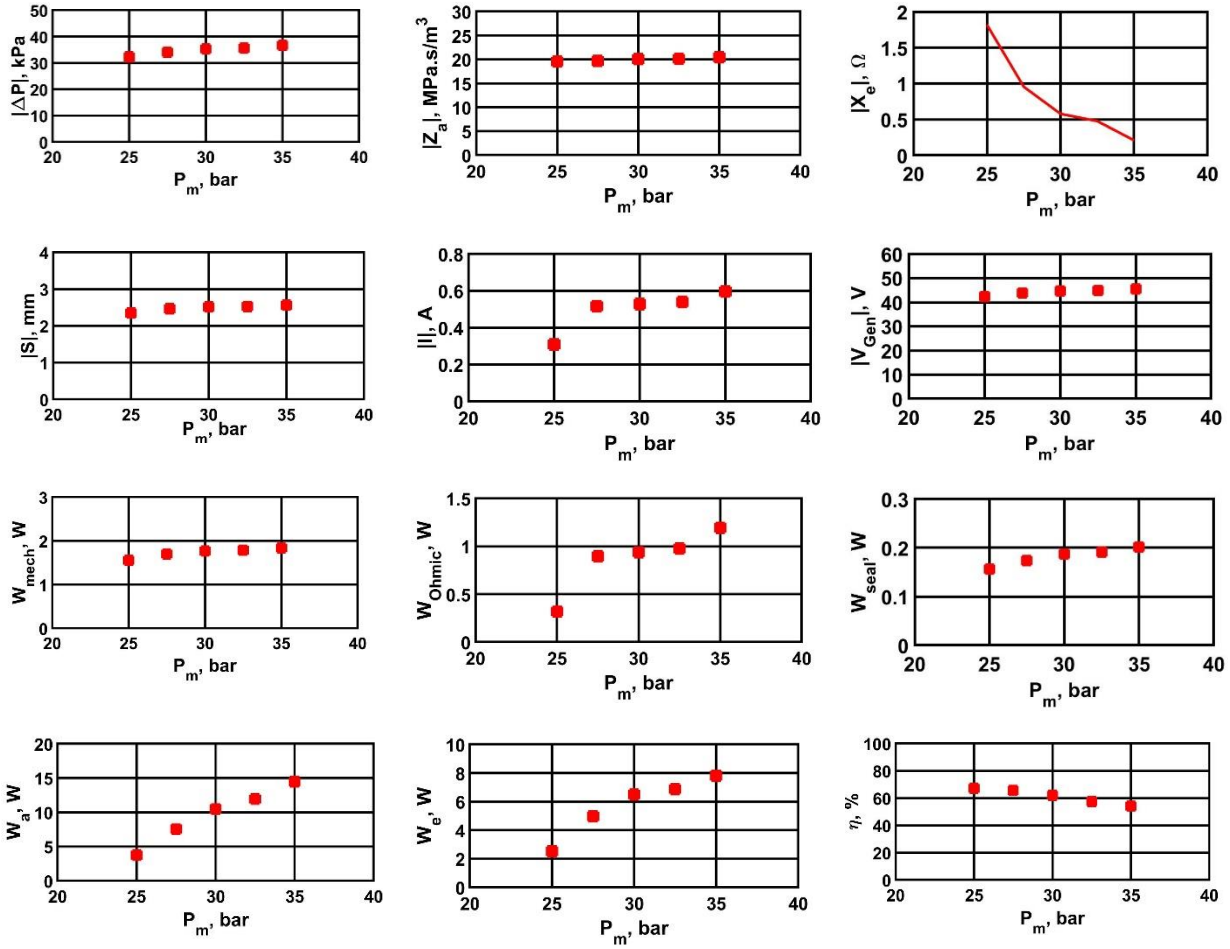

Figure 5-9. Linear alternator performance indices under mean gas pressure range 25-35 bar, This data is for a gas mixture consists of 60% helium/40% argon, dynamic pressure ratio 0.48% and an operating frequency of 56 Hz. The load consists of a rectifier in series with a 65 μF power-factor-correcting capacitor then connected with a 37V constant voltage DC-load.

Such as in the previous case of working under different input pressure ratios, the DC voltage load controls the change in the main performance indices.

Over a short range of mean gas pressures (25-35 bar), the absorbed acoustic power increases significantly. In spite of this increase, the DC voltage load experiences a small change and forces the mechanical stroke and the pressure difference across the linear alternator's piston to experience a small change in their values.

Fig (5-9) reveals the main consequences of the mentioned phenomena. The increase in the acoustic power is converted to an increase in the generated current under the small change in the absorbed voltage in the load. Which causes an increase in the generated electric power but the rate of increasing of the generated electric power is less than the rate of increasing in the acoustic power. Thus, the acoustic-to-electric conversion efficiency decreases as the mean gas pressure increases. From the perspective of generating a maximum electric power, working at high mean gas pressure is very useful. Conversely, working at low mean gas pressure has the advantage of high efficiency of the linear alternator.

The main differences between operation under linear loading and non-linear loading under the stated operating conditions in Table 5-1 and Table 5-3 are mentioned in Sec 5.2.1. These differences are valid over the studied range of the mean gas pressures as shown in Fig.5-3 and Fig.5-9. The operation under linear loading still has the same merits of higher efficiency and lower total loss over the operation under non-linear loading. On the other hand, the operation under non-linear loading produces higher generated electric power.

5.2.4 Effects of gas mixture

As illustrated in detail in Sec (5.2.4), the increase of the helium molar fraction in a gas mixture consists of helium and argon causes an increase in the speed of sound in the mixture that causes an increase in the absorbed acoustic power, the dynamic pressure difference across the piston of the linear alternator, and thus mechanical stroke.

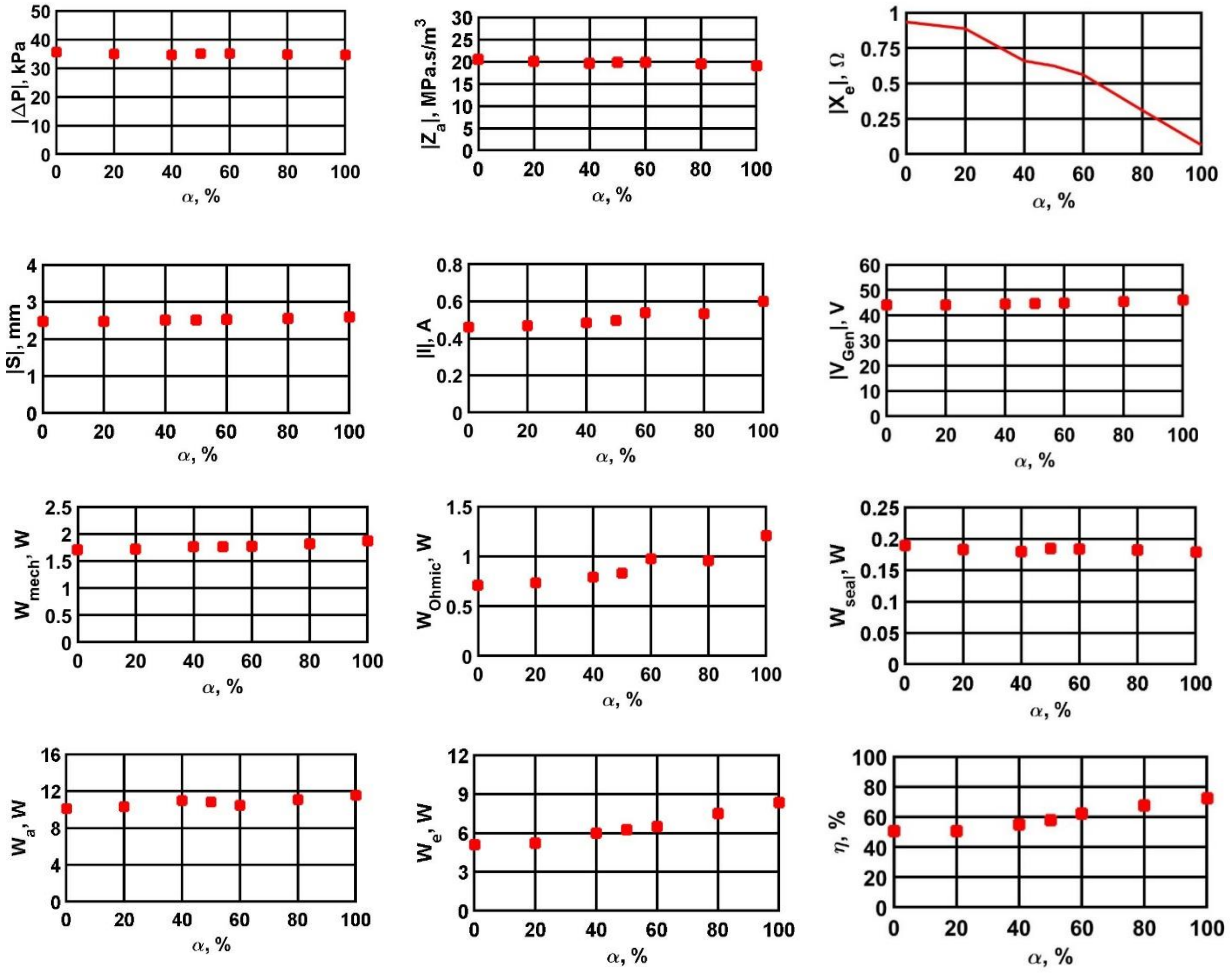

Figure 5-10. Linear alternator performance indices under helium molar fraction range 0-100 %, This data is for a mean gas pressure of 30 bar and dynamic pressure ratio 0.48% and an operating frequency of 56 Hz. The load consists of a rectifier in series with a 65 μF power-factor-correcting capacitor then connected with a 37V constant voltage DC-load.

The most of the increase of the absorbed acoustic power is converted to an increase in the generated current because the linear alternator is able to achieve the set DC load voltage (37 V) under these working conditions.

The nature of the constant DC voltage load affects the generated voltage that affects the mechanical stroke (Eq.(4-12) and the dynamic pressure difference across the piston of the linear alternator (Eq.(4-19)). Thus the increase factor (1.046) of the mechanical stroke over the range

of the change in the helium molar fraction from 0% to 100% is small in this case compared to the linear load case (1.22). Thus, the increase in the most of the performance indices is small compared to the linear load case.

The rate of the increase in the generated electric power (1.64) is more than the rate of the increase in the absorbed acoustic power (1.15) thus the acoustic-to-electric conversion efficiency increases. On the other hand, the increase in the pressure difference across the piston and the mechanical stroke is almost the same thus the acoustic impedance is almost constant. These observations are summarized in the Table 5-2 below.

Table 5-4.The increase factors of the main performance indices over the change in the helium molar fraction

Performance index	Value of the index at α = 0%	Value of the index at α = 100%	Ratio between two values
(|S|), mm	2.47	2.58	1.046
(W_{mech}), W	1.7	1.86	1.096(=1.046^2)-(Eq.4-30)
(W_a), W	10.07	11.55	1.147
(|I|), A	0.46	0.6	1.303
(W_{Ohmic}), W	0.71	1.2	1.69(=~1.3^2)- (Eq.4-31)
($\|V_L\|$), V	43.97	45.96	1.045-(Eq.(4-12)
(W_e), W	5.07	8.34	1.64

The main differences between operation under linear loading and non-linear loading under the stated operating conditions in Table 5-1 and Table 5-3, are mentioned in Sec 5.2.1. These differences are valid over the studied range of the gas mixtures as shown in Fig.5-4 and Fig.5-10. The operation under linear loading still has the same merits of higher efficiency and lower total loss over the operation under non-linear loading. On the other hand the operation under non-linear loading produces higher generated electric power.

5.2.5 Effects of DC load Voltage

The increase in the value of the DC load voltage causes an increase in the mechanical stroke (Eq. (4-12) that causes an increase in the absorbed acoustic power (Eq.(4-22)) and the pressure difference across the piston of the linear alternator (Eq.(4-19)).

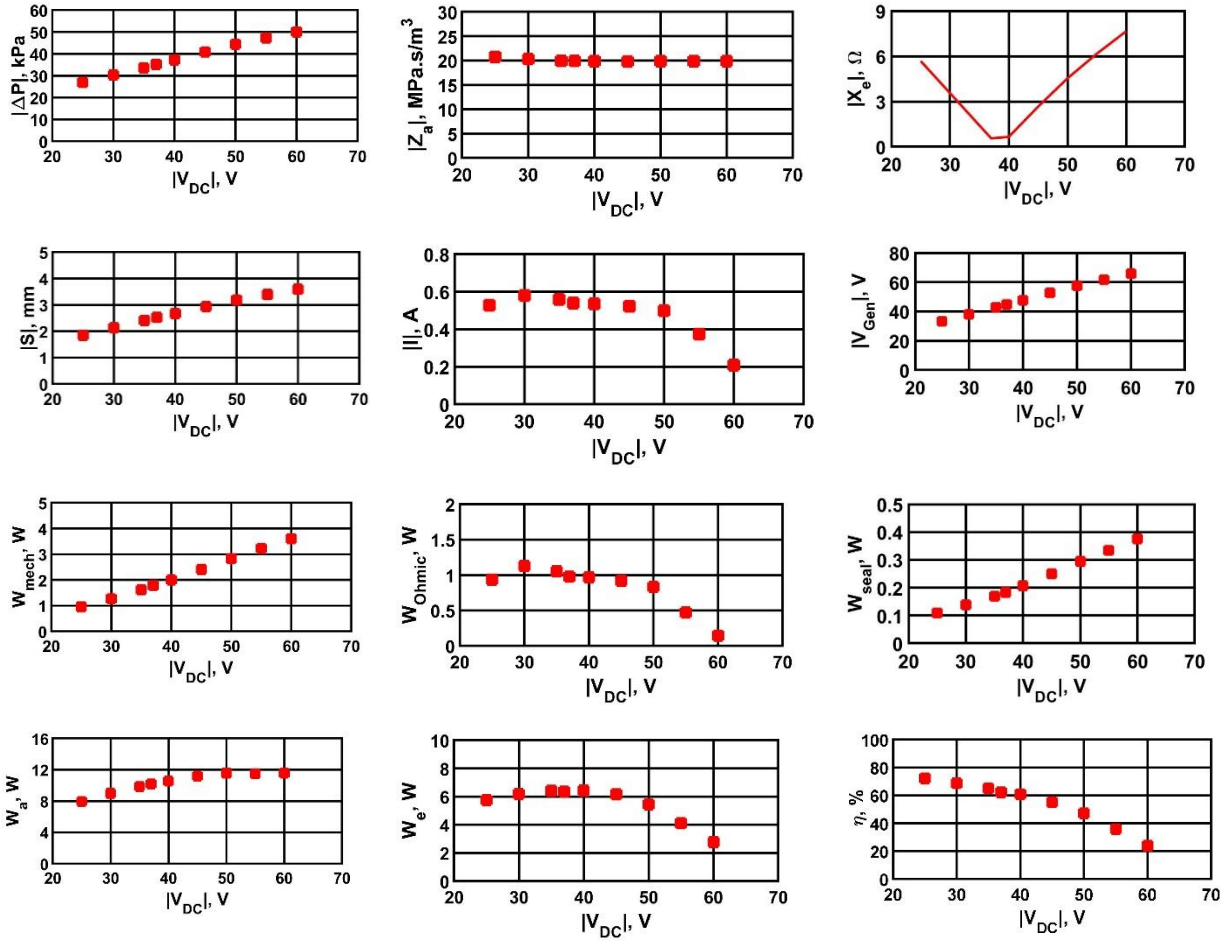

Figure 5-11. Linear alternator performance indices under constant voltage DC-load range 30-60 V, This data is for a gas mixture consists of 60% helium/40% argon, 30 bar and dynamic pressure ratio 0.48% and an operating frequency of 56 Hz. The load consists of a rectifier in series with a 65 μF power-factor-correcting capacitor then connected with a constant voltage DC-load.

The increase of the set voltage consumes the increase of the absorbed acoustic power. Thus, the generated current decreases with the increase in the set voltage.

The decrease in the generated current is more than the increase in the generated voltage. Thus, the generated electric power and the acoustic-to-electric conversion efficiency decreases.

It is worthy to note that the acoustic impedance under different DC load voltage is constant. The main cause is that the generated voltage is the main cause for changing the mechanical stroke and the pressure difference across the piston of the linear alternator as shown in Eq.(4-12) and

Eq.(4-19) thus, the percentage of the change is the same for the mechanical stroke and the pressure difference across the piston of the linear alternator.

The main differences between operation under linear loading and non-linear loading are mentioned in Sec 5.2.1.These differences are valid under the stated operation conditions in Table 5-1 and Table 5-3.These differences cannot be achieved over the studied load range due to the difference in the natures of the two types of loads.

5.2.6 Effects of power-factor-correcting capacitor

The value of the power-factor-correcting capacitor dramatically influences the value of the electric reactance. After connecting a low value power-factor-correcting capacitor the magnitude of the electric reactance decreases until the point of the electric resonance (65 µF) then it starts to increase. Thus, as shown in (Eq. 4-20) and as presented in Fig (5-12), the mechanical stroke experiences a decrease before the electric resonance point then an increase after the resonance point.

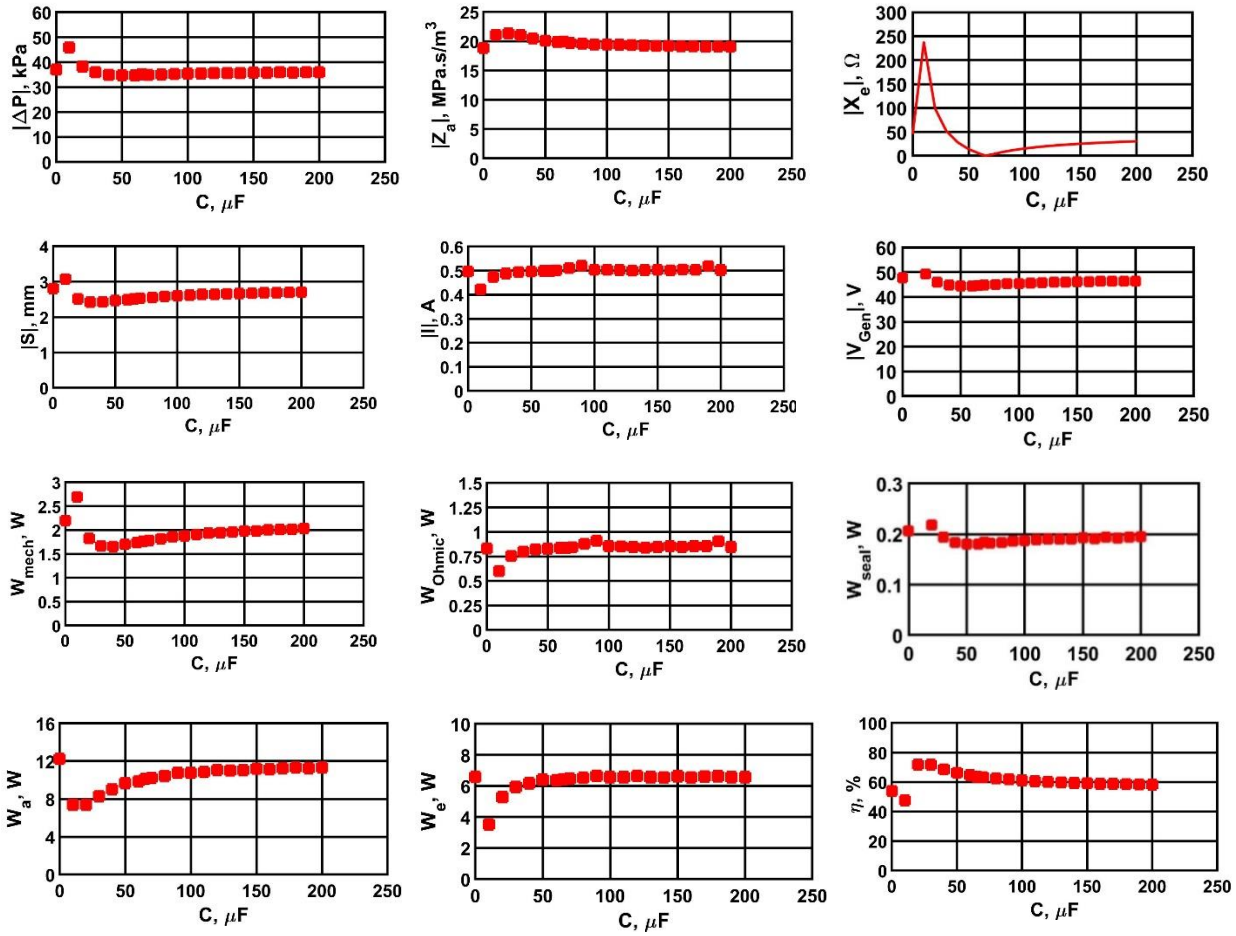

Figure 5-12. Linear alternator performance indices under power-factor-correcting capacitor range 0-204 µF, This data is for a gas mixture consists of 60% helium/40% argon, a mean gas pressure of 30 bar, dynamic pressure ratio 0.48% and an operating frequency of 56 Hz. The load consists of a rectifier in series with a power-factor-correcting capacitor then connected with a 37V constant voltage DC-load.

The performance indices of the linear alternator in the non-linear load case display the same behavior as in the linear load case over the change in the electric reactance and the power-factor-correcting capacitor.

Equation (4-18) shows that the acoustic impedance is a function of the electric reactance that appears in the numerator and denominator of this equation. Thus, the effect of the change in the electric reactance on the acoustic impedance is not significant especially in the case of high values of the load resistance and the mechanical reactance that is the case of this work. The acoustic impedance has a peak at point of 20 μF then it has a minor decrease over the increase of the power-facto-correcting capacitor.

Additionally, Eq. (4-1) reveals that the direct relationship between the mechanical stroke and the dynamic pressure difference across the piston of the linear alternator depends on the magnitude of the acoustic impedance as $|S|=|\Delta P|/(\omega * A * |Za|)$. From this relationship, it is clear that the mechanical stroke and the pressure difference display the same behavior when the operating frequency and the acoustic impedance are constants. This is supported by the results presented in Fig.5-6.Consquently, the mechanical motion loss (Eq. (4-30)) and the fluid seal loss (Eq. (4-29)) have the same behavior of the mechanical stroke and the dynamic pressure difference across the piston.

From Eq.(4-22), it is clear that the absorbed acoustic power has an inverse proportionality with the square of the magnitude of the acoustic impedance. This can explain the severe increase of the absorbed acoustic power with the decrease of the magnitude of the acoustic impedance. The DC electronic load converts the increase in the absorbed acoustic power after achieving the set voltage point into an increase in the generated current. Thus, the generated current, the Ohmic loss (Eq. (4-31)) and the dissipated electric power in the load Eq.(4-23) increase over the increase of the power-factor-correcting capacitor.

Additionally, Eq. (4-12) reveals that the generated voltage has a direct proportionality with the mechanical stroke. Thus, they display the same behavior.

From studying the point of the electric resonance (65 μF) under non-linear loading, it is clear that, it is not the point of the maximum efficiency, unlike the linear case.

But from the perspective of the total losses and the absorbed acoustic power, generated electric power and operating mechanical stroke, it can be found that this point has the merits of maximum generated electric power with average absorbed acoustic power, and the point of minimum total losses with low operating mechanical stroke, but an efficiency lower than the maximum efficiency.

The main differences between operation under linear loading and non-linear loading under the stated operating conditions in Table 5-1 and Table 5-3 are mentioned in Sec 5.2.1.These differences are valid over the studied range of the power-factor-correcting capacitors as shown in Fig.5-6 and Fig.5-12. The operation under linear loading still has the same merits of higher efficiency and lower total loss over the operation under non-linear loading. On the other hand the operation under non-linear loading produces higher generated electric power.

5.3 Summary of Parametric Study Results

In conclusion, the operating frequency in the linear load case affects the electric reactance, the mechanical reactance and the radial frequency of the linear alternator, thus, it affects the absorbed acoustic power and the matching between the linear alternator on one side and the thermoacoustic engine and the load on the other side. The operating frequency has different effects on the performance indices. All the performance indices show a peak at the mechanical resonance frequency (54 Hz) (Fig. 5-1), except the dynamic pressure difference across the piston and the seal loss, which show a peak at the free-damping frequency (56 Hz); the conversion efficiency and the acoustic impedance which both show a monotonic increase; and the electric reactance magnitude which decreases down to zero at the electric resonance point and then increases. It should be noticed that there is no single frequency that achieves the optimum performance in all indices.

In the non-linear load case, the generated current, Ohmic loss, dissipated electric power in the load, the absorbed acoustic power and the acoustic-to-electric conversion efficiency are very small or nearly zero at the low operating frequencies. At higher frequencies, the acoustic-to-electric conversion efficiency has a monotonic increase, while the remaining four indices have a peak at nearly 54 Hz. The dynamic pressure difference, fluid seal loss, and acoustic impedance have monotonic increase. The mechanical stroke and the generated voltage both increase till the set point and then remain almost constant. The electrical reactance behaves as before.

Increasing the input pressure ratio in the linear load causes an increase in all the performance indices, except the acoustic impedance and the acoustic-to-electric conversion efficiency, which are almost constant; and the electric reactance magnitude which decreases down to zero at the electric resonance point and then increases. In the non-linear load, all the performance indices increase except the electric reactance which behaves as in the linear load.

Increasing the mean gas pressure causes all the performance indices to increase in the linear load, except the acoustic impedance and the efficiency which remain constant as model data and there is a small change in the experimental data. For the model data this is because the dimensionless Wakeland [77] number, $\beta = (Bl)^2/(R_m r_e)$ remains unchanged. In the non-linear load, the increase in the mean gas pressure causes all the performance indices to increase,

except the acoustic impedance which is almost constant and the efficiency which decreases slightly. In both loads, the electric reactance behaves as before.

Increasing the helium molar fraction in the linear load causes an increase in the speed of sound in the mixture, which causes an increase in the absorbed acoustic power by the linear alternator, thus, all the values of the performance indices increase with the increase of the helium molar faction in the gas mixture, except the acoustic impedance and the conversion efficiency which are almost constant. In the non-linear load, all the indices increase, except the pressure difference across the piston (and hence the seal loss) and the acoustic impedance which remain almost constant. In both loads, the electric reactance behaves as before.

Increasing the load resistance in linear load case causes a monotonic increase in the dissipated voltage in the load, the mechanical stroke, the pressure difference across the linear alternator, the mechanical motion loss and the fluid seal loss. On the other hand, the generated current and the Ohmic loss experience a monotonic decrease. The acoustic impedance decreases at low values of the load resistance while at high values it is almost constant. Moreover, the load resistance exists in the numerator and the denominator of the absorbed acoustic power, dissipated electric power in the load and acoustic-to-electric conversion efficiency thus there is certain optimum load resistance that achieves the peak of the each of these performance indices. The electric reactance behaves as before.

Increasing the DC load voltage in the non-linear load case causes an increase in the mechanical stroke that causes an increase in the absorbed acoustic power, the pressure difference across the piston of the linear alternator and the seal loss. The increase of the set voltage consumes the increase of the absorbed acoustic power. Thus, the generated current decreases with the increase in the set voltage. Consequently, the Ohmic loss, the dissipated electric power in the load and the acoustic-to-electric conversion efficiency decrease. The acoustic impedance under different DC load voltages is constant. The electric reactance behaves as before.

Increasing the power-factor-correcting capacitor in the linear load case and in the non-linear load case under the mentioned operating conditions in Table 5-1 and Table 5-3 causes a decrease in the magnitude of the electric reactance that causes a decrease in the mechanical stroke, dissipated voltage in the load, dynamic pressure difference across the piston of the linear alternator, fluid seal loss and the mechanical motion loss. On the other hand, this

decrease causes an increase in the generated current, the Ohmic loss, the absorbed acoustic power, the dissipated electric power in the load, the acoustic-to-electric conversion efficiency. Additionally, the acoustic impedance has a peak at certain value of the power-factor-correcting capacitor. It is worth noting that the point of the electric resonance enjoys high generated electric power and linear alternator's efficiency accompanied by average absorbed acoustic power and low operating mechanical stroke, mechanical motion loss and generated voltage with respect to the other points at off-electric resonance conditions. The electric reactance behaves as before.

The comparison between the linear load and the non-linear load at the same pressure ratio, same operating frequency, and semi equal mechanical strokes, yields several significant findings. First, operating under the linear load is more efficient with less amount of the losses at low input dynamic pressure ratios. Second, at low input dynamic pressure ratios under non-linear load yields higher generated electric power and consumes more absorbed acoustic power.

6. Sensitivity Analysis

The fact that a thermoacoustic power converter consists of a thermoacoustic engine, a linear alternator and an electric load makes the linear alternator a very critical part that must be well matched both to the thermoacoustic engine and to the electric load. This matching affects both the thermal-to-acoustic and the acoustic-to-electric conversion efficiencies as well as the output power of the thermoacoustic power converter.

This mid position of the linear alternator make its selection, customization and the selection of its operating parameters a difficult and critical task that may improve some of the mechanical performance indicators at the expense of the electrical indicators, or vice versa.

For this reason, the current work presented an analytical model and a parametric study to fully understand how the operating factors affect the performance of the linear alternator.

Now, this chapter employs the technique of sensitivity analysis to determine how a certain small deviation in the values of the operating factors from a known reference condition quantitatively affects the response of the system.

This sensitivity analysis is very useful to properly select the operating factors if the design or operation does not allow simultaneous achievement of all the factors required for ideal operation and deviations in certain operating factors away from the values that optimize certain performance indices become inevitable; or, if during actual operation minor changes in any of the operating factors unavoidably take place, causing effects on the performance indices. Additionally, this analysis increases the understanding of the relationships between the operating factors and the system response and thus allows optimization of a certain performance index by targeting the operating factor(s) that affects it the most with minimum changes in other operating factors. Furthermore, this analysis makes it possible to assess the effects of uncertainties in the operating factors on each of the performance indices.

In this work, the linear load consists of a resistance (nominal value of 122 Ω, rated power of 350 W, supplied by Ohmite) preceded by a power-factor correcting capacitor that corrects for the alternator inductance (polypropylene film capacitor, run type, maximum operating voltage of 450 V, a capacitance of 71-μF). The purpose and effects of the power-factor-correcting capacitors on the overall performance of the linear alternator has been discussed in detail [44].

In this work, the values of the power-factor-correcting capacitors and the operating frequency are constant to achieve the electric and the mechanical resonance. The sensitivity analysis carried-out on the linear loads considers four operating factors, namely: the helium molar fraction (α), the mean gas pressure (P_m), the load resistance (R_L) and the input dynamic pressure ratio (β).

These factors are the most significant factors used to optimize the performance of thermoacoustic power converters.

The system response to ± 10% changes in these four operating factors around a set of given conditions (hereinafter known as the reference experiment) is characterized via certain key performance indices, namely the amplitudes of ten selected performance indices. These performance indices are the mechanical stroke amplitude ($|S|$), the generated current ($|I|$), the dissipated voltage in the load ($|V_L|$), the mechanical-motion loss (W_{mech}), the Ohmic loss (W_{Ohmic}), the fluid-seal loss (W_{seal}), the absorbed acoustic power (W_a), the generated electric power (W_e), the acoustic-to-electric conversion efficiency (η) and the acoustic impedance amplitude ($|Z_a|$) .

Table 6-1 shows the conditions of the reference experiment and the nominal values of the four operating factors and the nominal values of the ten performance indices for this study

The role of the reference experiment in this work is to set the range of nominal values of the four operating factors.

Then, based on the nominal values of the factors used in the reference experiment, the design-of-experiment methodology is utilized to systematically and efficiently set a scheme for 2^n experiments, where n is the number of factors considered in the analysis under full-factorial layout [79]. Data collected according to this design-of-experiment scheme allows for the efficient estimation of how the factors and *their combined interactions* affect the response variables (the ten performance indices in this work).

The sensitivity analysis of the four operating factors on the linear alternator performance indices is carried-out to reveal the impact of the ±10% variations in the nominal values of the operating factors on the ten linear alternator performance indices.

This analysis assumes the absence of any significant nonlinear behavior in the ±10% range around the nominal values. The validity of the results is limited to and around the nominal values of the reference experiment.

Table 6-1.Nominal values of the factors and performance indices in the reference experiment used for linear loading condition.

Factor studied	**Nominal value**	**Performance index**	**Nominal value**
Helium molar fraction, α	0.60	Mechanical stroke amplitude, $\|S\|$	2.2 mm
		Acoustic impedance amplitude, $\|Z_a\|$	21.5 Mpa. s/m^3
Mean gas pressure, P_m	30 bar	Dissipated voltage in the load amplitude, $\|V_L\|$	38 V
		Generated current amplitude, $\|I\|$	0.3 A
Input pressure ratio to the linear alternator, β	0.48%	Mechanical motion loss, W_{mech}	1.4 W
		Ohmic loss, W_{Ohmic}	0.3 W
Load resistance, R_L	122 Ω	Fluid seal loss, W_{seal}	0.1 W
		Absorbed acoustic power, W_a	7.0 W
Factors kept constants		Dissipated electric power in the load, W_e	5.0 W
Operating frequency, f	56 Hz	Acoustic-to-electric conversion efficiency, η	71.3 %
Power-factor-correcting capacitor, C	71 μF		

In this work, the experimental conditions used in the reference experiment are selected to be close to the conditions typically encountered in thermoacoustic power conversion, which typically are in the frequency range of 50-90 Hz, with working gases/gas mixtures made of argon and helium, and operating at a mean gas pressure in the range of 25-50 bar [17], [21] and [29].

Other studies that utilized this technique on *different* research problems include [43], [80] and [81].

This sensitivity analysis is carried-out when the linear alternator is connected to a linear (resistive) load examines the effects of four factors: helium molar fraction (α), mean gas pressure (P_m), electric load resistance (R_L) and pressure ratio (β) on ten responses, which are the key

performance indices of the linear alternator. This analysis is carried-out under constant operating frequency of 56 Hz. The linear load consists of load resistance (R_L) of a nominal value of 122 Ω preceded by a power-factor-correcting capacitor of 71 μF.

Table 6-2. Full factorial layout used in the sensitivity analysis of the factors α, β, P_m and R_L on the generated current (I). The ±1 statement refers to ±10 % variations in the factors with respect to the nominal values presented in Table 6-1. The conditions of the reference experiment are stated in Table 6-1.

i	α	P_m	R_L	β	|I|	ME (α)	ME (P_m)	ME (R_L)	ME (β)	ME (αP_m)	…	ME ($\alpha P_m R_L$)	…	ME ($\alpha\beta P_m R_L$)
1	-1	-1	-1	-1	0.24	-0.24	-0.24	-0.24	-0.24	0.24	…	-0.24	…	0.24
2	+1	-1	-1	-1	0.24	0.24	-0.24	-0.24	-0.24	-0.24	…	0.24	…	-0.24
3	-1	+1	-1	-1	0.30	-0.30	0.30	-0.30	-0.30	-0.30	…	0.30	…	-0.30
4	+1	+1	-1	-1	0.32	0.32	0.32	-0.32	-0.32	0.32	…	-0.32	…	0.32
5	-1	-1	+1	-1	0.22	-0.22	-0.22	0.22	-0.22	0.22	…	0.22	…	-0.22
6	+1	-1	+1	-1	0.22	0.22	-0.22	0.22	-0.22	-0.22	…	-0.22	…	0.22
7	-1	+1	+1	-1	0.28	-0.28	0.28	0.28	-0.28	-0.28	…	-0.28	…	0.28
8	+1	+1	+1	-1	0.29	0.29	0.29	0.29	-0.29	0.29	…	0.29	…	-0.29
9	-1	-1	-1	+1	0.29	-0.29	-0.29	-0.29	0.29	0.29	…	-0.29	…	-0.29
10	+1	-1	-1	+1	0.30	0.30	-0.30	-0.30	0.30	-0.30	…	0.30	…	0.30
11	-1	+1	-1	+1	0.36	-0.36	0.36	-0.36	0.36	-0.36	…	0.36	…	0.36
12	+1	+1	-1	+1	0.38	0.38	0.38	-0.38	0.38	0.38	…	-0.38	…	-0.38
13	-1	-1	+1	+1	0.26	-0.26	-0.26	0.26	0.26	0.26	…	0.26	…	0.26
14	+1	-1	+1	+1	0.27	0.27	-0.27	0.27	0.27	-0.27	…	-0.27	…	-0.27
15	-1	+1	+1	+1	0.34	-0.34	0.34	0.34	0.34	-0.34	…	-0.34	…	-0.34
16	+1	+1	+1	+1	0.35	0.35	0.35	0.35	0.35	0.35	…	0.35	…	0.35
Percent effect on Generated current amplitude (|I|)						1.1	7.3	-2.5	5.5	0.45	…	-0.12	…	-0.01

For this purpose, a set of 16 (=2^4) experiments are carried-out at the conditions prescribed by the design-of-experiment procedure, as shown in Table 6-2. This table shows the details of the 16 experiments based on the factor level combinations for a 15 factorial design and the response indicated in this Table is for the generated current amplitude (|I|). Similar tables are built for the nine other performance indices studied (mechanical stroke, dissipated voltage in the load, mechanical-motion loss, Ohmic loss and fluid-seal loss, absorbed acoustic power,

generated electric power, acoustic-to-electric conversion efficiency and acoustic impedance) and are not shown here but their results are summarized in Fig. 6-1 and Table 6-3.

Table 6-2 consists of 16 rows, where each row represents the conditions and the outcomes of a different experiment. The table consists of 21 columns: the first column shows the experiment number, from 1 to 16. Columns from the 2nd to the 5th show the +/- variations in the factors. The 6th column presents the measured amplitude of the generated current ($|I|$), in mm. The 7th to the 10th columns present the Main Effect (ME) of the factors α, P_m, R_L and β on the generated current, which is the multiplication of the values in the factor column times the values in the corresponding generated current column. For example, the main effect of the factor α is shown in the 7th column and is calculated as the product of the values in the α column (2nd column) times the measured values of the generated current ($|I|$) (6th column). Similarly, the 11th column presents the combined effect of the two factors α and P_m on the generated current, which is the triple multiplication of the values in the α and P_m columns times the measured value of the corresponding generated current. The main effects of tertiary interactions (e.g., $\alpha P_m R_L$) and quaternary interactions (e.g., $\alpha\beta P_m R_L$) are estimated similarly.

In this table, there are four single effects (α, β, P_m and R_L), six binary interactions (namely αP_m, αR_L, $\alpha\beta$, βP_m, βR_L and $P_m R_L$), four tertiary interactions (namely $\alpha P_m R_L$, $\alpha\beta P_m$, $\alpha\beta R_L$ and $\beta P_m R_L$) and a single quaternary interactions ($\alpha\beta P_m R_L$) summing up to 15 effects and interactions. One of the main powerful results of the sensitivity analysis technique is to reveal how combined interactions (binary, tertiary and quaternary effects) affect the performance indices.

The (+1/-1) signs in the table represent the corresponding (high/low) levels of each of the factor values, which are +/- 10 % of the nominal values, as set by the design-of-experiment methodology for a full-factorial layout.

For example, the first row represents an experiment made in which all the factors are set to 90% of their nominal values. The 4th row, for example, represents an experiment made in which the factors α and P_m are set to 110% of their nominal values, while the factors R_L and β are set to 90% of their nominal values.

The percent effects of a certain single factor or combined interaction of factors, ME_j, on any performance index is estimated from the main effects as [82]

$$ME_j = \frac{1}{2^{n-1}} * \sum_{i=1}^{2^n} \pm X_i \,, \qquad (6\text{-}1)$$

where n is the number of factors (four in this work), and X is the value of the performance index studied (shown in column 6 in Table 6-2) . The signs in Eq. (6-1) correspond to the appropriate combination for the j^{th} main effect of a single factor or combined interaction of factors. For example, the percent effect of factor α is estimated as the sum of the different main effects in the 7^{th} column divided by 2^3 as follows:

$$ME(\alpha) = 100*(- 0.24 + 0.24 – 0.30 + …+ 0.27– 0.34 + 0.35) / 8 = 1.1\ \%. \qquad (6\text{-}2)$$

Once the percent effects of the single factors and their combined interactions are estimated from Table 6-2, they are arranged in an ascending order, from $J = 1, 2, ..., N$, where N is the total number of the percent effects, given as $2^n - 1$ (15 percent effects in this work), then they are plotted on a normal probability plot along the abscissa. The ordinate values are computed as $(J - 0.5)/N$ as described in [82].

An important aspect in Eq. (6-1) is that the percent effect depends on the value of the performance index considered. For example, the percent effect of the helium molar fraction (α) on ($|V_L|$) is 111.9 %, where the nominal value $|V_L|$ is 38 V. In contrast, the percentage effect of the same factor α on ($|S|$) is 9.2 %, where the nominal value of $|S|$ is 2.2 mm. The results of the sensitivity analysis indicate the *order* on which the factors and their interactions affect the response and which direction.

On normal probability plot, the percent effects that produce no significant effect on the performance index studied (e.g., generated current) exhibit a normally distributed *random* behavior, and hence they fall near a *straight line* on this plot. Only the percent effects of a certain single factor or combined interaction of factors that affect the performance index under consideration significantly fall *away* from the line indicating significant factors or significant combination of factors. The relative distance from the line indicates the relative significance of the factor or combination of factor.

Results of the sensitivity analysis for the linear load are shown in Fig. 6-1 and indicate how the four factors studied and their eleven combinations affect the ten linear alternator performance indices considered. The most significant factors affecting all the performance indices can be read directly from Fig. 6-1 and are summarized in Table 6-3.

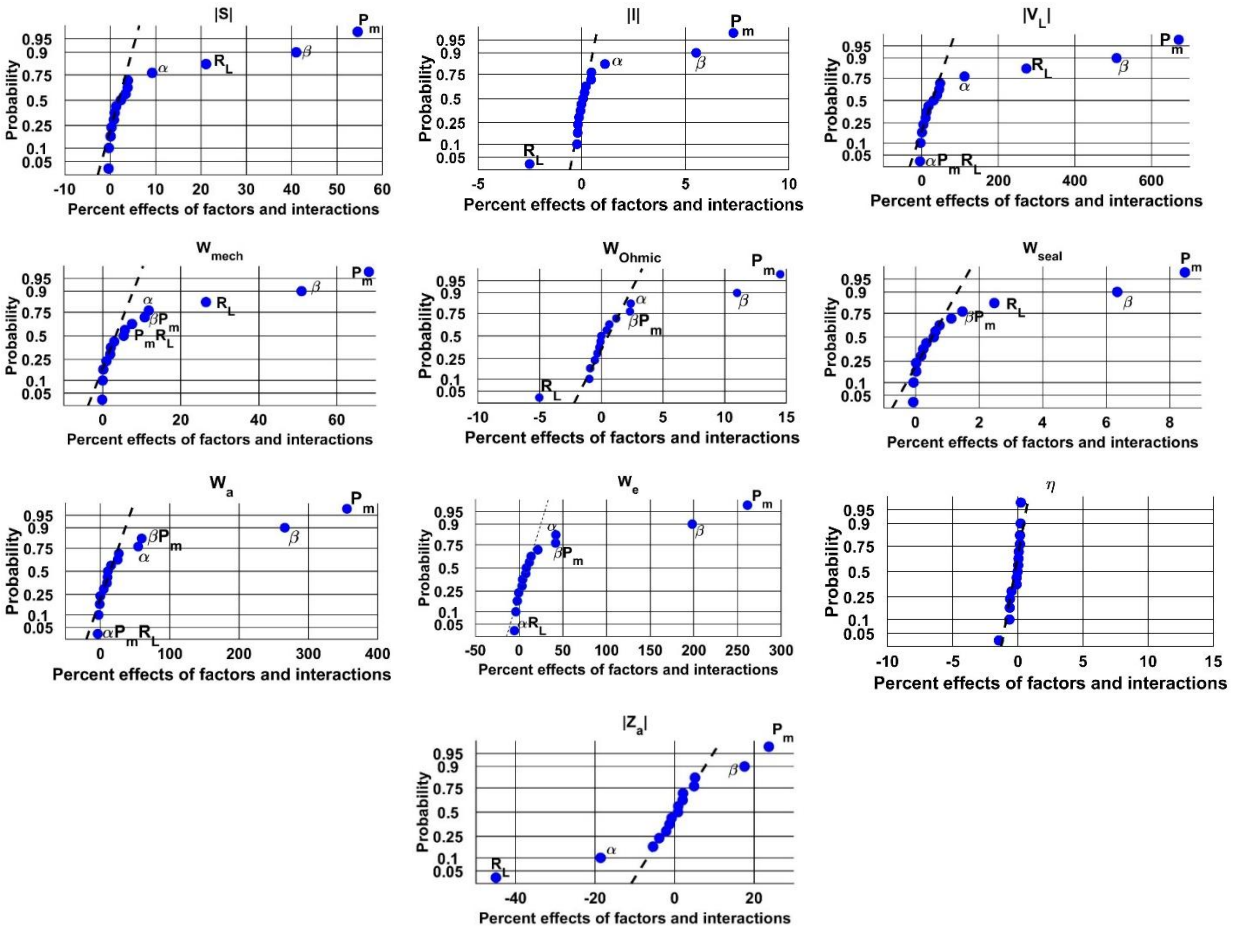

Figure 6-1. Percent effect of four operating factors and their eleven interactions for ±10% variations in the factors α, β, P_m and R_L on ten linear alternator performance indices for the linear load case. The conditions of the reference experiment are stated in Table 6-1.

The results of the sensitivity analysis indicate that the factors and their interactions affect the response in the order and directions presented in Table 6-3. Positive signs indicate direct relationships and negative indicate an inverse relationship. For example, an increase in the mean gas pressure P_m causes an increase in the mechanical stroke amplitude $|S|$, while a decrease in the load resistance R_L, causes an increases in the generated current ($|I|$).

Table 6-3. Most significant factors and interactions on the performance indices of linear alternators for ± 10% variations in the factors at the nominal conditions of the four working factors under linear loading condition. *The conditions of the reference experiment are stated in Table 6-1.*

Performance index	Most significant factors and interactions
Mechanical stroke amplitude, $\|S\|$	P_m (55.0%), β (41.0%), R_L (21.0%) and α (9.2%)
Acoustic impedance amplitude, $\|Z_a\|$	R_L (-44.9%), P_m (23.7%), α (-18.6%) and β (17.56%)
Dissipated voltage in the load amplitude, $\|V_L\|$	P_m (671.7%), β (508.8) %, R_L (273.4%) and α (111.9%)
Generated current amplitude, $\|I\|$	P_m (7.3%), β (5.5%), R_L (-2.5%) and α (1.1%)
Mechanical motion loss, W_{mech}	P_m (68.0%), β (51.0%), R_L (26.5%) and α (11.8%)
Ohmic loss, W_{Ohmic}	P_m (14.5%), β (11.0%), R_L (-5.0%) and α (2.4%)
Fluid seal loss, W_{seal}	P_m (8.5%), β (6.3%), R_L (2.5%) and βP_m (1.5%)
Absorbed acoustic power, W_a	P_m (355.8%), β (265.9%), βP_m (59.6%) and α (54.6%)
Dissipated electric power in the load, W_e	P_m (261.4%), β (198.3%), α (42.2%) and βP_m(41.9%)
Acoustic-to-electric conversion efficiency, η	As per Wakeland [77], the maximum acoustic-to-electric conversion efficiency depends only upon the dimensionless driver parameter, $\beta = (Bl)^2/(R_m r_e)$, which were not varied in this section.

The results of the sensitivity analysis indicate that, in linear loads, the mean gas pressure and the input dynamic pressure ratio are the most significant factors that affect *all* the values of the performance indices. This result can be explained in view of the parametric study presented in Chapter 5 and the model presented in Chapter 4. The results of the parametric study presented in Fig. 5-2 and Fig. 5-3 reveal the effects of the dynamic pressure ratio and the mean gas pressure on all the performance indices. These figures show that the dynamic pressure difference, ΔP, increases when either the mean gas pressure or the dynamic pressure ratio increase, and reveal that this increase is more pronounced for the mean gas pressure than for the dynamic pressure ratio. Additionally, Sec 4.2 indicated that all the ten performance indices are proportional to the ΔP, for the conditions used in the sensitivity analysis (constant operating frequency).

The effect of the helium molar fraction, α, is not as significant as the effect of the mean gas pressure and the input dynamic pressure ratio, which is further supported by the results of the parametric study shown in Sec 5.2 and Figs. 5-2, 5-3 and 5-4 which quantify the effects of β, P_m and α on the ten performance indices studied.

All the mechanical and the electrical performance indices studied are proportional to the helium molar fraction, except the acoustic impedance, which is inversely proportional to it. The reason is that the increase in the helium molar fraction increases the speed of the sound in the gas mixture, as well as the piston's velocity, u, thus causing the applied acoustic power to increase as shown in Eq.(1-4), and causing all the mechanical and electrical performance indices to increase accordingly.

In Eq. (1-4), the resonator pressure is kept constant because the mean gas pressure and the input dynamic pressure ratio were constants.

The results indicate that the amplitude of the acoustic impedance actually decreases with the molar helium fraction, indicating that the increase in the volumetric velocity, U, overweighs the changes that occur in the dynamic pressure difference, ΔP.

The results of Table 6-3 indicate that the load resistance, R_L, affects the performance indices on an order smaller than that of the P_m or β, as verified by the results presented in Figs. 5-2, 5-3 and 5-5 which quantify the effects of β, P_m and R_L, respectively on the ten performance indices studied.

Table 6-3 indicates that a decrease in (R_L) causes the linear alternator to deliver more current to the resistive load, which inevitable causes the generated voltage to drop. Because the mechanical stroke is proportional to the generated voltage at constant frequency as shown in Eq. (4-12) and explained in details [48], this causes a reduction in the mechanical stroke as well. As a matter of fact, these relationships were used to protect the linear alternator against potential over stroke events as depicted in [46].

The fact that the R_L factor is inversely proportional to the acoustic impedance can be seen from Eq. (4-18) which indicates that, for typical values in linear alternators, the numerator is controlled by the Bl product making $|Z_a|$ inversely proportional to the R_L value.

It is worthy to note that the value of the acoustic impedance is affected by the load parameters and the operating frequency. The effect of the load resistance is illustrated above and the effect of the power-factor-correcting capacitor which affects the value of the electric

reactance is illustrated in detail in Sec (5.1.5). From the experimental perspective the value of the power-factor-correcting affect the value of (P_f) thus, the value of the capacitor affects the ΔP value and the acoustic impedance value as shown in [44]. The operating frequency affects the values of the mechanical reactance and the electric reactance. It should be noted that the presented work in this section was conducted at constant values of the power-factor-correcting and operating frequency as mentioned before.

Reflecting on how the factor R_L affects the performance indices within ±10% of the nominal values reported reference experiment, it should be noted that the acoustic-to-electric conversion depends on R_L as shown in Eq.(4-24)

And that there exists an R_L value that causes a peak in W_e (Eq. 4-38), (6.7-9 Ω in this work, because the value of the electric reactance depends on the value of the mechanical stroke amplitude).

In this set of experiments, the changes caused by R_L on the W_a and W_e were insignificant, because the nominal R_L value (122 Ω) was much larger than the value that leads to the maximum output power. This is illustrated in more details in Fig. 5-5 that shows the effects of the load resistance on the performance indices of the linear alternator.

Reflecting on the effects on the fluid seal loss, we can infer that the mean gas pressure and the input dynamic pressure ratio are the most significant parameters that affects this performance index, where Eq. (4-29) supports this finding, because the fluid seal loss is a function of the maximum pressure difference across the piston of the linear alternator. Furthermore, the dynamic pressure ratio and the mean gas pressure are the two main parameters that affect the pressure difference across the piston of the linear alternator.

Additionally, the load resistance positively affects the value of the seal loss because the load resistance affects the pressure difference across the piston of the linear alternator. The effect of the load resistance on the pressure difference across the linear alternator can be illustrated by the relationship between the mechanical stroke and the dissipated voltage in the load and the relationship between the mechanical stroke and the pressure difference as shown in Eq. (4-19).

According to Eq. (4-19) and Eq. (4-20) the dynamic pressure difference across the piston of the linear alternator (ΔP) is proportional to the mechanical stroke (S). Noting that it is clear from Eq. (4-20) the increase in the load resistance does not affect the proportionality between

the (S) and (ΔP) because the value of the denominator (ω*Bl) is very large compared to value of the numerator ($A\sqrt{(R_{e+}^2 X_e^2)}$)

6.1 Summary of Sensitivity Analysis Results

In conclusion, all the factors are found to be significant. The most significant combination is βP_m. Around ± 10% variation of the nominal case considered, the most important factors that affect the mechanical stroke, the mechanical motion loss, the acoustic impedance amplitude, the dissipated voltage in the load are the mean gas pressure (55 %); the mean gas pressure (68%), the load resistance (-44.9%), and the mean gas pressure (671%), respectively. Similarly, the most important factors that affect the generated current, the Ohmic loss, fluid seal loss, the absorbed acoustic power, and the dissipated electric power in the load are the mean gas pressure (7.3%), the mean gas pressure (14.5%), the mean gas pressure (8.5%), the mean gas pressure (355.8%), the mean gas pressure (261.4%), respectively. In the range considered, no significant factors affect the conversion efficiency, this is because the dimensionless Wakeland [77] number, $\beta = (Bl)^2/(R_m r_e)$ remains unchanged. More details on the effects are presented in Table (6-3).

7. Summary and Future Work

The current work addresses matching the linear alternator and the thermoacoustic engine and improving the performance characteristics of the linear alternator in three main chapters: Chapter 4 introduces and validates an algebraic model that relates the mechanical and electrical variables and then optimize some of the main parameters. The model is validated in the same chapter. Chapter 5 presents a parametric study on the effects of several operating factors on the performance indices. Chapter 6 presents a sensitivity analysis that estimates the relative effects of each of the working factors around a basic point. In this chapter, the main findings are summarized below.

Chapter 4 introduces a detailed algebraic model for the estimation of the performance indices of the linear alternator under thermoacoustic-power-conversion conditions. The model introduces a new effective inductance of the linear alternator that is function of the inductance at zero mechanical stroke, the relative permeability, the operating stroke and the rated stroke.

The model presents the equivalent linear alternator impedance and relates both its real and imaginary parts to the mechanical reactance, electric reactance, load resistance, stator resistance, transduction coefficient, damping coefficient and the piston area.

The model's equations illustrate the relationships between the different performance indices, operating conditions and the linear alternator parameters, and thus relate the mechanical variables (mechanical stroke, mechanical motion loss, pressure difference across the piston, fluid-seal loss), electrical variables (generated voltage, current and electric power, Ohmic loss), acoustic variables (acoustic impedance, absorbed acoustic power) and acoustic-to-electric conversion efficiency to each other's.

Chapter 5 presents an experimental parametric study focused on determining the effects of the different working factors on the performance indices under two types of electric load. The considered working factors are the operating frequency, the mean gas pressure, the gas mixture composition, the input dynamic pressure ratio, the power-factor correcting capacitor and the load resistance in the linear load case or the DC electronic voltage in the non-linear load case.

Chapter 6 presents a sensitivity analysis that examines the sensitivity of four factors and their binary, tertiary and quaternary combinations utilizing the design-of-experiment approach.

The four factors considered are the helium molar fraction (α), the mean gas pressure (P_m), the load resistance (R_L) and the input dynamic pressure ratio (β).

7.1 Future Work

The presented model assumes laminar regime in the velocity and dynamic pressures and thus neglects the dissipation of kinetic energy into heat via turbulent fluctuations. The model also neglects harmonic generation and thus assumes that all the acoustic power is carried-out in the fundamental mode only. The model simulates the two main losses (mechanical-motion loss and Ohmic loss) while it ignores the minor losses (e.g., pressure drops and secondary flows associated with variations of the flow cross sectional area or fluid seal loss) for the sake of simplicity. The model ignores variations in the linear alternator parameters (i.e., the Wakeland [77] number remains constant) either with time or with the operating conditions, except for the variation of the effective inductance with the mechanical stroke, which was found to strongly affect the electric resonance and is discussed in Section 4.1.2. The model considers electric loads made of resistive and capacitive components and does not consider non-linear loads (e.g., the electric grid) for the sake of simplicity.

The main recommendation for future work is to extend the model validity to larger range of operating conditions. For example, it is useful to modify the validity of the model to larger dynamic pressure ratios by accounting for the variation in the linear alternator parameters such as the intrinsic stiffness, transduction coefficient, damping coefficient and stator resistance over the change in the operation conditions. For instance previous research has shown that the damping coefficient increases with the increase of pressure difference across the piston of the linear alternator [30]; the BL product decreases with the mechanical stroke [23]; the electrical resistance is enhanced at higher frequencies [9]; the effective inductance varies with power as well as frequency [9];

Additionally, to properly model the performance at large dynamic pressure ratios, the modified model should account for turbulent flow regimes and harmonic generation. It should also account for losses other than the mechanical-motion loss, Ohmic loss, and fluid seal loss such as eddy current loss and the thermal, mechanical and magnetic hysteresis losses. For this purpose, excessive vibration in the experimental setup should be eliminated or reduced to insignificant levels (especially at non-linear loading).

On another side, it may beneficial to use different simulating software rather than DELTAEC, such as Sage [11] because the DELTAEC does not directly model electric loads such as the load resistance and the load capacitance.

8. References

[1] Swift, Gregory W. *Thermoacoustics: A Unifying Perspective for Some Engines and Refrigerators*. Melville: Acoustical Society of America, 2002.

[2] Telesz, Mark P, "Design and testing of a thermoacoustic power converter," 2006. Masters Thesis. Georgia Institute of Technology, 2006.

[3] Jaworski, Artur J., and Xiaoan Mao. "Development of thermoacoustic devices for power generation and refrigeration." *Proceedings of the Institution of Mechanical Engineers, Part A: Journal of Power and Energy* 227.7 (2013): 762-782.

[4] Hariharan, N. M., P. Sivashanmugam, and S. Kasthurirengan. "Influence of stack geometry and resonator length on the performance of thermoacoustic engine." *Applied Acoustics* 73.10 (2012): 1052-1058.

[5] Ceperley, Peter H. "A pistonless Stirling engine—The traveling wave heat engine." *The Journal of the Acoustical Society of America* 66.5 (1979): 1508-1513.

[6] Tourkov, Konstantin, and Laura Schaefer. "Effect of regenerator positioning on thermoacoustic effect in a looped tube traveling wave thermoacoustic engine." *Energy Conversion and Management* 95 (2015): 94-100.

[7] Backhaus, Scott, and Greg W. Swift. "A thermoacoustic-Stirling heat engine: Detailed study." *The Journal of the Acoustical Society of America* 107.6 (2000): 3148-3166.

[8] De Blok, Kees. "Low operating temperature integral thermo acoustic devices for solar cooling and waste heat recovery." *Journal of the Acoustical Society of America* 123.5 (2008): 3541-3541.

[9] Reid, Gordon. "Chart Industries: Email communication." 2016.

[10] Bagg, S. D. "Linear alternator technologies used for free piston Stirling engines." Nuclear and Emerging Technologies for Space (2012).

[11] Metscher, Jonathan F., and Edward J. Lewandowski. "Development and Validation of Linear Alternator Models for the Advanced Stirling Convertor." *The American Institute of Aeronautics and Astronautics* (2014).

[12] Yarr, George A. Linear reciprocating alternator. United States of America: Patent 5,146,123. 8 September 1992.

[13] *First High-Efficiency Affordable STAR™ Reciprocating Motor*. n.d. 2018. <https://sbir.nasa.gov/SBIR/successes/ss/044text.html>.

[14] Qiu, Songgang. Linear electrodynamic system and method. United States of America: Patent 6,930,414. 16 August 2005.

[15] *Thales Cryogenics Flexure bearing technology*. 2016. Thales Cryogenics. 2018. <https://www.youtube.com/watch?v=YaPLXDtShE0>.

[16] Garrett, Steven L., Robert M. Keolian, and Robert W. Smith. High-efficiency moving-magnet loudspeaker. United States of America: Patent 6,307,287. 23 October 2001.

[17] Bi, Tianjiao, Zhanghua Wu, Limin Zhang, Guoyao Yu, Ercang Luo, and Wei Dai. "Development of a 5 kW traveling-wave thermoacoustic electric generator." *Applied Energy* 185 (2017): 1355-1361.

[18] Wang, Kai, Jie Zhang, Ning Zhang, Daming Sun, Kai Luo, Jiang Zou, and Limin Qiu. "Acoustic matching of a traveling-wave thermoacoustic electric generator." *Applied Thermal Engineering* 102 (2016): 272-282.

[19] Wilcox, Douglas Alan. "Experimental investigation of a thermoacoustic-stirling engine electric generator with Gedeon streaming suppression." MSc thesis. The Pennsylvania State University, 2011.

[20] Spoor, Philip S. "On the axial drift of free pistons in acoustic systems." *The Journal of the Acoustical Society of America* 129.4 (2011): 2411-2411.

[21] Abdelmwgoud, Moamen Bellah. "Integration of linear alternators in thermoacoustic heat Engines." Masters Thesis . The American University in Cairo, 2015.

[22] Abdou, M., Abdelwahed, A. Y., Ibrahim, A. H., & Abdel-Rahman, E. "An experimental setup to test linear alternators: design, operation and preliminary results." *Proceedings of the 22nd International Congress on Sound and Vibration*. Florence, Italy, 2015.

[23] Liu, Jin, and Steven Garrett. "Characterization of a small moving-magnet electrodynamic linear motor." *The Journal of the Acoustical Society of America* 118.4 (2005): 2289-2294.

[24] Luo, E. C., Z. H. Wu, W. Dai, and S. F. Li. "Study on a Thermoacoustic-Stirling Electrical Generator." *Proceedings of ISES Solar World Congress 2007: Solar Energy and Human Settlement*. Berlin, Heidelberg: Springer, 2008. 1833-1837.

[25] Wu Zhanghua, Dai Wei and Luo Ercang. "Theoretical investigation on linear alternator in thermoacoustic power generation system." *Acta Energiae Solaris Sinica* 4 (2008): 024.

[26] Rossi, Andrea, Fabio Immovilli, Claudio Bianchini, Alberto Bellini, and Giovanni Serra. "Design of linear alternators for thermoacoustic machines." *Energy Conversion Congress and Exposition*. IEEE, 2009. 2436-2440.

[27] Yu, Zhibin, Patcharin Saechan, and Artur J. Jaworski. "A method of characterising performance of audio loudspeakers for linear alternator applications in low-cost thermoacoustic electricity generators." *Applied acoustics* 72.5 (2011): 260-267.

[28] Saha, C. R., Paul H. Riley, J. Paul, Z. Yu, A. J. Jaworski, and C. M. Johnson. "Halbach array linear alternator for thermo-acoustic engine." *Sensors and Actuators A: Physical* 178 (2012): 179-187.

[29] Sun, D. M., K. Wang, X. J. Zhang, Y. N. Guo, Y. Xu, and L. M. Qiu. "A traveling-wave thermoacoustic electric generator with a variable electric RC load." *Applied energy* 106 (2013): 377-382.

[30] Wu, Zhanghua, Limin Zhang, Wei Dai, and Ercang Luo. "Investigation on a 1 kW traveling-wave thermoacoustic electrical generator." *Applied Energy* 124 (2014): 140-147.

[31] Rott, Nikolaus."Thermoacoustics." *Advances in Applied Mechanics.* 20 (1980): 135-175.

[32] Xiao, J. H. "Thermoacoustic heat transportation and energy transformation Part 1: Formulation of the problem." *Cryogenics* 35.1 (1995): 15-19.

[33] Xiao, J. H. "Thermoacoustic heat transportation and energy transformation Part 2: Isothermal wall thermoacoustic effects." Cryogenics 35.1 (1995): 21-26.

[34] Xiao, J. H. "Thermoacoustic heat transportation and energy transformation Part 3: Adiabatic wall thermoacoustic effects." Cryogenics 35.1 (1995): 27-29.

[35] Wang, Kai, Daming Sun, Jie Zhang, Ya Xu, Kai Luo, Ning Zhang, Jiang Zou, and Limin Qiu. "An acoustically matched traveling-wave thermoacoustic generator achieving 750 W electric power." *Energy* 103 (2016): 313-321.

[36] Timmer, Michael AG, Kees de Blok, and Theo H. van der Meer. "Review on the conversion of thermoacoustic power into electricity." *The Journal of the Acoustical Society of America* 143.2 (2018): 841-857.

[37] Abdelwahed, A. Y., A. H. Ibrahim, and Ehab Abdel-Rahman. "Experimental investigation of the effects of mechanical stroke on the acoustic impedance of linear alternators under thermoacoustic-power-conversion conditions." *Proceedings of the 23rd International Congress on Sound and Vibration*. Athens, Greece, 2016.

[38] Kankam, M. David, Jeffrey S. Rauch, and Walter Santiago. *Dynamic analysis of free-piston Stirling engine/linear alternator-load system-Experimentally validated*. Cleveland, Ohio: National Aeronautics and Space Administration-Lewis Research Center, 1992.

[39] Petach, Michael, Emanuel Tward, and Scott Backhaus. "Design of a high efficiency power source (HEPS) based on thermoacoustic technology." 2004", Los Alamos National Laboratory, Condensed Matter and thermal Physics group.

[40] Hoshino, Takeshi, and Shoichi Yoshihara. "Development of High Efficiency Linear Alternator for Stirling and Thermoacoustic Engines." *6th International Energy Conversion Engineering Conference (IECEC)*. 2008. 5637.

[41] Wang, Kai, Daming Sun, Jie Zhang, Ya Xu, Jiang Zou, Ke Wu, Limin Qiu, and Zhiyi Huang. "Operating characteristics and performance improvements of a 500 W traveling-wave thermoacoustic electric generator." *Applied Energy* 160 (2015): 853-862.

[42] Kankam, M. David, and Jeffrey S. Rauch. *Controllability of free-piston Stirling engine/linear alternator driving a dynamic load*. Cleveland, Ohio: National Aeronautics and Space Administration-Lewis Research Center, 1993.

[43] Arafa, N. M., A. H. Ibrahim, and E. E. Khalil. "Sensitivity analysis of a standing-wave thermoacoustic engine." *9th Annual International Energy Conversion Engineering Conference*. 2011.

[44] Abdelwahed, A. Y., A. H. Ibrahim, and Ehab Abdel-Rahman. "Effects of operation at and off-electrical resonance on the performance indices of linear alternators under ther-moacoustic-power-conversion conditions." *Proceedings of the 22nd International Congress on Acoustics*. Buenos Aires, Argentina, 2016.

[45] Abdelwahed, A. Y., A. H. Ibrahim, and Ehab Abdel-Rahman. “Performance of linear alternators using passive linear and non-linear loads under thermoacoustic-power-conversion conditions." *Proceedings of the 23rd International Congress on Sound and Vibration*. Athens, Greece, 2016.

[46] Ibrahim, A. H., A. Y. Abdelwahed, M. Abdou, and Ehab Abdel-Rahman. "Real-time measurements of linear alternator performance indices under thermoacoustic-power-conversion conditions." *Proceedings of the 23rd International Congress on Sound and Vibration*. Athens, Greece, 2016.

[47] Ibrahim, A. H., A. Y. Abdelwahed, and Ehab Abdel-Rahman. "Sensitivity analysis of linear alternator performance indices under thermoacoustic-power-conversion conditions." *Proceedings of the 23rd International Congress on Sound and Vibration*. Athens, Greece, 2016.

[48] Abdelwahed, A. Y., A. H. Ibrahim, and Ehab Abdel-Rahman. "Performance indicators of linear alternators at different electric loads under thermo-acoustic-power-conversion conditions." Proceedings of the 24th International Congress on Sound and Vibration. London, United Kingdom, 2017.

[49] Abdelwahed, Ahmed Y., A. H. Ibrahim Essawey, and Ehab Abdel-Rahman. "Numerical simulation of key linear alternator performance indicators under thermoacoustic-power-conversion conditions." *The Journal of the Acoustical Society of America* 141.5 (2017): 3737-373.

[50] Arafa, N. "Towards a Better Performance of Thermacoustic Devices." MSc Thesis. Cairo University, 2010.

[51] Arafa, N. M., A. H. Ibrahim, K. Addas, and Ehab Abdel-Rahman. "Design considerations for thermoacoustic engines for low onset temperature and efficient operation." *Forum Acusticum*. 2011.

[52] Ibrahim, Abdelmaged, Ahmed Elbeltagy, Mahmoud Emam, and Ehab Abdel-Rahman. "Development and analysis of non-linearity in the pressure waves resulting from thermoacoustic heat engines."*Proceedings of the Acoustics Conference.* Nantes, 2012.

[53] Ibrahim, A. H., M. Emam, Hosny Omar, Karim Addas, and Ehab Abdel-Rahman. "Performance evaluation of thermoacoustic engine using different gases." *ICSV19*. Vilnius, Lithuania, 2012.

[54] Ibrahim, A. H., and Ehab Abdel-Rahman. "Innovative solar-energy-driven power converter: Efficient operation of thermo-acoustic engines." *The 2nd International Conference on Renewable Energy: Generation and Applications*. AlAin, UAE, 2012. 4-7.

[55] El-Rahman, Ahmed Abd, Mohamed Serry, Sherif Sedky, and Ehab Abdel-Rahman. "Performance Characterization of a Microscale Thermoacoustic Energy Harvester." *ICSV19*. Vilnius, Lithuania, 2012.

[56] El-Rahman, Ahmed Abd, and Ehab Abdel-Rahman. "Numerical simulation of a thermoacoustic couple." *Proceedings of the Acoustics Conference*. Nantes, 2012.

[57] Emam, Mahmoud Mohamed. "Experimental investigations on a standing-wave thermoacoustic engine." MSc thesis. Cairo University, 2013.

[58] Ibrahim, A. H., A. A. Elbeltagy, M. Emam, Moamen Abdou, Hosny Omar, and Ehab Abdel-Rahman. "Suppressing harmonics in standing-wave thermoacoustic engines." *The Int'l Summer School and Workshop on Non-Normal and Nonlinear Effects In Aero-and Thermoacoustics*. Munich, 2013.

[59] Abd El-Rahman, Ahmed I., and Ehab Abdel-Rahman. "Characteristic-based non-linear simulation of large-scale standing-wave thermoacoustic engine." *The Journal of the Acoustical Society of America* 136.2 (2014): 649-658.

[60] Abdou, Moamen, A. H. Ibrahim, and Ehab Abdel-Rahman. "Control of onset temperature in standing-wave thermoacoustic engines." *ICSV22*. Florence, Italy, 2015.

[61] Ramadan, I. A., AI Abd El-Rahman, A. H. Ibrahim, and Ehab Abdel-Rahman. "Numerical investigation on the thermoacoustic streaming behavior." *ICSV22*. Florence, Italy, 2015.

[62] Islam A. Ramadan, Hélène Bailliet and Jean-Christophe Valière. "Experimental investigation of acoustic streaming." *ICSV24*. London, UK, 2017.

[63] Ibrahim, A., Hosny Omar, and Ehab Abdel-Rahman. "Constraints and challenges in the development of loudspeaker-driven thermoacoustic referierator." *the 18th International Congress on Sound and Vibration (ICSV18)*. 2011.

[64] Abd El-Rahman, Ahmed I., and Ehab Abdel-Rahman. "Computational fluid dynamics simulation of a thermoacoustic refrigerator." *Journal of Thermophysics and Heat Transfer* 28.1 (2013): 78-86.

[65] Rezk, M., A. H. Ibrahim, T. Tigim, A. I. Abd El-Rahman, A. A. Elbeltagy, and Ehab Abdel-Rahman. "Investigation of Vortex Formation in the Vicinity of Parallel Plates in Oscillating Flow Using Particle Image Velocimetry." *The Int'l Summer School and Workshop on Non-Normal and Nonlinear Effects In Aero-and Thermoacoustics*. 2013.

[66] Rezk, Michael. " Experimental Investigation of the Flow Characteristics inside a Thermoacoustic Refrigerator Using Particle Image Velocimetry." M.Sc. Thesis. American University in Cairo, 2013.

[67] Ramadan, I. A., AI Abd El-Rahman, A. H. Ibrahim, and Ehab Abdel-Rahman. "Numerical investigation of the thermoacoustic streaming behavior." *ICSV22*. Florence,Italy, 2015.

[68] Rezk, M., Ibrahim, A. H., Nigim,T., Abd El-Rahman, A. I., Elbeltagy, A.A. and Abdel-Rahman, E. "Particle-image-velocimetry investigation of flow morphology at sudden expansion and contraction in oscillating flows." *the 22nd International Congress on Acoustics*. 2016.

[69] Ramadan, Islam A., Ahmed I. Abd El-Rahman, A. H. Ibrahim, and Ehab Abdel-Rahman. "Transition To Turbulence in Oscillating Flows." *ICSV25*. 2017.

[70] Ramadan, Islam. "Transient to Turbulence in Oscillating Flows." Ph.D. Thesis. American University in Cairo, 2018.

[71] Ramadan, Islam A., Hélène Bailliet, and Jean-Christophe Valière. "Experimental investigation of the influence of natural convection and end-effects on Rayleigh streaming in a thermoacoustic engine." *The Journal of the Acoustical Society of America* 143.1 (2018): 361-372.

[72] Tijani, M. E. H., J. C. H. Zeegers, and A. T. A. M. De Waele. "Prandtl number and thermoacoustic refrigerators." *The Journal of the Acoustical Society of America* 112.1 (2002): 134-143.

[73] Wang, Kai, Daming Sun, Jie Zhang, Ya Xu, Jiang Zou, Ke Wu, Limin Qiu, and Zhiyi Huang. "Operating characteristics and performance improvements of a 500 W traveling-wave thermoacoustic electric generator." *Applied Energy* 160 (2015): 853-862.

[74] Gonen, Eran, and Gershon Grossman. "Gap seal dissipation in linear alternators." *The Journal of the Acoustical Society of America* 137.4 (2015): 1744-1755.

[75] Purcell, E. M. and Morin, D. M. *Handbook of electricity and magnetism*. Cambridge University Press, 2013.

[76] Juha, P., Tapani, J. and Valeria, H. *Design of rotating electrical machines*. John Wiley and Sons, 2009.

[77] Wakeland, Ray Scott. "Use of electrodynamic drivers in thermoacoustic refrigerators." *The Journal of the Acoustical Society of America* 107.2 (2000): 827-832.

[78] Veselý, Martin, and Tomáš Vít. "Difference between working gases in thermoacoustic engine." *EPJ Web of Conferences*. EDP Sciences, 2014. 02126.

[79] Davies, O.L. *Handbook of the Design and Analysis of Industrial Experiments*. New York : Imperial Hafner, 1960.

[80] Ibrahim, Essawey AH. "Microparticle detachment from surfaces by fluid flow." PhD thesis. Notredam University, 2005.

[81] Wu, Hongjing, Leonard M. Lye, and Bing Chen. "A design of experiment aided sensitivity analysis and parameterization for hydrological modeling." *Canadian Journal of Civil Engineering* 39.4 (2012): 460-472.

[82] Guttman, I., Wilks, S. and Hunter, J. *Handbook of Introductory Engineering Statistics*. New York: John Wiley & Sons, 1982.

9. Appendices

9.1 Appendix A- Experimental setup devices

1. Function generator (model AFG3251, supplied by Tektronix) -Datasheet here
2. Power amplifier (model 2734, supplied by Bruel and Kjaer)-Datasheet here

3. Acoustic driver and linear alternator (model 1S102D, supplied by Chart Industries).

1-2 Specifications

1-2-1 Basic Unit

The 2S102DX specifications are given in the Table 1.1 below.

Table 1.1: 1S102DX Specifications

Dimensions	
Diameter	4.0 in (10.2 cm)
Length	4.75 in (12.1 cm)
Ambient Operating Temperature	32° - 86°F (0°- 30°C)
Weight	3.5 lbs (1.6 kg) — approx.
Electrical Requirement	
Max. Operating Current	2 Amps RMS
Max. Fuse or Circuit Breaker Size	2.5 Amp
Motor Specifications	
Nominal Stroke	10 mm peak-to-peak (max)
Nominal input power (at 60 Hz)	125 Watts
Nominal output pV work (at 60 Hz)	100 Watts (including seal loss)
Maximum input power (at 60 Hz)	150 Watts
Voltage at nominal input power, assuming matched load at 60 Hz	~100 Volts AC rms

For additional information, such as piston diameter, interface bolt circles, and motor parameters, see attached motor data sheet and assembly drawings.

1-3 General Arrangement

The Qdrive 1S102DX Driver is designed to drive Stirling or acoustic Stirling (displacerless) coldheads by mechanically compressing and acoustically expanding helium gas for the Stirling cycle. It can also be DRIVEN by a Stirling engine pressure wave. The driver can be used with other acoustic loads or sources as well, but regardless of the type of load, maximum pV output cannot be obtained unless the load is matched to the driver.

1-3-1 Physical Description

The 1S102DX driver consists of a 1S102M STAR™ resonant linear motor-alternator, with a piston that inserts into a matching cylinder. The motor and cylinder are pre-assembled. The small annular gap ($\leq$ 0.001 inch) between the piston O.D. and the cylinder I.D. forms a non-contacting clearance seal, acoustically isolating the front side of the piston from the back side. For most applications, the cylinder is itself mounted into an assembly that includes a pressure vessel enclosing the motor, and enclosing a load which is addressed by the front side of the piston. The 1S102X may be used with any combination of inert gases, such as helium and argon, and other common gases such as air and

A. Acoustic driver parameters

DRiver serial 777

Test Date	Project	Motor Type	Serial Number	Mechanical Resistance R_m (N*s/m)	Stiffness K (kN/m)
May 5, 2014	1483AU	102	102 777-1	4.69	30.49
Free Decay Frequency f (Hz)	**Moving Mass m (kg)**	**Inductance L_e (mH)**	**Maximum Displacement S_{max} (mm)**	**Electrical Resistance R_e (Ω)**	**Transduction Coefficient $B\ell$ (N/A)**
40.51	0.4922	86.4	6.23	6.70	47.69

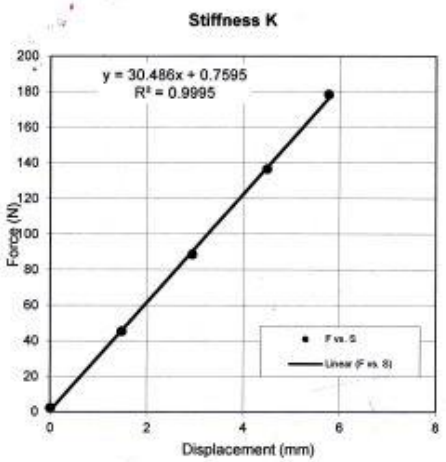

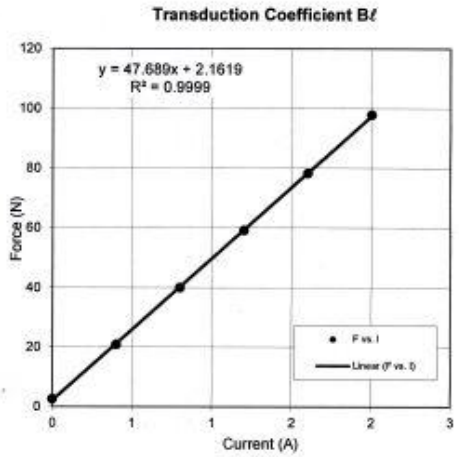

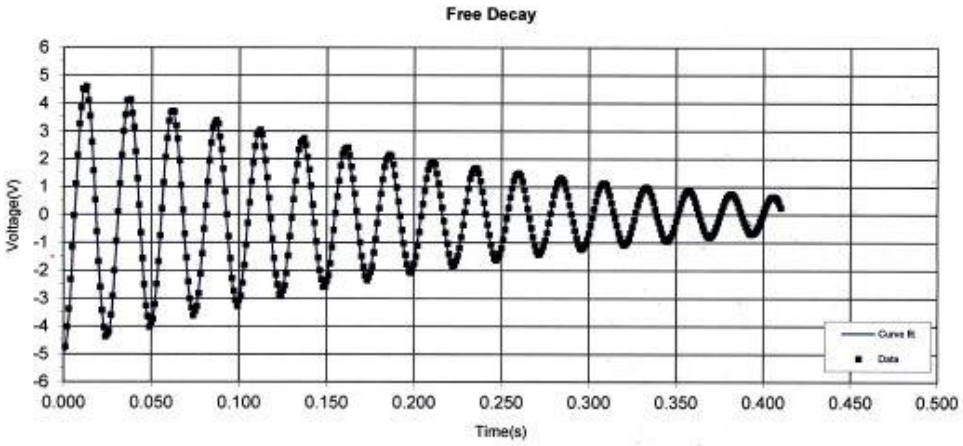

Excel module for calculating approximate piston seal gaps based on DC flow measurements

D218 (motor SN 102777.1 with piston sleeve)

Author: Phil Spoor Date: 5-May-14 WS

Driver

seal length = 12.7mm
seal gap = 18.7 μm

piston dia = 2 in.

CONSTANTS and FITTING PARAMETERS:

gil2=	0.064824	Coefficients for obtaining standard liter/min flow of helium
gil1=	0.606873	from Gilmont flow meter type GF-1560
gil0=	1.246088	(see gilmont_hi-p_calib.xls)

foo= 0.662 apparent power-law correlating std. flow to gilmont reading as a function of pressure

Po=	14.7	psi	ambient pressure, psi	viscosity=	2.00E-05 N*s/m^2
PoM=	101379.3	Pa	ambient pressure, Pa (Metric units)		
	2	in	piston		
dp=	0.0508	meter	diameter		
				seal length L=	0.5 in / 0.0127 meter
perim=	0.159593	meter	seal perimeter		

use SI in all Terms; it works!

DATA and CALCULATIONS:

data descriptor

pressure, psig: in flowmeter	pressure, psig: into seal	Gilmont reading	p absolute in pwg, Pa	He flow, std l/min	approx seal gap, mil
10.0	10.0	0.50	170344.8	2.207589	0.77
20.0	20.0	2.00	239310.3	4.801355	0.74
30.0	30.0	3.50	308275.9	8.695102	0.74
40.0	40.0	4.50	377241.4	12.62451	0.72
50.0	50.0	5.50	446206.9	17.45627	0.71
	0.0		101379.3	1.246088	
	0.0		101379.3	1.246088	

HORIZONTAL

$$\delta_j := \left[\frac{12 \cdot P_0 \cdot \mu \cdot L_{seal} \cdot U_j}{\left[(P_j)^2 - P_0^2\right] \cdot \pi \cdot d_p}\right]^{\frac{1}{3}}$$

Formula above is for two seals in parallel (e.g. a PWG.) in this case, we only have one piston, so 12 is replaced by 24.

Approximate effective radial seal gap= 0.74 mil or 18.7 microns

π * dp not π only

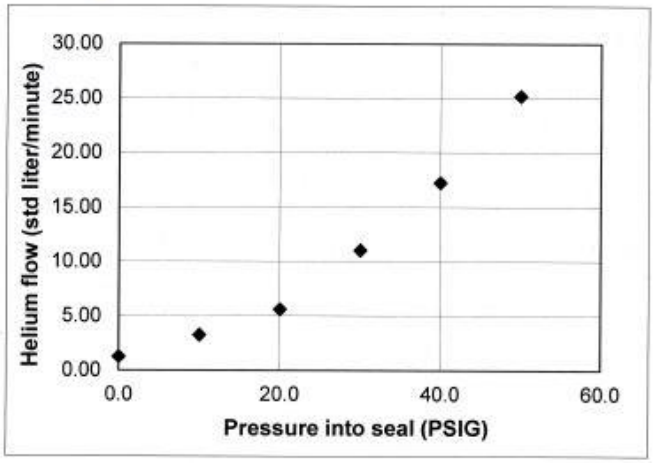

B. Linear alternator parameters

Alternator serial 774

Test Date	Project	Motor Type	Serial Number	Mechanical Resistance R_m (N*s/m)	Stiffness K (kN/m)
May 5, 2014	1482AU	102	102 774 - 1	4.55	30.94
Free Decay Frequency f (Hz)	**Moving Mass m (kg)**	**Inductance L_s (mH)**	**Maximum Displacement S_{max} (mm)**	**Electrical Resistance R_e (Ω)**	**Transduction Coefficient $B\ell$ (N/A)**
40.48	0.478	84.1	6.14	6.72	48.01

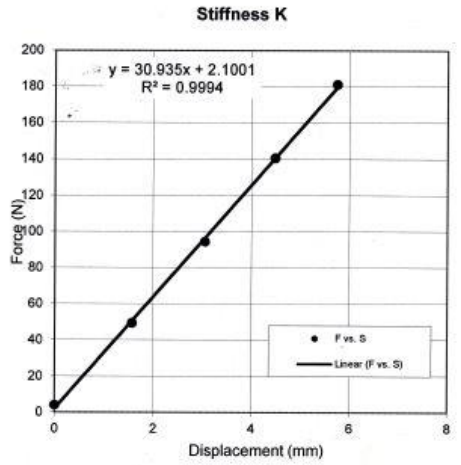

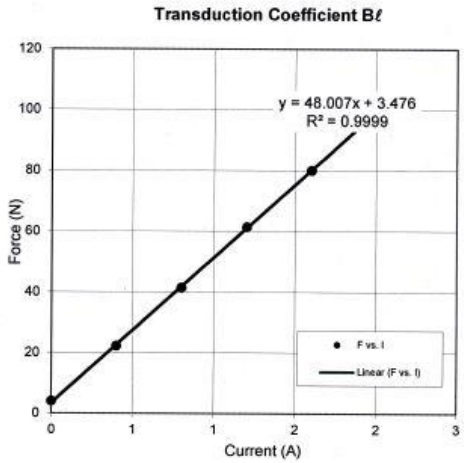

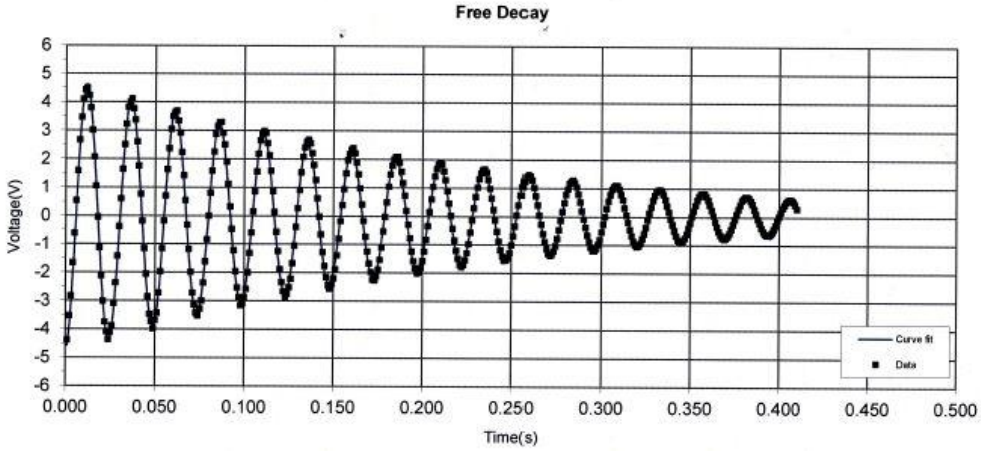

Excel module for calculating approximate piston seal gaps based on DC flow measurements

D219 (motor SN 102774.1 with piston sleeve)

Author: Phil Spoor Date: 5-May-14 WS

Alternator

CONSTANTS and FITTING PARAMETERS:

gil2=	0.064824	Coefficients for obtaining standard liter/min flow of helium
gil1=	0.606873	from Gilmont flow meter type GF-1560
gil0=	1.246088	(see gilmont_hi-p_calib.xls)

foo= 0.662 apparent power-law correlating std. flow to gilmont reading as a function of pressure

Seal length = 12.7 mm
Seal gap = 19.1 μm
piston dia = 2 inch

Po=	14.7	psi	ambient pressure, psi	viscosity=	2.00E-05 N*s/m^2
PoM=	101379.3	Pa	ambient pressure, Pa (Metric units)		
	2	in	piston		
dp=	0.0508	meter	diameter		
				seal length L=	0.5 in / 0.0127 meter
perim=	0.159593	meter	seal perimeter		

DATA and CALCULATIONS:

data descriptor

pressure, psig: in flowmeter	pressure, psig: into seal	Gilmont reading	p absolute in pwg, Pa	He flow, std l/min	approx seal gap, mil
10.0	10.0	0.50	170344.8	2.207589	0.77
20.0	20.0	2.00	239310.3	4.801355	0.74
30.0	30.0	4.00	308275.9	9.836271	0.77
40.0	40.0	5.00	377241.4	14.08357	0.75
50.0	50.0	6.00	446206.9	19.25976	0.74
	0.0		101379.3	1.246088	
	0.0		101379.3	1.246088	

Horizontal axis

$$\delta_j := \left[\frac{12 \cdot P_0 \cdot \mu \cdot L_{seal} \cdot U_j}{\left[(P_j)^2 - P_0^2\right] \cdot \Pi}\right]^{\frac{1}{3}}$$

Formula above is for two seals in parallel (e.g. a PWG.) in this case, we only have one piston, so 12 is replaced by 24.

Approximate effective radial seal gap= 0.75 mil or 19.1 microns

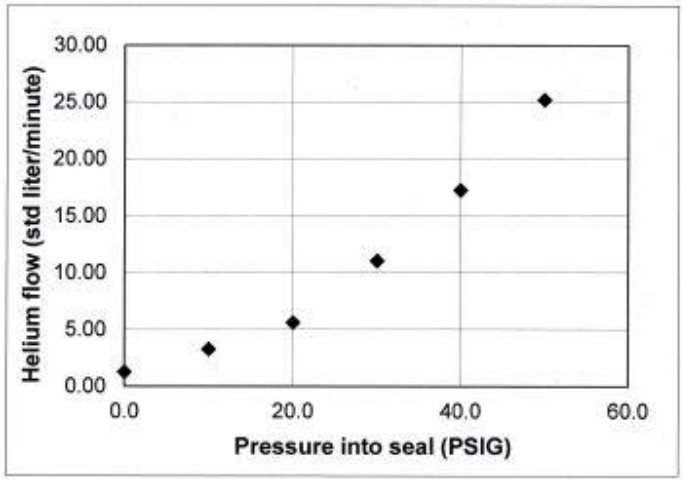

4. Three pressure microphones (model 8530B-500M5, piezo-resistive, range 0-500 PSI absolute, individually calibrated by the supplier, Meggitt)-Datasheet here

Aerospace
Energy
Measurement

Endevco®

Piezoresistive pressure transducer

Model 8530B -200, -500, -1000

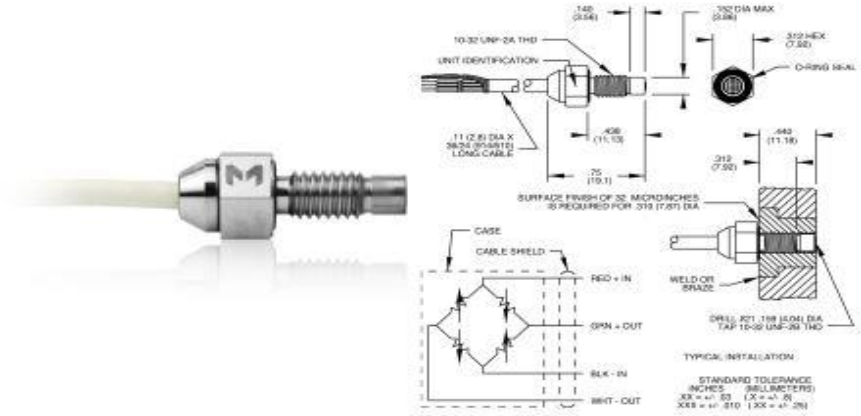

Key features

- 200, 500 and 1000 psia ranges
- Absolute reference
- 300mV full scale output
- Rugged, minature

Model 8530B is a miniature, high sensitivity piezoresistive pressure transducer for measuring absolute pressure. The volume behind the diaphragm is evacuated and glass sealed to provide an absolute pressure reference. Full scale output is 300 mV with high overload capability and high frequency response. It is available in ranges from 200 psia to 1000 psia. See model 8530C for lower pressure ranges.

Endevco brand pressure transducers feature an active four arm strain gage bridge diffused into a sculptured silicon diaphragm for maximum sensitivity and wideband frequency response. Self-contained hybrid temperature compensation provides stable performance over the temperature range of 0°F to 200°F (-18°C to +93°C). Endevco brand transducers also feature excellent linearity and provide stable performance over the temperature range of -65°F to +250°F (-54°C to +121°C). Meggitt's Endevco brand transducers also feature excellent linearity (even to 3X range), high shock resistance, and high stability during temperature transients.

Recommended electronics for signal conditioning and power supply are the Endevco brand model 126 and 136 general purpose three channel conditioners, ultra low noise 4430A conditioner, or the 4990A-X (Oasis) multi-channel rack mount system.

Meggitt Sensing Systems

Our measurement product competencies:
Piezoelectric accelerometers | Piezoresistive accelerometers | Isotron accelerometers | Variable capacitance accelerometers | Pressure transducers | Acoustic sensors | Electronic instruments | Calibration systems | Shakers | Modal hammers | Cable assemblies

MEGGiTT
smart engineering for
extreme environments

Aerospace
Energy
Measurement

Endevco®

Piezoresistive pressure transducer

Model 8530B -200, -500, -1000

Specifications

The following performance specifications conform to ISA-RP-37.2 (1982) and are typical values, referenced at +75°F (+24°C) and 100 Hz, unless otherwise noted. Calibration data, traceable to National Institute of Standards and Technology (NIST), is supplied.

Dynamic characteristics	Units	-200	-500	-1000
Range	psia	0-200	0-500	0-1000
Sensitivity [1]	mV/psi	1.5 ±0.5	0.6 ±0.2	0.3 ±0.1
Combined: non-linearity, non repeatability, pressure hysteresis [2]	% FSO RSS max	0.50	0.50	1.0
Non-linearity, independent	% FSO typ	0.2	0.2	0.2
Non-repeatability	% FSO typ	0.1	0.1	0.1
Pressure hysteresis	% FSO typ	0.1	0.1	0.1
Zero measurand output [3]	mV max	±20	±20	±20
Zero shift after 3X over range	±% 3X FSO max (typ)	0.2 (0.05)	0.2 (0.05)	
after 2.5X over range	±% 2.5X FSO max (typ)			0.2 (0.1)
Thermal zero shift				
From 0 to 200°F (-18°C to +93°C)	±% FSO max	3	3	3
Thermal sensitivity shift				
From 0 to 200°F (-18°C to +93°C)	±% max	4	4	4
Resonant frequency	Hz	750 000	1 000 000	> 1 000 000
Non-linearity at 3X over range	% 3X FSO	1.5	2.0	2.0 @ % 2.5X FSO
Thermal transient response per	psi / °F	0.02	0.02	0.04
ISA-S37.10, PARA. 6.7, procedure I	psi / °C	0.04	0.04	0.07
Photoflash response [4]	equiv psi	5	10	20
Warm-up time [5]	ms	1	1	1
Acceleration sensitivity	equiv. psi/g	0.0003	0.0002	0.0002
Burst pressure (diaphragm)	psia min	800	2000	4000
Case pressure [6]	psia min	1000	5000	5000

Electrical	
Full scale output	300 ±100 mV at 10.0 Vdc
Supply voltage [7]	10.0 Vdc standard, 18 Vdc maximum
Electrical configuration	Active four-arm piezoresistive bridge
Polarity	Positive output for increasing pressure
Resistance	
Input	2000 ±800 ohms
Output	1500 ±600 ohms
Isolation	100 megohms minimum at 50 Volts, leads to case, leads to shield, shield to case
Noise	5 microvolts rms typical, DC to 50 000 Hz; 50 microvolts rms maximum, DC to 50 000 Hz

Mechanical	
Case, material	Stainless steel (17-4 PH CRES)
Cable, integral	Four conductor No. 32 AWG Teflon insulated leads, braided shield, silicone jacket
Dead volume port (+)	0.0003 cubic inches (0.005 cc)
Mounting/torque	10-32 UNF-2A threaded case 0.438 inch (11.12 mm) long / 15 ±5 (lbf-in (1.7 ±0.6 Nm)
Weight	2.3 grams (cable weighs 9 grams/meter)

Environmental	
Media [8] [9]	Clean dry gas. Contact factory for protective modifications for other media.
Temperature [10]	-65°F to +250°F (-54°C to +121°C)
Vibration	1000 g pk
Acceleration	1000 g
Shock	20 000 g, 100 microsecond haversine pulse
Humidity	Isolation resistance greater than 100 megohms at 50 V when tested per MIL-STD-202E, method 103B, test condition B

Calibration data [11]
Data supplied for all parameters in Certified Performance section. Optional calibrations available for all parameters in Typical Performance section.

A. Pressure microphone in the acoustic driver enclosure (SN#29821)-Test report

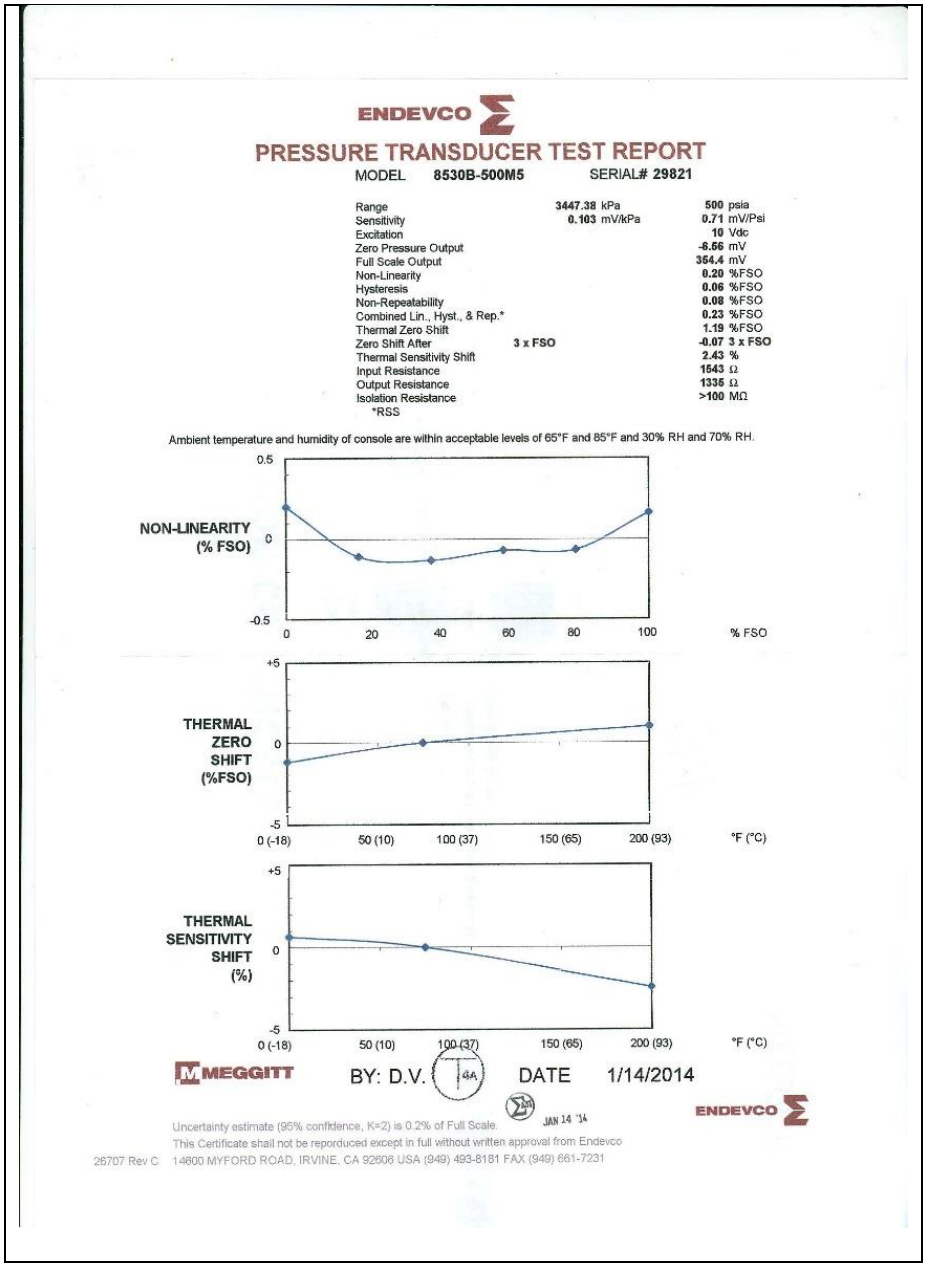

ENDEVCO

PRESSURE TRANSDUCER TEST REPORT

MODEL 8530B-500M5 SERIAL# 29821

Range	3447.38 kPa	500 psia
Sensitivity	0.103 mV/kPa	0.71 mV/Psi
Excitation		10 Vdc
Zero Pressure Output		-6.66 mV
Full Scale Output		354.4 mV
Non-Linearity		0.20 %FSO
Hysteresis		0.06 %FSO
Non-Repeatability		0.08 %FSO
Combined Lin., Hyst., & Rep.*		0.23 %FSO
Thermal Zero Shift		1.19 %FSO
Zero Shift After	3 x FSO	-0.07 3 x FSO
Thermal Sensitivity Shift		2.43 %
Input Resistance		1543 Ω
Output Resistance		1335 Ω
Isolation Resistance		>100 MΩ

*RSS

Ambient temperature and humidity of console are within acceptable levels of 65°F and 85°F and 30% RH and 70% RH.

MEGGITT BY: D.V. 4A DATE 1/14/2014

JAN 14 '14

ENDEVCO

Uncertainty estimate (95% confidence, K=2) is 0.2% of Full Scale.

26707 Rev C 14600 MYFORD ROAD, IRVINE, CA 92606 USA (949) 493-8181 FAX (949) 661-7231

B. Pressure microphone in the front of the linear alternator piston (SN#29822)-Test report

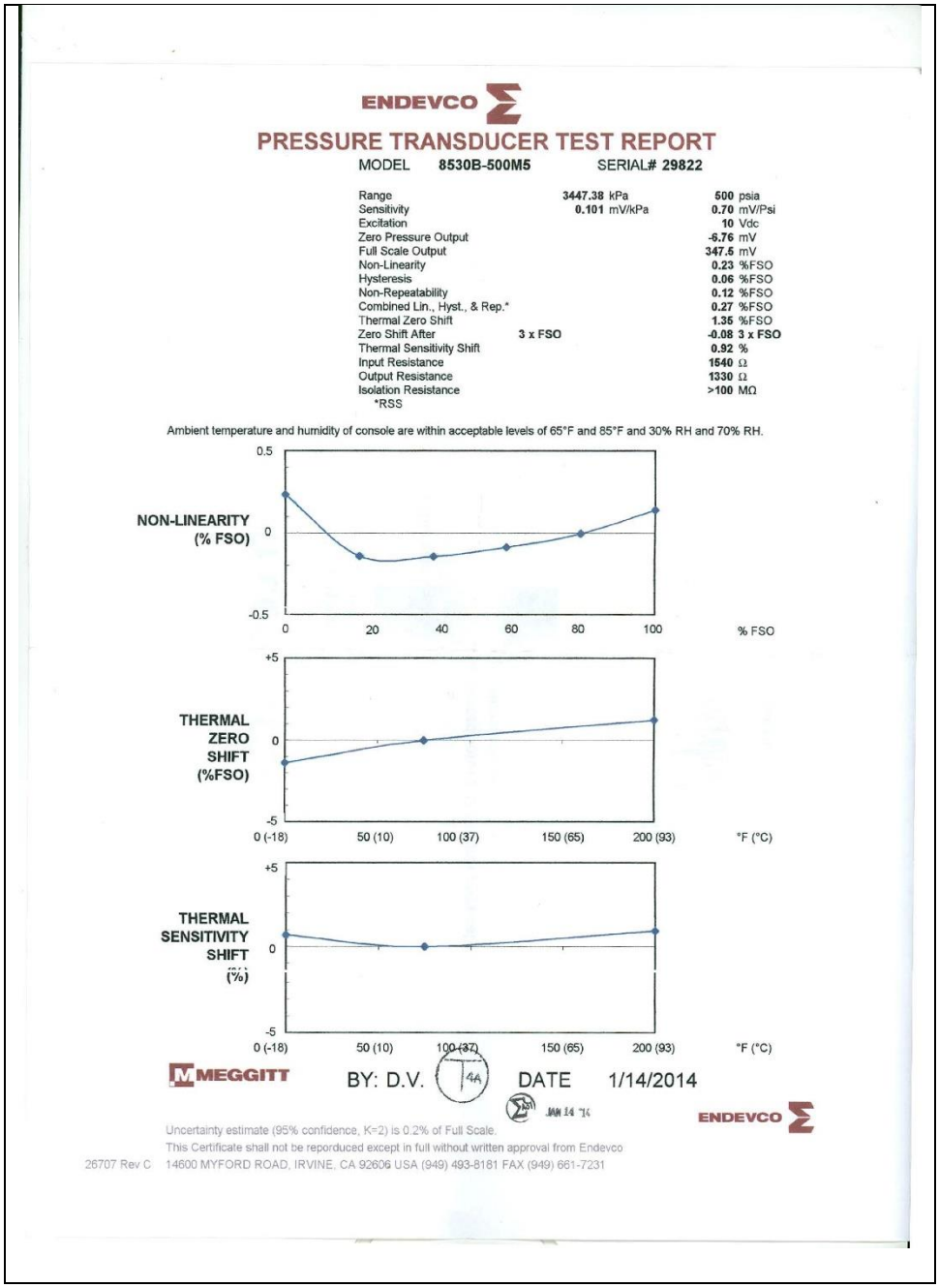

ENDEVCO

PRESSURE TRANSDUCER TEST REPORT

MODEL **8530B-500M5** SERIAL# **29822**

Range	**3447.38** kPa	**500**	psia
Sensitivity	**0.101** mV/kPa	**0.70**	mV/Psi
Excitation		**10**	Vdc
Zero Pressure Output		**-6.76**	mV
Full Scale Output		**347.5**	mV
Non-Linearity		**0.23**	%FSO
Hysteresis		**0.06**	%FSO
Non-Repeatability		**0.12**	%FSO
Combined Lin., Hyst., & Rep.*		**0.27**	%FSO
Thermal Zero Shift		**1.35**	%FSO
Zero Shift After	**3 x FSO**	**-0.08**	**3 x FSO**
Thermal Sensitivity Shift		**0.92**	%
Input Resistance		**1540**	Ω
Output Resistance		**1330**	Ω
Isolation Resistance		**>100**	MΩ

*RSS

Ambient temperature and humidity of console are within acceptable levels of 65°F and 85°F and 30% RH and 70% RH.

MEGGITT BY: D.V. DATE 1/14/2014 ENDEVCO

Uncertainty estimate (95% confidence, K=2) is 0.2% of Full Scale.

26707 Rev C 14600 MYFORD ROAD, IRVINE, CA 92606 USA (949) 493-8181 FAX (949) 661-7231

C. Pressure microphone in the linear alternator enclosure (SN#29823)-Test report

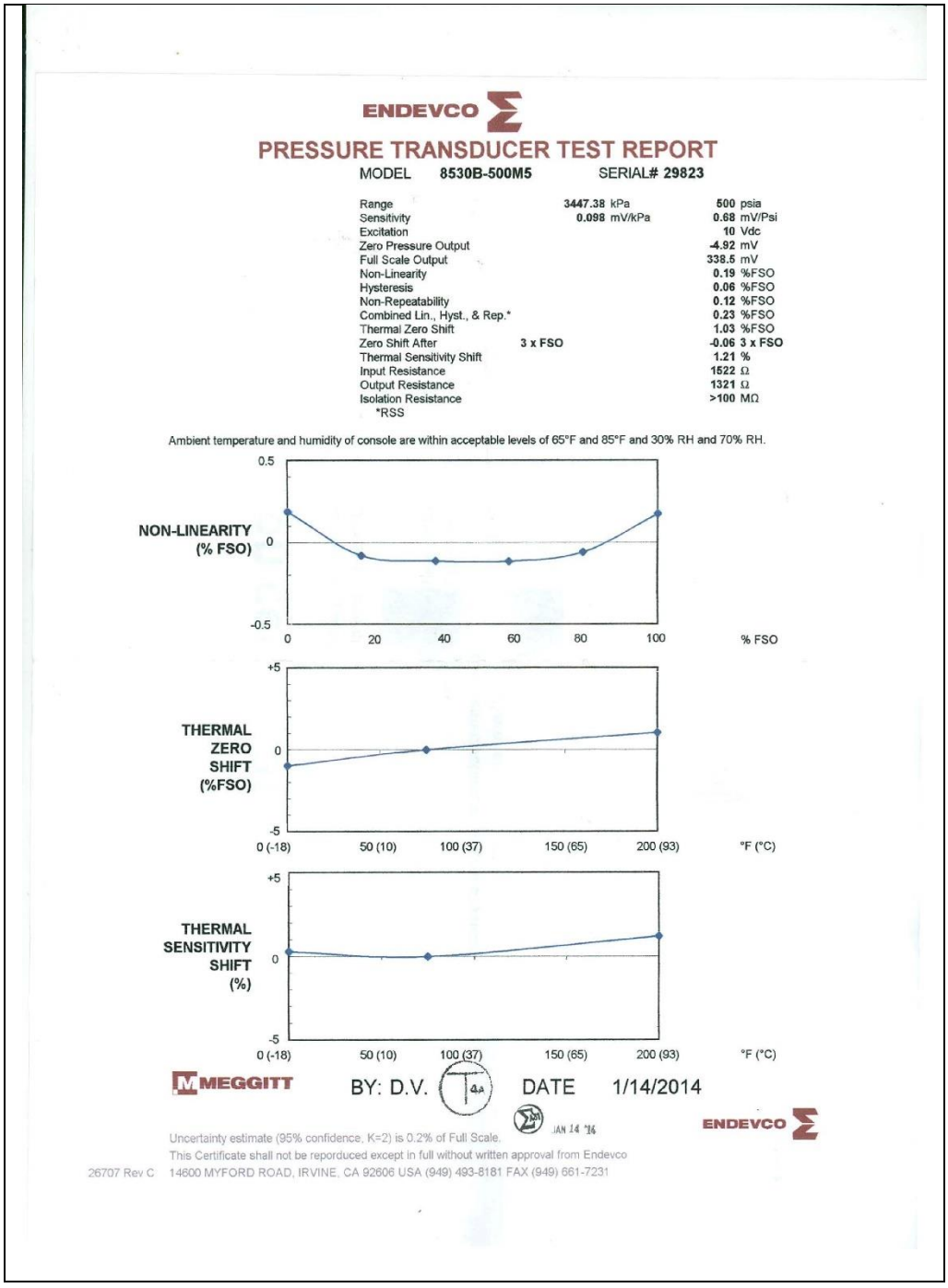

ENDEVCO

PRESSURE TRANSDUCER TEST REPORT

MODEL **8530B-500M5** SERIAL# **29823**

Range	**3447.38** kPa	**500** psia	
Sensitivity	**0.098** mV/kPa	**0.68** mV/Psi	
Excitation		**10** Vdc	
Zero Pressure Output		**-4.92** mV	
Full Scale Output		**338.5** mV	
Non-Linearity		**0.19** %FSO	
Hysteresis		**0.06** %FSO	
Non-Repeatability		**0.12** %FSO	
Combined Lin., Hyst., & Rep.*		**0.23** %FSO	
Thermal Zero Shift		**1.03** %FSO	
Zero Shift After	**3 x FSO**	**-0.06**	**3 x FSO**
Thermal Sensitivity Shift		**1.21** %	
Input Resistance		**1522** Ω	
Output Resistance		**1321** Ω	
Isolation Resistance		**>100** MΩ	

*RSS

Ambient temperature and humidity of console are within acceptable levels of 65°F and 85°F and 30% RH and 70% RH.

MEGGITT BY: D.V. DATE 1/14/2014

JAN 14 '14

ENDEVCO

Uncertainty estimate (95% confidence, K=2) is 0.2% of Full Scale.

26707 Rev C 14600 MYFORD ROAD, IRVINE, CA 92606 USA (949) 493-8181 FAX (949) 661-7231

5. Signal conditioner unit (Model 136 amplifier, supplied by Meggitt)-Datasheet here

Aerospace
Energy
Measurement

Endevco®

DC amplifier
Model 136

Endevco® model 136 is a three-channel, DC amplifier that is manually or computer programmable. Manual control is accomplished at the front panel by means of a "select channel" push-button, three (3) "channel LEDs", one "select function" push-button, five "function LEDs", a four character LED display, showing the state of each function/channel, and four "edit" push-buttons to change the entries in the LED display. There are three LEDs used as fault status indicators for the auto zero function.

There are two modes of operation, normal and programming/setup. Both modes of operation utilize the front panel LED display. In the normal mode, there are two states, monitoring mode and no-monitoring. In the monitoring mode the LED display indicates the RMS reading of the signal present at the output of the selected channel. The non-monitoring mode turns off the LED display for lower noise applications and to minimize power consumption. In the programming mode, the unit is ready for manual programming or editing of existing channel setups. The unit will automatically return to the normal mode of operation after 20 seconds of inactivity of the front panel or after pressing the "select function" push-button while the "monitoring state" function LED is flashing.

The rear panel contains (on a per-channel basis) a BNC output connector, a 9-pin "D" input connector, the RS-232 connector (RS-232 communication is no longer supported), and the input power connector. Three model 136 units may be configured in a 19-inch rack mount adapter. The standard unit is powered by 90-264 VAC, 50/60 Hz. The -1 option is powered by 9 to 18 VDC, making it ideal for portable use or for automobile test applications.

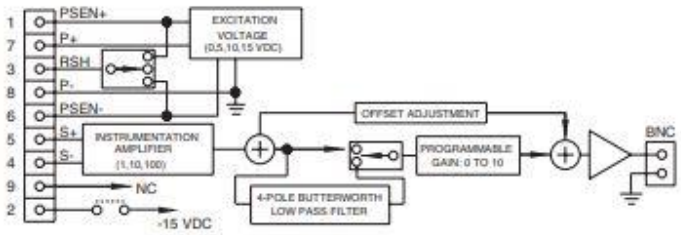

Key features

- Three-channel DC differential voltage amplifier
- 200 kHz bandwidth (-3dB corner)
- Auto-zero and shunt calibration
- Gain range 0 to 1000
- Four selectable excitation voltage levels
- 12 VDC power option
- Default 4-pole Butterworth low-pass filter
- Optional low-pass filter module with different corner frequencies

Meggitt Sensing Systems

Our measurement product competencies:
Piezoelectric accelerometers | Piezoresistive accelerometers | Isotron accelerometers | Variable capacitance accelerometers | Pressure transducers | Acoustic sensors | Electronic instruments | Calibration systems | Shakers | Modal hammers | Cable assemblies

MEGGiTT
smart engineering for extreme environments

Aerospace
Energy
Measurement

Endevco®

DC amplifier
Model 136

Specifications

The following performance specifications conform to ISA-RP-37.2 (1966) and are typical values, referenced at +75°F (+24°C) and 100 Hz, unless otherwise noted. Calibration data, traceable to National Institute of Standards and Technology (NIST), is supplied.

Inputs	
Input impedance	1 Meg Ohm minimum
Input range: differential	0 to ±10 VDC or peak VAC, 9 pin "D" connector for each bridge sensor
Common mode	±10 VDC or pk VAC, inclusive of signal 50 Vpk without damage
Common mode rejection	70 dB minimum, 200Ω or less input imbalance, DC to 60 kHz
Input imbalance adjustment	±100 mVDC, 100 ≤ gain ≤ 1000 ±1 VDC, 10 ≤ gain ≤ 100 ±10 VDC, 0 ≤ gain ≤ 10
Outputs	
AC/DC voltage	Single-ended, short circuit protected
Output impedance	10 ohm typical
Linear output	10 V pk
Current output	10 mA, minimum
Output DC bias stability temp	±5 µV/°C RTI or ±0.1 mV/°C RTO
Output DC bias stability time	±20 µV RTI or ±5 mV RTO, whichever is greater, for 24 hours, after a 1 hour warmup
Excitation voltage	0, 5.0, 10.0, or 15.0 VDC, front panel or computer selected; 1 selection for all 3 channels
Excitation voltage accuracy	±1%
Excitation current	30 mA maximum, short circuit protected
Noise and ripple	1 mV rms maximum, 10 Hz to 50 kHz, with 1 kOhm load
Transfer characteristics	
Gain	
Range	Programmable from 0 to 1000
Resolution	0.0025, 0 ≤ gain ≤ 10 0.025, 10 ≤ gain ≤ 100 0.25, 100 ≤ gain ≤ 1000
Accuracy	±0.5% of full scale maximum, DC to 1kHz, filters disabled
Linearity	0.1% of full scale, best fit straight line at 1 kHz reference
Stability	±0.2% of full scale, 0°C to +50°C
Noise	20 µV rms RTI plus 1 mV rms RTO, whichever is greater, DC to 50 kHz, with a 1 kOhm source resistance unit in Non-monitoring state, 10 kHz internal lowpass filter enabled
Broadband frequency response	±5%, DC to 50 kHz, referenced to 1 kHz; -3 dB at 200 kHz
Filter characteristics/type	4-pole Butterworth
Corner frequency (-3 dB)	10 kHz ±12% (other corners available by changing internal module 31875: 10 Hz to 80 kHz)
Crosstalk between channels	80 dB RTI
Power requirements	
Voltage	Standard unit: 90-264 VAC 50 to 60 Hz; -1 option: 9-18 VDC
Power dissipation	10 Watts typical
Isolation	No isolation channel to channel or signal ground to caseground
Physical characteristics	
Dimensions	5.57" x 2.52" x 12"
Weight	4 lbs typical
Case	Black aluminum cover, medium grey plastic bezel

MEGGiTT
smart engineering for
extreme environments

6. Linear Variable Differential Transformers (LVDT's) (model XS-C 499, sensitivity of 1.27 mm/V, supplied by Measurement Specialties)-Datasheet here

TE connectivity SENSOR SOLUTIONS

RoHS

XS-C SERIES

High Pressure Sealed AC LVDT

SPECIFICATIONS

- **Operating pressures to 3,000 PSI**
- **Bulkhead mounting**
- **Stroke ranges from ±0.25 to ±1 inch**
- **AISI 304 stainless steel housing**
- **Magnetically shielded**
- **Wide operating temperature range**
- **Shock and vibration tolerant**

The XS-C Series high pressure sealed LVDTs are the ideal solution for displacement measurement in pressure-sealed chambers, hydraulic actuators and pressure vessels. Constructed with heavy-wall 304 Series stainless steel, the all-welded XS-C is highly resistant to corrosive environments. It is suitable for operating pressures up to 3,000 PSI (proof pressures up to 4,500 PSI) and temperatures up to +300°F [+150°C].

The XS-C is available in stroke ranges of ±0.25 inch [±6.35mm] to ±1 inch [±25.4mm], with imperial or metric threaded cores. All models incorporate internal magnetic and electrostatic shielding, protecting it from external magnetic influences. The XS-C Series is compatible with all Measurement Specialties LVDT signal conditioners, controllers and readouts.

FEATURES

- Sealed 304 Series stainless steel housing
- High pressure and temperature operation
- Bulkhead mount design
- 400Hz to 5KHz operating frequency range
- Shock and vibration tolerant
- Calibration certificate supplied with all units

APPLICATIONS

- Hydraulic actuators
- Pressure chambers & vessels
- Continuous casting mold clamping
- Tundish slide valve position feedback
- Automatic transmission servo testing
- Rolling mill gap feedback

PERFORMANCE SPECIFICATIONS

ELECTRICAL SPECIFICATIONS			
Parameter	**XS-C 249**	**XS-C 499**	**XS-C 999**
Stroke range	±0.25 [±6.35]	±0.50 [±12.7]	±1.00 [±25.4]
Sensitivity V/V/inch [mV/V/mm]	1.7 [66.9]	1.0 [39.4]	0.8 [31.5]
Output at stroke ends *(*)*	425mV/V	500mV/V	800mV/V
Phase shift	+5°	+2°	-1°
Input impedance (PRIMARY)	800Ω	938Ω	770Ω
Output impedance (SECONDARY)	940Ω	1130Ω	1400Ω
Non-linearity (% of FR), maximum	±0.25		
Input voltage, sine wave	3 VRMS		
Input frequency range	400Hz to 5kHz		
Test input frequency	2.5kHz		
Null voltage, maximum	0.5% of FRO		

ENVIRONMENTAL SPECIFICATIONS & MATERIALS	
Parameter	**All Models**
Operating pressure	3,000 PSI [207 bars]
Proof Pressure	4,500 PSI [310 bars]
Operating temperature	-67°F to +302°F [-55°C to +150°C]
Shock survival	1, 000 g (11ms half-sine)
Vibration tolerance	20 g up to 2KHz
Housing material	AISI 304 Series stainless steel
Electrical connection	Six lead-wires, stranded 28 AWG, PTFE insulated, 1 foot [0.3m] long *(longer wires optional)*
IEC 60529 rating	IP61

Notes:
Dimensions are in inch [mm]
All values are nominal unless otherwise noted
Electrical specifications are for the test frequency indicated in the table
(*): Unit for output at stroke ends is millivolt per volt of excitation (input voltage)
FR: Full Range is the stroke range, end to end; FR=2xS for ±S stroke range
FRO (Full Range Output): Algebraic difference in outputs measured at the ends of the range

MECHANICAL SPECIFICATIONS

Parameter	**XS-C 249**	**XS-C 499**	**XS-C 999**
Main body length "A"	3.00 [76.2]	4.65 [118.1]	7.88 [200.2]
Core length "B"	1.80 [45.7]	3.00 [76.2]	3.80 [96.5]
Core null position "C"	1.39 [35.3]	2.23 [56.6]	3.25 [82.6]
Body weight, oz [g]	3.88 [110]	4.62 [131]	6.04 [171]
Core weight, oz [g]	0.12 [3.4]	0.30 [8.5]	0.37 [10.5]

7. Signal conditioner (Model LDM1000)-Datasheet here

RoHS CE

LDM-1000

LVDT/RVDT Signal Conditioning Module

SPECIFICATIONS

- **10 to 30VDC operation**
- **Standard DIN rail form factor**
- **4 to 20mA and VDC outputs**
- **Zero, span and phase adjustable**
- **2.5, 5 and 10kHz excitation frequencies**
- **Low noise, 3-pole Butterworth filter**
- **Master/slave capability**
- **Compatible with 4, 5 & 6-wire LVDTs/RVDTs**
- **Works with very low input impedance LVDTs and RVDTs**

FEATURES

- Standard DIN rail form factor
- Voltage and current output signals
- Phase correction
- Status LED's for power and loop integrity
- Multiple LVDT master/slave capability

APPLICATIONS

- Gas and steam turbine control systems
- Process control systems
- Reeler/dereeler control systems
- Automotive test track instrumentation
- Paper head box control

The **LDM-1000** is an extremely versatile and popular LVDT/RVDT signal conditioning module and the perfect choice for industrial applications requiring the DIN standard rail mount. The LDM-1000 provides everything you will need for accurately interfacing an AC operated Linear or Rotary Variable Differential Transformer to your industrial position control system.

The LDM-1000 was designed with maximum sensor/system compatibility in mind. A wide range of gains, excitation voltages and frequencies ensure compatibility with virtually all LVDT and RVDT type transducers. A full-wave synchronous demodulator eliminates quadrature and harmonics to maximize external noise rejection.

The LDM-1000 also provides several different input/output options to accommodate varying PLC and analog I/O requirements:

- ✓ Single-ended voltage outputs with the use of 100% zero suppression to maximize the sensor stroke utilization while simplifying programming (no need to deal with sign)
- ✓ Bipolar voltage output to maximize A/D bit usage with most PLC analog input modules, for applications requiring high resolution
- ✓ 4-20mA current output for applications requiring long signal runs or where noise immunity may be an issue. The 4-20mA loop is driven by an internal power supply, provided by the LDM-1000.

Finally, the frequency response is internally selectable and so is the master/slave function which allows synchronization of multiple LDM-1000 modules to prevent beat frequencies and cross talk between transducers.

PERFORMANCE SPECIFICATIONS

ELECTRICAL SPECIFICATIONS	
Supply voltage	18 to 30VDC or 10 to 18VDC *(jumper selectable, 18 to 30VDC as shipped)*
Supply current	65mA maximum
Output types and ranges	±5VDC, 0 to 5VDC, 0 to 10VDC, and 4 to 20mA *(DIP switch selectable, ±5VDC as shipped)*
Temp. coefficient of output	±0.02% of FSO per °F [±0.036% of FSO per °C] over the operating temperature range
Voltage output noise & ripple	5mV RMS maximum
Current output noise & ripple	25µA RMS maximum
Current loop resistance	700Ω maximum *(with 18 to 30VDC supply voltage)*
Frequency response	250 or 1000Hz @ -3 dB *(3-pole Butterworth, DIP switch selectable, 250Hz as shipped)*
Non-linearity	±0.02% of FSO
Input sensitivity range	0.05 to 2.50 VRMS
Transducer excitation	
Voltage	1 or 3 VRMS *(DIP switch selectable; 3VRMS as shipped, with 18 to 30VDC supply voltage only)*
Current	25mA RMS
Frequency	2.5, 5 or 10kHz *(DIP switch selectable, 2.5kHz as shipped)*
Transducer requirements	
Transducer type	LVDT or RVDT with 4, 5 or 6 electrical connections
LVDT/RVDT input impedance	50Ω minimum @ 1 VRMS excitation ; 150Ω minimum @ 3 VRMS
LVDT/RVDT full scale output	0.05 to 2.50 VRMS
ENVIRONMENTAL AND MECHANICAL SPECIFICATIONS	
Operating temperature range	-13°F to +185°F [-25°C to 85°C]
Storage temperature range	-67°F to +257°F [-55°C to 125°C]
Mounting	Standard DIN-3 rail mount
Size	3.90 [99.0] high x 0.89 [22.5] wide x 4.51 [114.5] Deep
Wire terminal size	24 to 12 AWG [0.2 to 2.5mm]
IEC 60529 rating	IP60

Notes:
All values are nominal unless otherwise noted
Dimensions are in inch [mm]
FSO (Full Scale Output) is the largest absolute value of the outputs measured at the range ends

8. Power supply (model RXN305D, supplied by Zhaoxin)-Datasheet here

9. Two down transformers

10. Data acquisition card (model NI 6225, 40 differential-input analog channels, 16-bit resolution, maximum sampling rate of 250,000 Samples/S, quantization resolution of 0.3 mV and supplied by National Instruments)-Datasheet here

DEVICE SPECIFICATIONS

NI 6225

M Series Data Acquisition: 16 Bit, 250 kS/s, 80 AI, 2 AO, 24 DIO

The following specifications are typical at 25 °C, unless otherwise noted. For more information about the NI 6225, refer to the *M Series User Manual* available at *ni.com/manuals*.

Analog Input

Number of channels	40 differential or 80 single ended
ADC resolution	16 bits
DNL	No missing codes guaranteed
INL	Refer to the *AI Absolute Accuracy* section
Sample rate	
Single channel maximum	250 kS/s
Multichannel maximum (aggregate)	250 kS/s
Minimum	No minimum
Timing accuracy	50 ppm of sample rate
Timing resolution	50 ns
Input coupling	DC
Input range	±0.2 V, ±1 V, ±5 V, ±10 V
Maximum working voltage for analog inputs (signal + common mode)	±11 V of AI GND
CMRR (DC to 60 Hz)	92 dB
Input impedance	
Device on	
AI+ to AI GND	>10 GΩ in parallel with 100 pF
AI- to AI GND	>10 GΩ in parallel with 100 pF

Device off	
AI+ to AI GND	820 Ω
AI- to AI GND	820 Ω
Input bias current	±100 pA
Crosstalk (at 100 kHz)	
Adjacent channels	-75 dB
Non-adjacent channels	-90 dB[1]
Small signal bandwidth (-3 dB)	700 kHz
Input FIFO size	4,095 samples
Scan list memory	4,095 entries
Data transfers	
PCI/PXI	DMA (scatter-gather), interrupts, programmed I/O
USB	USB Signal Stream, programmed I/O
Overvoltage protection for all analog input and sense channels	
Device on	±25 V for up to two AI pins
Device off	±15 V for up to two AI pins
Input current during overvoltage condition	±20 mA maximum/AI pin

Settling Time for Multichannel Measurements

Accuracy, full-scale step, all ranges	
±90 ppm of step (±6 LSB)	4 µs convert interval
±30 ppm of step (±2 LSB)	5 µs convert interval
±15 ppm of step (±1 LSB)	7 µs convert interval

[1] Channel AI <0..15> crosstalk to channel AI <64..79> is -71 dB. This applies to channels with 64-channel separation. Example: AI (*x*) and AI (*x* + 64).

11. High-power and low-inductance variable-resistances (Model RLS350E, maximum resistance of 350 Ω, power rating of 150 W and supplied by Ohmite)-datasheet here

Rheostats

(Potentiometers) Wirewound

MODELS H, J, G, K, L

Model	Type	Watts	Ohmic range	Core	Max. Voltage (RMS)*	Behind panel "B" (in./mm Ref.)	Diameter "D" (in./mm Ref.)	Dimension "C" (in./mm Ref.)	Shaft torque	Rotation (±5°)
H	RHS/RHL	25	1.0-25K	open	500	1.375/34.93	1.560/ 39.62	0.940/23.88	0.25-0.5 lb. in.	300°
J	RJS	50	0.5-50K	open	750	1.375/34.93	2.31 / 58.67	1.56 /39.62	0.25-2 lb. in.	300°
G	RGS	75	0.5-50K	open	900	1.750/44.45	2.75 / 69.25	1.78 /45.21	0.5-2 lb. in.	300°
K	RKS	100	0.5-50K	open	1000	1.750/44.45	3.125/ 79.38	1.91 /48.51	0.5-2 lb. in.	300°
L	RLS	150	0.5-50K	open	1200	2.000 / 50.8	4.00 /101.60	2.28 /57.91	0.5-3 lb. in.	300°

• Models H, J, G, and K also available in enclosed versions.

• See Catalog #203 for complete details.

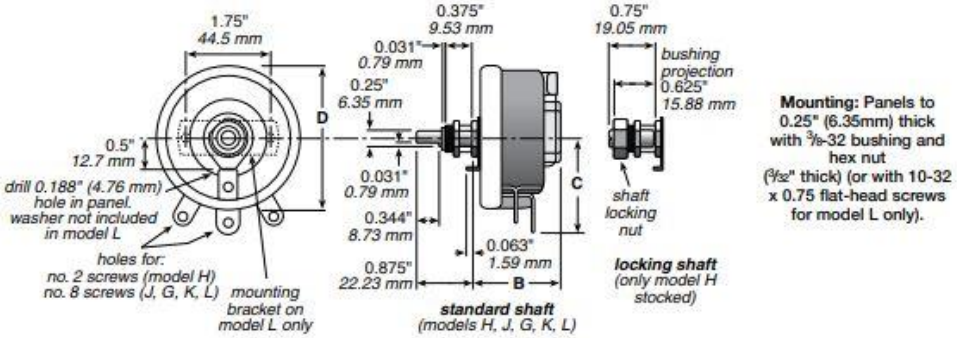

MODELS P, N, R, U

Model	Type	Watts	Ohmic range	Core	Max. Voltage (RMS)*	Behind panel "B" (in./mm Ref.)	Diameter "D" (in./mm Ref.)	Dimension "C" (in./mm Ref.)	Shaft torque	Rotation (±5°)
P	RPS	225	1.0-30K	open	1300	2.125/53.98	5.00 /127.00	2.97 /75.44	2.5-4 lb. in.	310°
N	RNS	300	1.0-50K	open	1225	2.375/60.33	6.00 /152.40	3.44 /87.38	2.5-5 lb. in.	320°
R	RRS	500	1.0-20K	open	1450	2.125/53.98	8.00 /203.20	4.31/109.47	4.5-7 lb. in.	325°
U	RUS	1000	1.0-20K	open	1600	3.000 / 76.2	12.00 /304.80	6.38/162.05	3.5-7 lb. in.	335°

• See Catalog #203 for complete details.

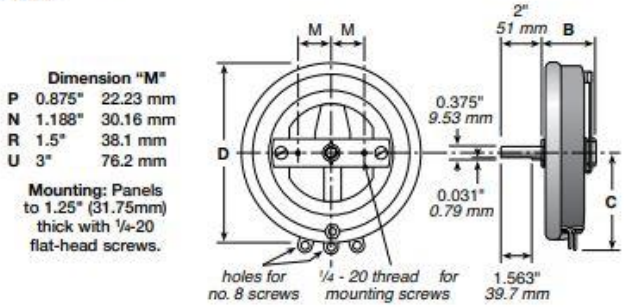

12. Power-factor correcting capacitor that corrects for the alternator inductance (polypropylene film capacitor, run type, maximum operating voltage of 450 V)-datasheet here.

MotorCap P2 (S2) Aluminum Can

Single Capacitance, B32330/B32332/B32333 Series

EPCOS

Technical data

Type/ series		B32330/ B32332	B32330/ B32332 Super MotorCap	B32333 Super MotorCap	
Terminals		Single fast-on Double fast-on		Wire cable terminals	
Electrical ratings					
Rated voltage	V_R	250	450	450	V AC
Rated capacitance	C_R	4 ... 60	1 ... 60	1 ... 60	µF
Rated frequency	f_R	50/ 60			Hz
Capacitance tolerance		±5			%
Max. permissible voltage	V_{max}	$1.1 \cdot V_R$			V
Max. permissible current	I_{max}	$1.3 \cdot I_R$			A
Dissipation factor (20 °C, 120 Hz)	tan δ	$\leq 1.0 \cdot 10^{-3}$			
Safety					
Safety class		P2 (S2) to IEC 60252-1			
Life expectancy to IEC/EN 60252		250 V: 10 000 h (class B)	450 V: 30 000 h (class A)	450 V: 30 000 h (class A)	
Climatic parameter to IEC 60068-1					
Temperature limit	T_{min}/ T_{max}	-25/ +85	-25/ +85	-25/ +85	°C
Test duration (damp heat test)	t_{test}	21			days
Construction					
Reference standards		IEC 60252-1, EN 60252, UL 810			
Can		Aluminum can with overpressure disconnection device			
Terminal top		UL 94 V2/V0 compatible; glow wire test to IEC/EN 60695-2-1/1; compatible to IEC/EN 60335-1 as an option			
Dimensions		Ø 30 ... 40 mm H: 68 ... 103 mm	Ø 30 ... 40 mm H: 52 ... 103 mm	Ø 30 ... 40 mm H: 74 ... 125 mm	
Approvals					
		UL 810 component	VDE UL 810 component CQC on request TÜV	VDE UL 810 component TÜV	
Mounting options					

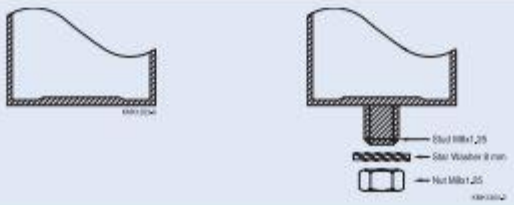

13. DC electronic load (model 8540, rated at 150 W, BK precision)-datasheet here.

INSTRUCTION MANUAL

BK PRECISION

Model 8540

Model 8540
60V/30A/150W DC Electronic Load

Specifications

Parameter		8540	
Input rating (0 - 40 ℃)	Voltage	0 – 60 V	
	Current	1 mA – 30 A	
	Power	150 W	
Load Regulation	Range	Accuracy	Resolution
	0-10 V	±(0.05%+0.1%FS)	1 mV
	0-60 V	±(0.05%+0.1%FS)	10 mV
	0-3 A	±(0.1%+0.1%FS)	1 mA
	0-30 A	±(0.1%+0.15%FS)	10 mA
CV Mode Regulation	0.1-60 V	±(0.05%+0.1%FS)	10 mV
CC Mode Regulation	0-3 A	±(0.1%+0.1%FS)	1 mA
	0-30 A	±(0.1%+0.15%FS)	10 mA
CR Mode Regulation	0.1-10 Ω	±(1%+0.8%FS)	0.001 Ω
	10-99 Ω	±(1%+0.8%FS)	0.01 Ω
	100-999 Ω	±(1%+0.8%FS)	0.1 Ω
	1K-4K Ω	±(1%+0.8%FS)	1 Ω
Current Measurement	0-3 A	±(0.1% + 0.1%FS)	1 mA
	0-30 A	±(0.1% + 0.15%FS)	10 mA
Voltage Measurement	0-10 V	±(0.05% + 0.1%FS)	1 mV
	0-60 V	±(0.05% + 0.1%FS)	10 mV
Power Measurement	0-10 W	±(1%+0.5%FS)	1 mW
	10-99 W	±(1%+0.5%FS)	10 mW
	100-150 W	±(1%+0.5%FS)	100 mW
Dimension (W x H x D)	88 x 175 x 282 mm 3.5 x 6.9 x 11.10 inches		
Weight (net)	2.7 kg 6 pounds		

Specifications and information are subject to change without notice. Please visit www.bkprecision.com for the most current product information.

9.2 Appendix B-LabView Code

1. User interface screen-Link of the code here

A. Sampling parameters

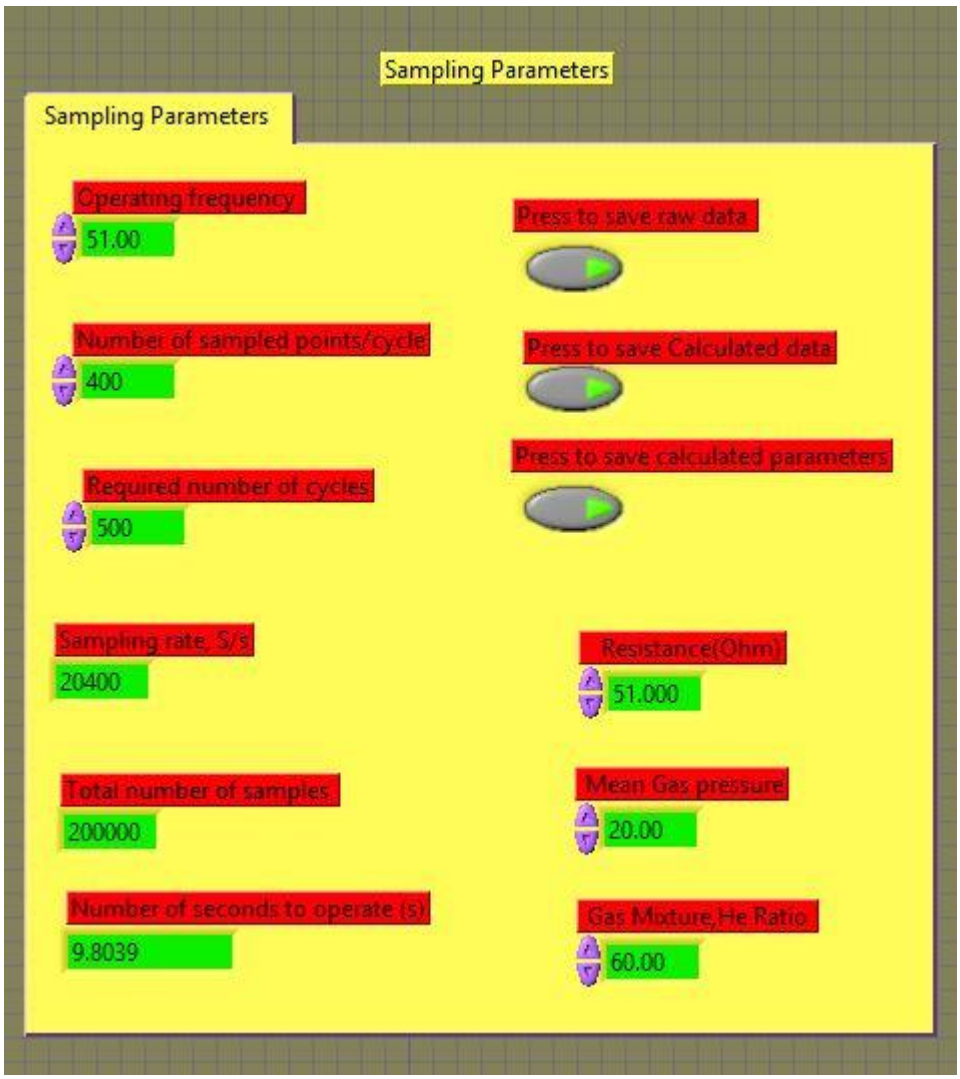

B. Calculated parameters

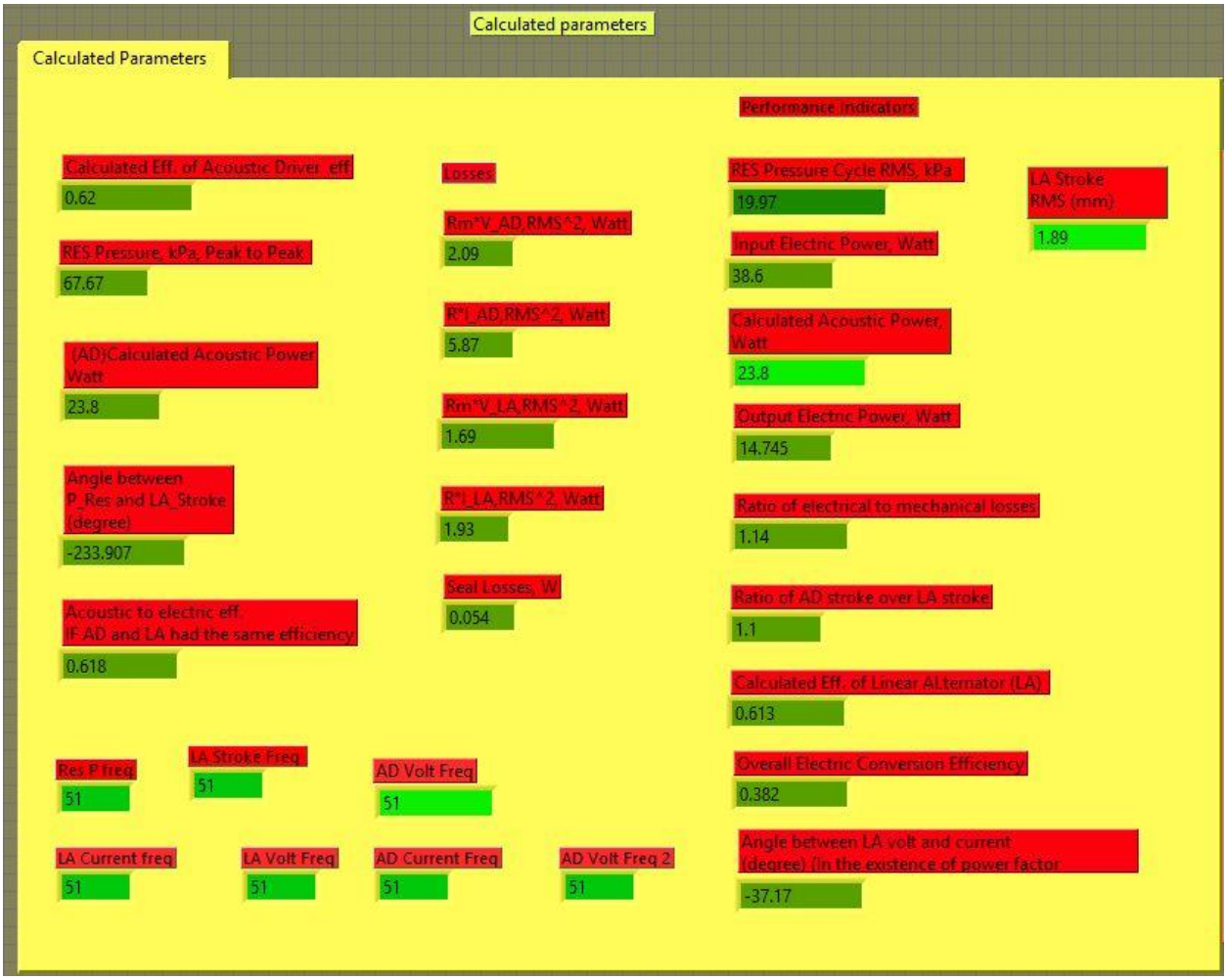

C. Seal loss parameters

2. Remove mean function

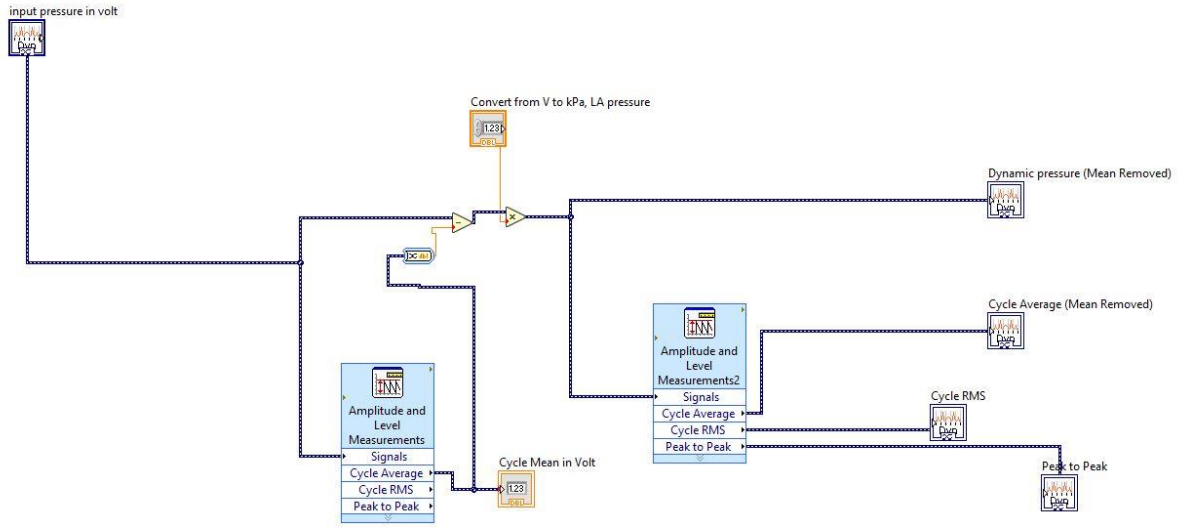

3. Data files

A. Raw data (Signals volts) file

Signal/ Sample#	AD stroke	LA stroke	AD pressure	Resonator pressure	LA pressure	AD current	LA current	AD volt	LA volt
1									
……									
Total number of Samples									

B. Calculated data (Performance indices signals) file

Signal/ Sample#	AD stroke, mm	LA Stroke ,mm	AD pressure ,kpa	Resonator pressure ,kpa	LA pressure, kpa	AD current, A	LA current, A	AD volt, V	LA volt, V
1									
……									
Total number of Samples									

C. Values (Performance indices of the acoustic driver and the linear alternator) file.

Performance index	**Value**
AD stroke, rms ,mm	
LA stroke, rms, mm	
AD PRESSURE, rms, kpa	
Resonator PRESSURE, rms, kpa	
LA PRESSURE, rms, kpa	
AD current, rms, A	
LA current, rms, A	
AD volt, rms, V	
LA volt, rms, V	
Input electric power, W	
Output electric power, W	
AD velocity, rms, m	
LA velocity, rms, m	
Measured Frequency, HZ	
Sampling rate, S,s	
Total Number of samples	
acoustic power(LA_V*Res_p),W	
Overall conversion Eff,%	
Theoretical LA efficiency Eff,%	
Calculated acoustic power, W	
Calculated LA efficiency Eff,%	

Input electric power, W	
LA Mechanical losses, W	
LA electric losses, W	
Ratio between LA losses	
Measured Frequency, HZ	
Ratio between AD stroke and LA stroke	
Angle between Res_P and LA_stroke via dot product, Deg	
Angle between Res_P and LA_stroke, Deg	
Number of cycles	
Number of points	
AD PF	
LA PF	
AD efficiency,%	
AD Mechanical losses, W	
AD electric losses, W	
user operating frequency	
Mean gas pressure	
HE ratio	
Angle between Res_P and LA_P, Deg	
Seal Impedance	
Seal losses, W	

9.3 Appendix C-DELTAEC code

```
Freq simulation
  0 BEGIN
              3.0000E+6 a Mean P Pa
                 60.000 b Freq   Hz
                 300.00 c TBeg   K
Gues         -5.3199E+4 d |p|    Pa
                 0.0000 e Ph(p)  deg
                 0.0000 f |U|    m^3/s
                 0.0000 g Ph(U)  deg
                 0.6000 j nL
Optional Parameters
HeAr          Gas type
   1 ANCHOR     Energy dissipation
   2 DUCT       Acoustic driver enclosure
              8.0000E-3 a Area   m^2                5.3159E+4 A |p|    Pa
                 0.8600 b Perim  m                   -180.0 B Ph(p)  deg
              4.9000E-2 c Length m                1.5787E-3 C |U|    m^3/s
                 0.0000 d Srough                    89.756 D Ph(U)  deg
Master-Slave Links                                 -0.17895 E Htot   W
Optional Parameters                                -0.17895 F Edot   W
ideal         Solid type
   3 VESPEAKER  Qdrive (ls102d-x) - Acoustic Driver (S/N:777)
              2.0000E-3 a Area   m^2                1.5442E+4 A |p|    Pa
                 6.7000 b R      ohms                30.821 B Ph(p)  deg
              8.6400E-2 c L      H                  1.5787E-3 C |U|    m^3/s
                 47.690 d BLProd T-m                 89.747 D Ph(U)  deg
                 0.4922 e M      kg                  6.2913 E Htot   W
              3.0490E+4 f K      N/m                 6.2913 F Edot   W
                 4.6900 g Rm     N-s/m               12.240 G WorkIn W
Gues             75.016 h |V|    V                   75.016 H Volts  V
Gues             274.87 i Ph(V)  deg                 1.1329 I Amps   A
                                                     73.259 J Ph(V/I)deg
                                                   6.6890E+4 K |Px|   Pa
ideal         Solid type                            6.7934 L Ph(Px) deg
   4 RPN        Acoustic driver efficiency
                 0.0000 a G or T                    51.400   A %
3F 3G / 100 *
   5 RPN        Acoustic driver stroke (amplitude)
              5.0000E-3 a G or T                  2.0938E-3  A ChngeMe
3C 3a / w /
   6 RPN        Acoustic driver volt (amplitude)
  AD volt setting by this RPN
                 110.00 a G or T                    75.016   A deg
3H
   7 RPN        Acoustic driver current (amplitude)
                 0.5100 a G or T                    1.1329  A ChngeMe
3I
   8 RPN        Phase between input volt and current
             9.9075E+18 a G or T                    73.259   A ChngeMe
3J
   9 RPN        Applied acoustic power on the piston of linear alternator
Targ             4.4200 a =A?                       6.2913  A ChngeMe
3F
  10 RPN        Input electric power
                 12.240 a G or T                    12.240   A ChngeMe
3G
  11 RPN        pressure amplitude on the piston of linear alternator
              1.0400E+4 a G or T                  1.5442E+4  A pa
```

```
pl mag
   12 DUCT       Resonator
              2.0000E-3 a Area   m^2     Mstr       1.5713E+4 A |p|    Pa
                0.39354 b Perim  m       12a          30.191  B Ph(p)  deg
              5.0000E-2 c Length m                  1.4777E-3 C |U|    m^3/s
                 0.0000 d Srough                     87.430  D Ph(U)  deg
Master-Slave Links                                   6.2823  E Htot   W
Optional Parameters                                  6.2823  F Edot   W
ideal        Solid type
   13 IESPEAKER  Qdrive (ls102d-x) - Linear Alternator(S/N:774)
              2.0000E-3 a Area   m^2               4.9755E+4 A |p|    Pa
                 6.7200 b R      ohms                -2.3111 B Ph(p)  deg
              8.4100E-2 c L      H                 1.4776E-3 C |U|    m^3/s
                48.000  d BLProd T-m                 87.445  D Ph(U)  deg
                 0.4780 e M      kg                  0.15677 E Htot   W
              3.0940E+4 f K      N/m                 0.15677 F Edot   W
                 4.5500 g Rm     N-s/m               -4.6211 G WorkIn W
Gues           -0.27524 h |I|    A                   35.118  H Volts  V
Gues             989.95 i Ph(I)  deg                 0.27524 I Amps   A
                                                    -197.03  J Ph(V/I)deg
                                                   3.7466E+4 K |Px|   Pa
ideal        Solid type                             -15.335  L Ph(Px) deg
   14 RPN        Linear alternator efficiency
                 0.0000 a G or T                     73.557   A %
13G 12F / -100 *
   15 RPN        Linear alternator stroke (amp)
              2.3320E-3 a G or T                   1.9597E-3  A m
13C 13a / w /
   16 RPN        angle between volt and current in linear alternator
                180.00 a G or T                    -197.03    A deg
13J
   17 RPN        Load Impedance (Real part and Imaginary part magnitudes)
  A: Imaginary
  B: Real
                 0.0000 a G or T                    -37.36    A ohm
                                                    122.00    B ohm
13H 13I / 13J cos * -1 * ; 13H 13I / 13J sin * -1 *
   18 RPN        Load Resistance
Targ             122.00 a =A?                       122.00    A ChngeMe
17B
   19 RPN        Magnitude and phase of electric load impedance
                 0.0000 a G or T                    127.59    A Ohm
                                                   -377.03    B Degree
                                                  -0.30623    C Tangent
13J 180 - ; # tan ; a<>b ; 13H 13I /
   20 RPN        Resistance and capacitance values
                 0.0000 a G or T                    122.00    A Ohm
                                                   7.1000E-5  B Farad
18A ; 19C ~ inv w / 18A / a<>b
   21 RPN        Capacitor value
Targ          7.1000E-5 a =A?                     7.1000E-5  A ChngeMe
20B
   22 RPN        Output electric power
                 6.0000 a G or T                     4.6211  A ChngeMe
-1 13G *
   23 DUCT       Linear alternator enclosure volume
     Same  2a  8.0000E-3 a Area   m^2               4.9793E+4 A |p|    Pa
                 0.8600 b Perim  m                   -2.3115 B Ph(p)  deg
```

```
117       Same  2c  4.9000E-2 c Length m                  9.2812E-13 C |U|    m^3/s
118                   0.0000 d Srough                        -73.451 D Ph(U)   deg
119   Master-Slave Links                                   7.4695E-9 E Htot    W
120   Optional Parameters                                  7.4695E-9 F Edot    W
121   ideal          Solid type
122      24 HARDEND     Rigid termination
123   Targ              0.0000 a R(1/z)                    4.9793E+4 A |p|     Pa
124   Targ              0.0000 b I(1/z)                      -2.3115 B Ph(p)   deg
125                                                        9.2812E-13 C |U|    m^3/s
126                                                          -73.451 D Ph(U)   deg
127                                                        7.4695E-9 E Htot    W
128                                                        7.4695E-9 F Edot    W
129                                                        7.9188E-12 G R(1/z)
130                                                       -2.3181E-11 H I(1/z)
131    25 RPN         Mechanical motion loss
132   Rm*u^2=4.55 N.S/m
133                   0.0000 a G or T                        1.2421  A ChngeMe
134   4.55 13C * 0.002 / 13C * 0.002 / 1.414 / 1.414 /
135    26 RPN         Ohmic loss
136   I^2*R, R=6.72
137                   0.0000 a G or T                       0.25461 A ChngeMe
138   6.72 13I * 13I * 1.414 / 1.414 /
139    27 RPN         Acoustic-to-electric conversion efficiency, %
140                   0.0000 a G or T                        73.452  A %
141   13G 3F / -100 *
```

9.4 Appendix D-Publications from this thesis work

Conference papers:

1. Abdou, M., Abdelwahed, A. Y., Ibrahim, A. H. and Abdel-Rahman, E. An experimental setup to test linear alternators: design, operation and preliminary results, The 22nd International Congress on Sound and Vibration, Florence, Italy, 12-16 July,2015.
2. Ibrahim, A. H., Abdelwahed, A. Y. and Abdel-Rahman, E . Real-time measurements of Linear alternator performance indices under thermoacoustic-power-conversion Conditions. The 23*rd* International Congress on Sound and Vibration, Athens, Greece, 2016.
3. Abdelwahed, A. Y., Ibrahim, A. H. and Abdel-Rahman, E . Performance of linear alternators using passive linear and non-linear loads under thermoacoustic-power-conversion conditions. The 23*rd International Congress on Sound and Vibration*, Athens, Greece, 2016.
4. Ibrahim, A. H., Abdelwahed, A. Y. and Abdel-Rahman, E. Sensitivity Analysis of linear alternator performance indices under thermoacoustic-power-conversion conditions. The 23*rd* International Congress on Sound and Vibration, Athens, Greece, 2016.
5. Abdelwahed, A. Y., Ibrahim, A. H. and Abdel-Rahman, E . Experimental investigation of the effects of mechanical stroke on the acoustic impedance of linear alternators under thermoacoustic-power-conversion conditions. The 23rd International Congress on Sound and Vibration, Athens, Greece, 2016.
6. Abdelwahed, A. Y., Ibrahim, A. H. and Abdel-Rahman, E. Effects of operation at and off electrical resonance on the performance indices of linear alternators under thermoacoustic-power-conversion conditions, The 22nd International Congress on Acoustics, Argentina, 2016.
7. Abdelwahed, A. Y., Ibrahim, A. H., and Abdel-Rahman, E. Performance indicators of linear alternators at different electric loads under thermoacoustic-power-conversion conditions. In Proceedings of the 24th International Congress on Sound and Vibration, London, United Kingdom, 2017.

Acoustical Society of America Meetings:

1. Ibrahim, A. H., Yassin, A. and Abdel-Rahman, E .Sensitivity analysis of the performance of a linear alternator at mechanical resonance under thermoacoustic power conversion conditions. The Journal of Acoustical Society of America,139(4),2031, 2016.
2. Abdelwahed, A. Y., Ibrahim, A. H., and Abdel-Rahman, E. Numerical Simulation of key linear alternator performance indicators under thermoacoustic-power-conversion conditions. The Journal of Acoustical Society of America,141(5),3737, 2017.

Research-Gate Profile: https://www.researchgate.net/profile/Ahmed_Abdel-Wahed

LinkedIn Profile: https://www.linkedin.com/in/ahmed-ibrahim-49bb0583/